Prerequisites for numerical pollen forecasts: distribution maps and a parameterization of pollen emission

KATRIN ZINK

1119619

DISSERTATION

submitted to the

FACULTY OF GEO- AND ATMOSPHERIC SCIENCES

at the

LEOPOLD FRANZENS UNIVERSITY OF INNSBRUCK

Innsbruck, July 2014

Dedicated to my husband Marcel and my son Nicolas.

Zusammenfassung

Allergien gehören zu den Gesundheitsproblemen, die am weitesten verbreitet sind. Pollenvorhersagen sind ein wichtiges Hilfsmittel für Allergiker, um die Symptome ihrer Pollenallergie abzuschwächen, da Gebiete mit hohen Pollenkonzentrationen gemieden werden können. Trotz ihrer Wichtigkeit wurden Pollenvorhersagen lange Zeit aufgrund von empirischem Wissen, numerischen Wettervorhersagen und gemessenen Pollenkonzentrationen erstellt. Die Pollenkonzentrationen wurden nicht direkt mithilfe eines numerischen Wettervorhersagemodells simuliert. Werden Pollen in ein Wettervorhersagemodell eingebaut, damit ihre Ausbreitung direkt berechnet werden kann, ist eine zusätzliche Gleichung nötig, die die Emission, den Transport und die Entfernung der Pollen aus der Atmosphäre beschreibt. Insbesondere ist eine mathematische Beschreibung des Quellterms der Pollen notwendig, der die folgenden Fragen beantwortet: (1) Wann werden Pollen emittiert? (2) Wo werden Pollen emittiert? (3) Wieviele Pollen werden emittiert? Die Güte solcher Ausbreitungsmodelle hängt stark von der Qualität dieses Quellterms ab. Die vorliegende Doktorarbeit nimmt die Herausforderung an, diesen Quellterm zu verbessern. Es werden dabei zwei Themen besonders betrachtet: (A) die numerische Parametrisierung der Pollenemission, und (B) die Verbreitungskarte, die die Standorte und Anzahl der pollenproduzierenden Pflanzen anzeigt.

Zu Beginn dieser Doktorarbeit gab es nur sehr wenige ausgereifte Parametrisierungen der Pollenemission. Diese sind für Baumpollen entwickelt worden. Bei der Verwendung für kleinere Pflanzen (wie z.B. Ambrosia) zeigen sie einige Nachteile. Es wurde daher in dieser Doktorarbeit eine neue Parametrisierung der Pollenemission (EMPOL) für die Anwendung in numerischen Wettervorhersagemodellen entwickelt. Die Grundidee von EMPOL ist die Verwendung von Parametern, die durch Feld- oder Laborexperimente bestimmt werden können. EMPOL ist so aufgebaut, dass die biologischen und physikalischen Prozesse, die zur Pollenemission führen, schrittweise beschrieben werden. Dies führt dazu, dass die Parametrisierung in zwei Teile aufgespalten ist: (1) die Freisetzung der Pollen aus den Blüten in ein sogenanntes Pollenreservoir (dieser Prozess wird auch 'Pollenpräsentation' genannt), und (2) die Einbringung der Pollen aus dem Reservoir in die Atmosphäre. Die Formulierungen sind dabei sehr flexibel gehalten, sodass neue Pollenarten relativ

einfach einzubauen sind (vorausgesetzt die artspezifischen Parameter sind bekannt, z.B. die Reaktion der Pflanze auf sich ändernde Temperaturen oder Feuchtigkeit). Am Beispiel der Birkenpollensaison 2012 wird gezeigt, dass EMPOL bessere Resultate erbringt als eine frühere Parametrisierung. Wird berücksichtigt, dass die Formulierungen in EMPOL nicht mit gemessenen Daten kalibriert werden konnten (wegen des Fehlens hochaufgelöster Daten), so kann gesagt werden, dass EMPOL ein großes Verbesserungspotential hat: mithilfe geeigneter Experimente könnte die Genauigkeit der Parametrisierung nochmals verbessert werden.

Der wichtigste Eingangsparameter bei numerischen Pollenvorhersagen sind Karten, die die räumliche Verteilung und Menge der pollenproduzierenden Pflanzen zeigen. In der Literatur sind verschiedene Methoden beschrieben, wie solche Karten generiert werden können. Diese Methoden basieren auf verschiedenen Arten von Daten: Inventardaten, Landnutzungsdaten, jährlichen Pollensummen oder auf ökologischer Modellierung. Wegen ihrer unterschiedlichen Art haben alle diese Karten ihre besonderen Vor- und Nachteile. In dieser Doktorarbeit habe ich daher den Einfluss der verschiedenen Methoden auf die Güte der Pollenvorhersagen untersucht. Am Schluss werden Empfehlungen abgegeben, wie solche Verbreitungskarten am besten herzustellen sind. In zwei separaten Studien werden verschiedene Verbreitungskarten zusammengestellt, die alle dieselbe Region abdecken: Karten, die auf verschiedenen Arten von Inventardaten beruhen, eine Karte, die auf Landnutzungsdaten und jährlichen Pollensummen beruht und verschiedene Karten, die auf ökologischer Modellierung beruhen. Diese Karten werden in Simulationen der Ambrosiapollensaison 2012 in Frankreich und der Schweiz verwendet. Die simulierten Pollenkonzentrationen werden statistisch mit gemessenen verglichen, um herauszufinden, welche der Karten die beste Vorhersage produziert. Es werden zwei verschiedene Szenarien untersucht: eine Region mit geringer lokaler Emission, die hauptsächlich von entfernten Pollenquellen beeinflusst wird (die Schweiz), und eine Region, die hauptsächlich von lokalen Pollenquellen beeinflusst wird (Frankreich). Es wird gezeigt, dass Karten, die auf Landnutzungsdaten in Kombination mit jährlichen Pollensummen beruhen, die besten Ergebnisse liefern, falls alle Regionen betrachtet werden. In der Quellregion selbst sind Vorhersagen, die auf Inventarkarten mit detaillierter Mengenangabe beruhen, noch besser. Allerdings sind Qualität und Verfügbarkeit solcher Inventardaten beschränkt, sodass solche Karten trotzdem nur eingeschränkt nutzbar sind.

Das letzte Kapitel schließlich stellt die Ergebnisse der einzelnen Studien zusammen. Es gibt Anleitungen und Empfehlungen, wie Pollenvorhersagen für eine neue Pollenart aufgesetzt werden sollten.

Summary

Allergies are one of the most widespread health problems. Pollen forecasts are an important tool for allergic people to reduce symptoms of pollen allergies by avoiding areas with high pollen concentrations. Despite their importance, pollen forecasts have long been based on empirical knowledge, numerical weather forecasts and observations of pollen concentrations. The pollen concentrations have not been simulated directly with the use of numerical weather prediction (NWP) models. Introducing pollen into NWP models to explicitly simulate their dispersal requires an additional balance equation accounting for the emission, transport and removal of the pollen grains. In particular, a mathematical description of the pollen source term is needed, answering the following questions: (1) When are pollen grains emitted? (2) Where are pollen grains emitted? (3) How many pollen grains are emitted? The performance of such models depends strongly on the quality of this source term. This thesis takes on the challenge to improve the source term by focusing on two sub-topics: (A) the numerical parameterization of the pollen emission processes, and (B) the distribution map displaying the locations and abundance of pollen sources.

Only very few sophisticated parameterizations of pollen emission had been published when this thesis started. Having been developed for tree pollen, they showed some drawbacks when applied to smaller plants such as ragweed. A new parameterization of pollen emission (EMPOL) was therefore developed in this thesis for the use within NWP models. The underlying idea of EMPOL is the use of parameters that can be derived from laboratory or field experiments. EMPOL is designed to describe the biological and physical processes leading to pollen emission in a stepwise manner. This leads to a separation of the parameterization into two major parts: (1) the release of the pollen from the flowers into a so-called pollen reservoir (i.e. pollen presentation), and (2) the entrainment of the pollen from the reservoir into the atmosphere. The formulations are kept flexible allowing for new pollen species to be introduced rather easily (if the species-specific dependencies are known, e.g., the response of the plant to changing temperatures or humidities). Using the birch pollen season of 2012 as an example, it is shown that EMPOL performs better than a previous parameterization. Considering the fact that the formulations in EMPOL could not be tuned with measured values (due to lack of highly resolved data),

EMPOL has considerable potential for improvement by dedicated experiments, thus even increasing its accuracy.

The main input parameter in numerical pollen forecasting are maps showing the spatial distribution and abundance of the pollinating plants. Different methods have been described in the literature to derive such maps. These make use of different kinds of data: inventory data, land use data, annual pollen counts or the output of ecological models. Due to the different nature of these maps, they all have their drawbacks and advantages. In this thesis, I thus investigate the impact of different methods on the predictive power of pollen forecasts. Furthermore, I give recommendations on the best practice of producing such distribution maps.

In two separate studies, a set of different distribution maps covering the same region is assembled: maps based on different kinds of inventory data, a map based on land use data and annual pollen counts and different maps based on ecological modeling. These maps are used to simulate the ragweed pollen season of 2012 in France and Switzerland. The simulated pollen concentrations are statistically compared to measurements in order to investigate which of the maps produces the best forecast. Two different settings are investigated: a region with low local pollen emission that is mainly influenced by remote pollen sources (Switzerland) and a region that is mainly influenced by local pollen sources (France). It is shown that maps based on land use data in combination with annual pollen counts render the best results if all regions are considered. In the source region, forecasts based on inventory maps with detailed quantitative information are even better. However, the quality and availability of inventory data are limited, thus reducing the usability of such maps.

Combining the results of the different studies, the last chapter gives instructions and recommendations on how to set up pollen forecasts for a new species.

Contents

List of Figures

List of Tables

Chapter 1

Introduction

"Allergic diseases are increasing in prevalence worldwide and are now the most frequent reasons patients seek medical care. Allergies are also becoming more complex, and patients frequently have multiple allergic disorders. Even the less severe allergic diseases can have a major adverse effect on the health of hundreds of millions of patients and diminish quality of life and work productivity. Allergy is a major problem for the 21st century, and this problem is predicted to worsen as this century moves forward."

Pawankar et al. (2008)

Although the term 'allergic diseases' in this citation comprises different types of allergies, pollen grains are amongst the three major causes for allergies (Pawankar et al. 2008). Taking ragweed (*Ambrosia artemisiifolia* L.) as an example, about 12% of the population living in areas that are influenced by strong ragweed pollen concentrations suffer from allergies against these pollen (Taramarcaz et al. 2005). In Germany, the yearly costs in the health sector that are evoked by ragweed allergies are estimated to be between 19 and 50 Mio Euro (Reinhardt et al. 2003). To reduce these costs and to enhance the quality of life of allergic people, detailed pollen forecasts are certainly helpful. Even though medication is possible, avoiding the aeroallergens is still the best way to reduce symptoms (van Moerbeke 1997). Less than a decade ago, forecasts of airborne pollen concentrations were basically handmade: derived from empirical knowledge about typical pollen seasons, current weather forecasts and measurements of airborne pollen concentrations. In the last few years, however, numerical forecasts of pollen concentrations have increasingly been used. This can be seen in the numerous recent publications that deal with different aspects of numerical pollen simulations. When my PhD project started in the end of 2009, there were only a handful of publications dealing with numerical pollen simulations. Today, numerical pollen forecasts are issued operationally on a day-to-day basis in several countries.

1.1   Simulating pollen concentrations in numerical weather prediction models

Numerous models that were built to simulate and investigate air pollution have recently been extended for the use with pollen grains. Examples are the models COSMO-ART (**Co**nsortium for **S**mall-scale **Mo**delling - **A**erosols and **R**eactive **T**race Gases, Vogel et al. 2008), SILAM (System for Integrated modeLling of Atmospheric coMposition, Sofiev et al. 2006), MM5/CMAQ (Mesoscale Meteorological Model - Community Multiscale Air Quality, Efstathiou et al. 2011), CHIMERE (Menut et al. 2013), or WRF-MEGAN-CMAQ (Weather Research & Forecasting - Model of Emissions of Gases and Aerosols from Nature - Community Multiscale Air Quality, Zhang et al. 2014).

Generally, pollen grains are treated as passive tracers that are not subject to physical or chemical transformations and do not feed back on meteorological processes (e.g., radiation). Thus, simulating pollen concentrations in numerical weather prediction (NWP) models requires an additional balance equation describing the processes that affect pollen grains: the emission of pollen into the air, advective transport, turbulent diffusion, sedimentation and washout. In Seinfeld and Pandis (2006), the motion of an aerosol particle in a fluid is discussed. They find that for particles smaller than 20 μm inertial effects can be neglected. For particles larger than that a drag coefficient needs to be considered additionally. To this respect, the pollen grains of the species that are considered in this thesis (ragweed and birch) are a borderline case: their diameter is approximately 20 μm. Because of that, Sofiev et al. (2006) tested the assumptions behind the balance equations for aerosols on their applicability for pollen grains. Using the Navier-Stokes equation as a basis and birch pollen properties as an example, Sofiev et al. (2006) find that (1) for typical atmospheric conditions, pollen grains follow the airflow including turbulent eddies, (2) the inertia of pollen grains is insufficient to penetrate the near-surface laminar layer, and (3) diffusion is negligible for the dry deposition of pollen grains. The washout (called 'wet deposition' in the original publication) was not studied in detail. Sofiev et al. (2006) conclude that the existing formulations for aerosols can be used for pollen grains as well. They state that the errors introduced by the balance equation of aerosols are smaller than the errors introduced by the source term of pollen grains and uncertain meteorological parameters.

Taking the NWP model COSMO-ART as an example, the additional pollen balance equation describes the transport with the mean wind (1), the vertical turbulent

diffusion (2), the sedimentation (3), the washout (4) and the emission (5) of the total pollen density q (Vogel et al. 2008):

$$\rho \frac{dq}{dt} = \rho \left(\underbrace{\frac{\partial q}{\partial t} + \vec{v} \bullet \nabla q}_{1} \right) = \underbrace{-\frac{\partial \overline{\rho w' q'}}{\partial z}}_{2} \underbrace{-\frac{\partial (\rho q v_s)}{\partial z}}_{3} \underbrace{-\lambda q}_{4} \underbrace{+S}_{5} . \tag{1.1}$$

Here, ρ is the density of the air, $\vec{v}$ the wind speed, w' the turbulent fluctuations of the vertical wind velocity, q' the turbulent fluctuations of the total pollen density q, v_s the settling velocity of the pollen grains, λ the washout coefficient and S the source term. The total pollen density q is the ratio between the total number of pollen per m^{-3} (N_P) and the total number of particles per m^{-3} (N, including air molecules): $q = N_P/N$. The turbulent pollen flux is parameterized in accordance to the fluxes of scalars (e.g., temperature and specific humidity) (Doms et al. 2011):

$$\overline{w' q'} = -K^H \frac{\partial \overline{q}}{\partial z}, \tag{1.2}$$

with K^H being the turbulent diffusion coefficient for heat. The settling velocity v_s of pollen grains is needed to calculate their sedimentation:

$$v_s = \sqrt{\frac{4 \, \rho_P \, d_P \, g}{3 \, \rho \, c_D}}. \tag{1.3}$$

This equation takes into account the density of the pollen grains ρ_P, their diameter d_P, the acceleration of gravity g and the drag coefficient c_D. In COSMO-ART, c_D is parameterized according to Fuchs (1964) and Friedlander (1977). The washout in COSMO-ART is parameterized after Rinke (2008). The corresponding equation for λ can be found in Vogel et al. (2008).

The most difficult part of the balance equation for pollen is the source term S. The emission processes differ greatly between biogenic or anthropogenic aerosols and pollen grains. Because of that, the formulations describing the emission of aerosols or gases cannot be used for pollen grains. Hence, the introduction of pollen into NWP models requires a parameterization that relates environmental conditions and emission rates. Additionally, the phenological state of the plants has to be taken into account. Different approaches to tackle this problem are described in Section 1.2. Furthermore, the distribution of possible pollen sources is needed as an input parameter. Naturally, this corresponds to a map showing the locations and quantities of the pollen emitting plants. The different methods to create such distribution maps are presented further down in Section 1.3.

1.2   Models for pollen emission

Simulating pollen concentrations with a NWP model requires a mathematical description of the source term controlling the following aspects: (A) When does emission take place?, and (B) How many pollen grains are emitted? The emission of pollen grains is a complex succession and interaction of different processes. Roughly speaking, three processes have to be considered that are indispensable for pollen emission to take place: (1) the ripening of pollen grains in the anthers, (2) the opening of the anthers, and (3) the entrainment of the pollen grains into the atmosphere. Considering these processes, two time scales have to be distinguished: seasonal and daily variations of the source term.

The **seasonal variations** of pollen emission can be mainly attributed to the growth of the plant, the development of flowers and the ripening process of the pollen grains. Naturally, the onset of flowering of a given plant species takes place in a certain time range. Different meteorological conditions at different plant locations lead to a shift of the flowering season, e.g., colder temperatures usually result in a delayed flowering season. However, not only different environmental conditions have an impact on the timing of the flowering: even plants that are growing side by side can have a different timing of their flowering phases (e.g., due to genetic differences, different soils, ...). Additionally, even individual flowers of the very same plant can be in different stages of flowering. Since a numerical pollen forecast cannot account for individual plants or flowers, the seasonal variations of pollen emission are described as a curve giving the percentage of flowers that are mature at a specific point in time. This leads to some sort of bell-shaped curve: in the beginning and end of the season only a small percentage of the flowers are mature, while at the height of the season a great majority of flowers are ready to release their pollen grains.

The **daily variations** of pollen emission are caused by the current weather: both the opening of the mature anthers and release of the ripe pollen grains (also known as 'pollen presentation') and the entrainment of the pollen into the atmosphere can only take place under certain (plant-specific) meteorological conditions. For example, anthers of ragweed flowers need low relative humidities to open and present their pollen grains. Once anthers are open and the pollen grains presented, the level of the atmospheric turbulence determines the percentage of pollen grains actually lifted up into the air.

Parameterizations describing pollen emission in NWP models differ strongly in their complexity. The most simple approaches use a temporally and spatially uniform emission flux (e.g., Pasken and Pietrowicz 2005). Obviously, such an approach is limited to the use with short-term case studies in a small region where it might be justified to neglect both the seasonal and daily variations of pollen emission. As soon

as the model is meant to be used for numerical pollen forecasts covering the entire pollen season or a greater heterogeneous area, some sort of mathematical description of the state of the pollen season and the short-term influences on pollen emission are essential.

The simplest approach to define the **onset and duration of flowering** is the so-called null model: mean climatological dates (e.g., Sofiev et al. 2006). Maps of these phenological dates are available for entire Europe (Siljamo et al. 2007). However, the year-to-year variability (e.g., due to favorable or unfavorable weather conditions) is not taken into account. A commonly used approach to forecast the start of the pollinating season is the accumulation of heat units. These models are based on the assumption that a plant's development depends on accumulated temperatures (Réaumur 1735). According to this method, flowering starts when the accumulated daily temperatures reach a certain threshold temperature sum. Despite this rather simple basic idea, various parameters need to be determined: e.g., the date when the summing up of temperatures is started, the base temperature above which a daily temperature value is considered, the weighting of the different temperature values, whether chilling is considered or not, etc. The exact realization of the temperature sum model not only depends on the plant species but also on the region and the method to determine these parameters. The large number of publications describing a specific realization of the model in a certain region and for a certain species give evidence of that fact (e.g., Chuine et al. 1998; Duhl et al. 2013; Pauling et al. 2014). Physiology-based models take into account both promoting and inhibiting forces during the previous weeks/months. The best combination and weighting factors of these forces are determined statistically, e.g., using multiple regression (e.g., Galán et al. 1998; Schaber and Badeck 2003). Again, the particular realizations (i.e., the choice of promoting and inhibiting forces and the fitting procedure) differ between plant species and regions. A comparison between a temperature sum model and a regression model to forecast the onset and duration of flowering of ragweed in the area of Lyon can be found in Laaidi et al. (2003). They found the regression model to be more accurate than the temperature sum model. A combination of both methods is described in Makra et al. (2011): they predict the start and end dates of the pollen season with regression analyses using the cumulated daily mean temperature as one of its predictors. Prank et al. (2013) suggest a combination of heat accumulation and photoperiod for the prediction of ragweed flowering. They have observed that a model using temperature sums only works well in northern European regions. In southern European regions, the onset of flowering is rather dependent on the shortening of the photoperiod below a certain daily threshold value. The calculation of the end of the ragweed pollen season also divided into two submodels: in northern Europe, the season is terminated by low temperatures while in southern Europe it ends when the

photoperiod falls below a certain threshold.

To be used in the source term of a NWP model, the mathematical description of the pollen season not only has to calculate the starting and ending dates of flowering but also the **course of the pollen season** between these dates. Simple approaches can be found in Helbig et al. (2004) who assume a parabola-shaped pollen season with a fixed length of 30 days or in Duhl et al. (2013) who define a log-normal pollen season distributed over 14 days. Both methods do not account for year-to-year differences of the length of the pollen season due to favorable or unfavorable meteorological conditions (e.g., precipitation, very hot or very cold seasons). In the literature, only very few attempts can be found to consider variable lengths of the pollen season. One of them is described in Prank et al. (2013) who use a Gaussian function to describe the ragweed pollen season. The length of the season, and thus the width of the curve, is variable and determined by calculating the starting and ending date of the season taking into account temperature and photoperiod (as described above). The same basic form of a Gaussian function is used to describe the pollen season in Marceau et al. (2011). The parameters of the Gaussian function are estimated using the least squares method taking into account daily mean values of temperature and humidity. A very different approach is described in Sofiev et al. (2013b): while the start of the birch pollen season is determined via a temperature sum, the pollinating season ends when the model runs out of pollen grains. The total number of pollen grains available for the entire season is derived semi-manually using observations of the previous year. The up-swing of the pollen season is altered using relaxation functions that allow a small proportion of the pollen grains to be released before the threshold temperature sum defining the beginning of the season is reached. Likewise, the down-swing of the pollen season at the end is altered using a similar relaxation function. Both relaxation functions depend on the temperature sum.

Even though the **daily course of pollen emission** as observed from measurements has been described frequently in literature, only a few publications can be found that deal with models or parameterizations calculating these daily variations (e.g., Martin et al. 2010; Viner et al. 2010). Parameterizations that can be used within a NWP model are even more sparse. The first comprehensive parameterization of tree pollen emission that was used within a NWP model system is described in Helbig et al. (2004). The strength of the pollen emission flux is calculated from a simple seasonal description (see above) and terms that include the annual pollen production, the leaf area index (LAI), the height of the canopy, the friction velocity u_* (describing the shear stress in velocity units), temperature, relative humidity and wind speed. A detailed description of this parameterization can be found in Chapter 2. Being the first in its field, this parameterization has been adapted and modified for other pollen species (e.g., ragweed) and for the use in several other NWP models (e.g., Vogel et al.

2008; Zink et al. 2012; Efstathiou et al. 2011; Zhang et al. 2014). Efstathiou et al. (2011) and Zhang et al. (2014) modify the meteorological influences on pollen emission. Additionally, Zhang et al. (2014) drop the LAI from the formula describing pollen emission and they use the STaMPS model (Duhl et al. 2013) to determine the current state of the pollen season. The emission of maize pollen has been described using a combination of two distributions (Marceau et al. 2011): a log-normal distribution for the first part of the day and a normal distribution for the second part of the day. This accounts for the fact that maize pollen emission can exhibit both unimodal and bimodal daily courses. The model accounts for the influences of relative humidity, temperature and wind speed. The third independent approach to parameterize pollen emission within a NWP model is described in Sofiev et al. (2013b). Taking the parameterization of the pollen season as a basis (see above), the daily variations of pollen emission result from the influences of relative humidity, precipitation and wind speed. Chapter 2 gives a detailed description of this parameterization.

1.3 Generating distribution maps

Since pollen grains can only be emitted where pollinating plants are present, it is obvious that one of the key input fields for numerical pollen simulations is a detailed map of the pollen sources. The different methods to derive such maps make use of various combinations of the following types of data:

- inventory data

- land use/land cover data

- seasonal pollen indices (SPIs)

- daily pollen measurements

Maps based on inventory data

The most obvious way to generate a distribution map is to assemble inventory data. Such an approach makes direct use of the quantitative and spatial information registered in plant/forest inventories. It requires complete, comprehensive and up-to-date inventories. For long-living plants like trees, such inventories exist in many countries. Sofiev et al. (2006) and Skjøth et al. (2008) have assembled European-wide distributions for tree species. Bullock et al. (2012) have collected ragweed inventory data on the European scale. Unfortunately, the limitations of this approach are manifold:

- Forest inventories only cover forested areas disregarding trees that are growing outside of forests, e.g., in cities or alleys (Pauling et al. 2012).

- Inventories for short-living or spreading plants (e.g., annual or bi-annual herbaceous plants) are less accurate than for trees, since inventories are usually not updated at short intervals.

- Inventories differ strongly regarding the degree of detail in the quantitative information: plant abundance is given as exact numbers, as abundance classes or as presence/absence information (Alberternst et al. 2006).

- The spatial resolution of inventories varies largely: information is given as exact locations, with respect to an underlying grid, or only with respect to counties or countries (Bullock et al. 2012).

- Sometimes the original data is not available and inventories are only available as images (Bullock et al. 2012).

- For many species and regions, data is incomplete or missing entirely (Alberternst et al. 2006).

- In many countries, inventories are not centralized and have to be collected from many different sources. This introduces uncertainty with respect to the completeness as well as to the quality and comparability of the data (Alberternst et al. 2006).

Maps based on land use data and seasonal pollen indices

In order to bypass the limitations of inventory data, Skjøth et al. (2010) have developed another approach using a combination of land use data and SPIs on the example of ragweed in the Pannonian Plain. The method has also been applied to France (Thibaudon et al. 2014). In a first step, the classes of the land use data set are sorted into two groups with respect to their suitability as ragweed habitats ('suitable' or 'not suitable'). In a second step, the 'local infection level' at each measurement site of the pollen network is calculated based on the percentage of suitable land use classes and the mean SPI of the site. Additionally, an elevation filter is introduced that suppresses ragweed plants above a certain elevation threshold. Finally, the local infection level is interpolated to the entire area. The main advantage of this approach is the independency from inventory data. Land use data sets are generally available for the entire globe (with varying quality and degree of detail), e.g., the Global Land Cover 2000 data set (GLC2000, European Comission 2003) or the Corine Land Cover 2006 data set (European Environment Agency 2012). The disadvantages of

this approach relate to the underlying assumptions and the availability, completeness and quality of the data:

- The method is limited to regions where the SPI is dominated by local pollen sources. It cannot be used in regions that are mainly influenced by transported pollen grains.

- It is indispensable to have access to measurements of airborne pollen concentrations covering the entire area of interest.

- The land use data set should resolve small habitats that are suitable for the plant in question. For example, ragweed preferably grows in ruderal areas like river banks or edges of roadways, which in many inventories are not resolved.

- The land use data set should be detailed with respect to the land use categories. For example, for ragweed it would be beneficial to differentiate between different crop types.

- Like for inventory data sets, the land use data set should be updated regularly.

- The method assumes that a certain land use class exhibits the same suitability for a specific plant throughout the entire domain. However, the treatment of the soil or actions controlling the spread of the plant might be different in different countries/regions.

Maps based on inventory data, land use data and seasonal pollen indices

Another comprehensive approach has been reported by Pauling et al. (2012). They use a combination of forest inventory data, two land use data sets and SPIs to derive a distribution map of birch trees. In a first step, a birch distribution map is derived in a small region with good data coverage (Switzerland). This is done by assigning typical birch densities to the classes of a highly resolved and detailed regional land use data set: within forested areas these values are taken from a highly resolved forest inventory, outside forested areas the values are assigned according to ground surveys and botanical knowledge. The resulting birch distribution map in Switzerland is then used to calibrate the classes of a coarser and less detailed land use data set covering a larger area (GLC2000). This results in mean birch densities for each land use class of the GLC2000 data set in Switzerland. Regarding these values as typical for the specific class, the birch density is then extrapolated to a larger region where inventory data of such high quality is not available. The resulting distribution map is weighted with interpolated SPIs to respect local differences in the birch densities.

The applicability of this method to other species is limited by the assumptions that have to be made and the availability, completeness and quality of the data sets:

- The accuracy of assigned typical plant densities to the regional land use classes depends highly on the quality of the inventory data.

- In areas where inventory data is not available (here: non-forested areas), a typical plant density has to be assigned to the land use classes of the regional land use data set. Due to lack of data, such an assignment is rather subjective.

- This method assumes that a certain land use class contains the same amount of plants throughout the entire domain. Depending on the class, region and plant species, this assumption can be rather critical.

- The weighting of the distribution map with the mean SPI assumes that the SPI is dominated by local sources. Hence, the method cannot be applied to regions that are mainly influenced by transported pollen grains.

Maps based on ecological modelling and pollen measurements

A very different approach has been described by Bullock et al. (2012) and Prank et al. (2013) to derive a ragweed distribution map covering Europe. They simulate the spatial progression of the plant with the means of an ecological model. Starting in 1960 (when ragweed was still rather rare/sporadic in Europe), the model simulates the on-going spread of ragweed within the regions that are ecologically suitable for a full life cycle of the plant. The model takes into account both biological factors (such as air temperature or photoperiod) and antropogenic factors (e.g., human-related introduction of seeds or plant extinction). The dispersion model SILAM is then used for a tuning procedure: airborne pollen concentrations are simulated using the derived distribution map as an input parameter. The mean deviations between simulated and measured values are then used as a calibration factor for the distribution map. This procedure is repeated several times until the simulated values correspond well enough to the measured pollen concentrations. The uncertainties of this approach relate mainly to the many underlying assumptions (and thus the goodness of the model) and the quality, completeness and availability of data that is used to build and calibrate the model:

- Unsystematic human influences (e.g., eradication campaigns or seed introduction) can only be taken into account stochastically. The derived map can therefore only represent one of the possible current states of the spread of the plant.

- The different parameters of the ecological model are selected by comparing the computed distribution map to plant inventories. However, for ragweed the spatial coverage of inventory data is incomplete (e.g., high quality data for northern Italy is missing even though this region is one of the major sources of ragweed pollen in Euruope (Bullock et al. 2012)).

- The calibration using measured pollen concentrations attributes all systematic model errors to the emission term (Prank et al. 2013). Even more: the errors are attributed to only one factor of the emission term: the distribution map. In view of the uncertainties regarding the parameterization of pollen emission, this assumption seems rather rough.

- Additionally, such a calibration relates both measured and simulated pollen concentrations to local emission neglecting that both are influenced by transport processes. This approach is thus problematic in regions that have only small local populations but are in the area of influence of a remote pollen source. An example of such a situation is the northern part of Switzerland with respect to ragweed: being fairly free from local sources, the measured pollen concentrations are assumed to originate in the highly infested area of Rhône-Alpes in France (Clot et al. 2002).

- The efficiency of such a calibration depends on the number of available pollen measurements (Prank et al. 2013).

Suitability of the different approaches

All of these methods have their drawbacks, either with respect to low data coverage and low quality of the data or with respect to the underlying assumptions. Most of these approaches have been developed based on the example of one species only. Therefore, their suitability for another plant species needs to be considered carefully. Especially when adapting the method for a different kind of plant (e.g., when a method that was developed for trees should be used for a herbaceous plant), the assumptions of the different methods need to be carefully scrutinized. Given so many uncertainties, it might be beneficial to use an ensemble approach to assess the uncertainty of the different methods.

1.4   Evaluation of simulated pollen concentrations using measured values

When setting up a new model, its results have to be evaluated. This can be done, e.g., by comparing simulated and measured values of the parameter in question. Regarding pollen concentrations, different parameters and processes influence the resulting concentrations, both in the model and the observations:

- the distribution of pollen sources,

- the phenological state of the plants,

- the emission flux of pollen grains,

- the transport in and removal processes from the atmosphere.

Theoretically, each of these influencing factors should be evaluated separately. However, due to lack of data this is not possible. Inventory data of the plant distribution is usually neither complete nor detailed nor up-to-date. The phenological network does not record the course of the pollen season. Measurements of the emission fluxes are rare and usually do not coincide with measurements of meteorological parameters. Tracer experiments that study the transport in and removal of pollen from the atmosphere do not exist.

The only data that is available for evaluation are operationally recorded pollen concentrations. Obviously, this data includes both locally emitted pollen and transported pollen. Hence, the evaluation using pollen concentrations always is an evaluation of the overall performance of the model, not of the individual parameters and processes that affect both the simulated and the measured pollen concentrations. Depending on the specific problem, different subsets of the measured and/or simulated pollen concentrations can be identified that enhance the significance of the statistical comparison. For example, if local pollen concentrations are of interest, only days with low horizontal wind speeds should be taken into account to reduce the influence of transported pollen. In contrast, if transported pollen concentrations are of interest, days with a predominant flow from the source region to the receptor region should be identified. In some cases, it can also be beneficial to only use measured pollen concentrations above a certain threshold. An example for this approach is the calibration of the emission flux under ideal conditions: naturally, 'ideal conditions' should lead to a strong emission flux and thus high pollen concentrations. Therefore, days with low pollen concentrations should not be used for such a calibration.

An additional obstacle with this kind of data is the coarse resolution: (1) there are only a few observational sites for pollen compared to the observational sites for

meteorological parameters (e.g., in Switzerland, pollen concentrations are recorded at 14 observational sites), (2) most of the data is available in a daily resolution only (in some countries, 'highly resolved' data is available, giving a 2-hourly resolution). Furthermore, it has to be noted that the measurements are 'point values' (representative of a certain area of influence) while the simulated concentrations represent an areal mean for the grid cell.

To reduce the randomness of simulated and measured values, it can be beneficial to create clusters of observational sites that represent a certain region. In this thesis, this has been done several times to produce subsets that represent, e.g., the main source region, the main receptor region, or regions that are only marginally affected. The low temporal resolution of the measurements poses a problem for the evaluation of processes that take place in a timeframe of seconds, minutes or a few hours. An example for such a process is the influence of different meteorological parameters on the current emission flux. It is obvious that daily resolved pollen concentrations cannot be used to evaluate these processes individually. In this thesis, the parameterization of emission is evaluated as a whole: the performance of the entire model is evaluated using two different emission parameterization while all other parameters and processes are kept identical. While it is not possible to evaluate the individual steps within the parameterization of emission, they should at least be checked to be biologically and physically sound.

1.5 Aims and structure of this thesis

This thesis consists of three publications that take on two of the main issues regarding numerical pollen forecasts: (1) the mathematical description of pollen emission, and (2) the spatial distribution of pollinating plants. Taking the two topics together, this thesis answers the following questions in the context of numerical modeling:

- When are pollen grains emitted?

- Where are pollen grains emitted?

- How many pollen grains are emitted?

At the beginning of my doctorate, only one sophisticated parameterization of pollen emission had already been published by Helbig et al. (2004). However, this parameterization displays several drawbacks that needed to be overcome. Therefore, a new parameterization was developed. **Chapter 2** describes the underlying ideas of the parameterization, its mathematical realization and implementation into a NWP model. Birch pollen concentrations are simulated using both the new parameterization and the existing parameterization of Helbig et al. (2004). The performance of the

two model versions is compared statistically.

Secondly, the suitability of plant inventories to be used for the construction of distribution maps is investigated. **Chapter 3** describes exemplary simulations of ragweed pollen concentrations using a set of nine different distribution maps that are based on inventory data. The different maps show a varying degree of detail in two aspects: (1) the quantitative information of the inventory data, and (2) the spatial resolution of the distribution map. Nine maps are used to simulate the ragweed pollen season of 2012. Particularly, it is investigated how a large but distant pollen source influences the pollen concentrations in an area that is practically free of local pollen sources. Using French ragweed populations as the large pollen source, their influence on Swiss pollen concentrations is investigated using statistical analyses.

Chapter 4 investigates the suitability of different methods to produce such distribution maps. Six different ragweed distribution maps are assembled representing three methodologies of generating distribution maps: (1) maps based on inventory data, (2) maps that combine land use data and annual pollen counts, and (3) potential maps derived from spatial distribution modeling. These maps are used to simulate the ragweed pollen season of 2012 in France. The simulated pollen concentrations are compared to measured concentrations in France using different statistical scores. A ranking of the different maps is derived based on these scores. In the end, a specific procedure to derive a distribution map for the use in a NWP model is recommended.

Chapter 5 summarizes the main results of the thesis and presents some ideas for future research. Finally, this chapter includes a guideline for the setup up of pollen forecasts and gives recommendations for the generation of distribution maps.

Chapter 2

EMPOL 1.0: A new parameterization of pollen emission in numerical weather prediction models

K. **Zink**[1], A. **Pauling**[1], M. W. **Rotach**[2], H. **Vogel**[3], P. **Kaufmann**[1], B. **Clot**[1]

[1] *Federal Office of Meteorology and Climatology MeteoSwiss, Switzerland*

[2] *Institute for Meteorology and Geophysics, University of Innsbruck, Austria*

[3] *Institute for Meteorology and Climate Research, Karlsruhe Institute of Technology, Germany*

Abstract

Simulating pollen concentrations with numerical weather prediction (NWP) systems requires a parameterization for pollen emission. We have developed a parameterization that is adaptable for different plant species. Both biological and physical processes of pollen emission are taken into account by parameterizing emission as a two-step process: (1) the release of the pollen from the flowers, and (2) their entrainment into the atmosphere. Key factors influencing emission are: temperature, relative humidity, the turbulent kinetic energy and precipitation.

We have simulated the birch pollen season of 2012 using the NWP system COSMO-ART, both with a parameterization already present in the model and our new parameterization EMPOL. The statistical results show that the performance of the model can be enhanced using EMPOL.

2.1   Introduction

In industrialized countries, a relatively high proportion of the population suffer from pollen allergies. Different allergenic plant species shed their pollen at different times of the year leading to several pollen seasons (e.g., birch pollen season, grass pollen season). In Central Europe, the most important periods for patients are the tree pollen season in spring, the grass pollen season in late spring and early summer and the ragweed pollen season in late summer and autumn (only in regions where this invasive plant is present). Even though medication is possible, the best way to reduce allergic symptoms remains complete avoidance of the allergens (van Moerbeke 1997). Therefore, it is of great importance to forecast the distribution of airborne pollen a few days in advance. Currently, pollen forecasts are mainly based on pollen monitoring, weather forecasts, climatological information about the pollen seasons and the experience of the forecaster. The available technology (Hirst type traps (Hirst 1952)) for pollen monitoring demands a lot of manpower since the pollen grains have to be counted manually. Therefore, the density of the pollen sites is low compared to that of meteorological sites. Thus, the spatial resolution of pollen forecasts is very low (essentially, forecasts are only available at the observational sites themselves). Recently, pollen dispersion has been integrated into numerical weather prediction (NWP) models. The knowledge of the simulated spatial and temporal evolution of pollen concentrations enables the forecaster to make nationwide predictions instead of forecasts for the pollen sites only. The prerequisite for reliable numerical simulations of pollen concentrations are (i) an up-to-date distribution map of the plant that indicates the pollen sources, (ii) a NWP system that can deal with particles (including transport, deposition, washout of the particles etc.), and (iii) a parameterization of

the emission process.

Assuming that the first two prerequisites – the distribution map of the plant and the NWP system including particle dispersion – are available, this work is focused on the emission of pollen grains which is a combination of physical and biological processes that are characteristic for each plant species. Thus, the emission parameterization has to address two questions: (i) When does emission take place? (ii) How many pollen grains are emitted? To answer these questions, we have to look closer at the biological and physical processes leading to pollen ripening and release. Two time scales can be distinguished that require the use of two sub-models within the emission parameterization:

1. The seasonal cycle of pollen emission depends on the number of mature flowers or inflorescences, hence the development of the plants. It is driven by the weather conditions during the preceding weeks or months and usually is described via phenological models (e.g. Sarvas 1974; García-Mozo et al. 2009).

2. The diurnal cycle of pollen emission is driven by the current meteorological conditions that lead to a rupture of the anthers (thus, the release of pollen grains from the flowers) and to the entrainment of the pollen grains into the atmosphere. This process happens in a time frame of seconds to hours.

Although the processes leading to pollen emission have been described in the literature, the information that can be found is mainly of qualitative nature (e.g. Bianchi et al. 1959). Additionally, both the development of the plants and the release of the pollen are processes that are characteristic for each plant species. Hence, an emission parameterization that is supposed to work for different plant species has to be very flexible regarding these biological and physical processes.

In Section 2.2, we briefly describe the meteorological model that is used in our study. A comparison between different pollen emission parameterizations is given in Section 2.3. In Section 2.4, a new parameterization for pollen emission is developed, followed by a description of a basic tuning. The application of this parameterization and a comparison of the results to an existing parameterization can be found in Sections 2.5 and 2.6. Finally, Section 2.7 contains the summary and conclusions.

Throughout the publication, we have used the following terms to describe the different processes and parameters in the context of pollen emission:

- **anthesis:** opening of the anthers.

- **pollen release:** release of the pollen from the anthers, either into a reservoir or into the atmosphere directly.

- **pollen presentation:** making the pollen grains available for entrainment into the atmosphere. Usually, this is the result of the combined processes of anthesis and pollen release.

- **entrainment:** uplifting of the pollen from the reservoir or from the anthers into the atmosphere.

- **pollen emission:** refers to the combined processes of pollen release and entrainment into the atmosphere. This term is used when the different steps during the emission process are not distinguished. This formulation is necessary since many emission parameterizations treat pollen release and entrainment as a single process.

- **pollen production:** amount of pollen that is produced per square meter and per year.

- **pollen concentration:** concentration of airborne pollen, given in number of pollen grains per cubic meter of air.

2.2   The NWP model system COSMO-ART

COSMO (**Co**nsortium for **S**mall-scale **Mo**delling) is a non-hydrostatic regional NWP model that is used for operational weather forecasts in various European countries (Steppeler et al. 2002). Vogel et al. (2009) have developed an extension ART (**A**erosols and **R**eactive **T**race Gases) to COSMO in order to study the interaction between aerosols and the atmosphere. Information about the code availability can be found in the supplementary materials.

Physical processes that are incorporated into COSMO-ART include transport by the mean wind, turbulent diffusion, dry and wet deposition, coagulation, condensation, wash-out and sedimentation of the aerosols and reactive trace gases. ART includes, amongst others, a module to simulate the emission and dispersion of pollen grains (Vogel et al. 2008; Zink et al. 2012). The default parameterization of pollen emission follows the suggestions of Helbig et al. (2004) and Vogel et al. (2008).

At MeteoSwiss, COSMO-ART has been used as an operational tool for birch pollen forecasting since 2011, using a modified version of the Helbig et al. (2004) emission parameterization. The modification includes the influence of temperature, humidity and wind speed and the description of the pollen season and is designed to better model the physiological processes in the plants. Since the quantitative relationships between the meteorological parameters and pollen emission are largely unknown, the implementation of the qualitative knowledge about plant physiology is somewhat subjective. The error between model and observations was evaluated as

a function of temperature, relative humidity and wind speed. Using these results, the meteorological functions in the emission parameterization of Helbig et al. (2004) were adapted. This was done based on observational data in Switzerland.

2.3 Available emission parameterizations

The approaches to parameterize pollen emission that can be found in the literature differ greatly in complexity. Very simple solutions use spatially and temporally uniform emission fluxes (e.g. Pasken and Pietrowicz 2005). More sophisticated versions include current meteorological conditions and/or a curve representing the typical pollinating season (e.g. Helbig et al. 2004; Schueler and Schlünzen 2006; Marceau et al. 2011; Sofiev et al. 2013b). Additionally to the current meteorological conditions, the model of Martin et al. (2010) also includes previous values of relative humidity.

In this section, we describe in some detail the differences and analogies of three different emission parameterizations. These are:

- The parameterization of Helbig et al. (2004), in the following referred to as 'H$_{orig}$'. It was used to simulate both birch (Vogel et al. 2008) and ragweed (Zink et al. 2012) pollen concentrations.

- The parameterization that has been used for operational numerical birch pollen forecasts at MeteoSwiss, an optimized formulation of H$_{orig}$. In the following referred to as 'H$_{opt}$' (compare Section 2.2).

- The parameterization of Sofiev et al. (2013b). In the following referred to as 'S13'. It has been implemented into the dispersion model system SILAM and was applied for birch pollen emission.

These are the only comprehensive parameterizations that are incorporated into NWP systems for the application over wider regions that we are aware of. The comparison is divided into three parts reflecting the nature of the parameterizations: the first part describes the seasonal cycle, the second part the daily cycle of pollen emission. Part three explains additional features of the parameterizations. A table summarizing the differences between the parameterizations can be found in the supplementary materials.

2.3.1 Description of the pollen season

The amount of pollen that is ripe and available for emission depends greatly upon the state of the pollen season. At the beginning and the end of the season only a few

plants flower, hence, the amount of available pollen grains is small, regardless of the meteorological conditions. It is therefore essential to introduce a mathematical model that describes the course of the pollen season on a daily basis. H_{orig} assumes the birch pollen season to last for 30 days and to have a fixed shape of a parabola. In H_{opt}, a more sophisticated description of the pollen season is used. Following measured pollen data in Switzerland, the shape of the pollen curve is chosen to be positively skewed. A similarly skewed shape of the pollen curve has been reported for Central Europe by Grewling et al. (2012). Additionally, the length of the season is variable depending on the temperature during the pollen season. This takes into account that a warm spring season results in a short and intense birch pollen season whereas a cool spring tends to lengthen the birch pollen season because not all birch trees flower at the same time. S13 introduces an internal model that reflects the seasonal pollen curve. It uses temperature sums to predict the start and course of the pollen season. The season ends when a certain amount of pollen has been emitted. The up- and downswing of the pollen curve is parameterized using relaxation functions describing the probability for a single tree to bloom at a certain day.

2.3.2   Meteorological influences

Naturally, emission has to be linked to a velocity scale since the pollen grains have to be lifted into the air by wind currents. In H_{orig} and H_{opt}, the friction velocity u_* is taken as the parameter influencing the amount of emitted pollen. A threshold friction velocity u_{*t} has to be reached in order to allow emission. The value of u_{*t} is derived using a parameterization for dust entrainment and a meteorological correction factor (see below). Emission by free convection is not taken into account. S13 uses both the 10 m wind speed and the convective velocity scale w_* to take into account both ways of pollen entrainment into the atmosphere.

Theoretically, if unlimited amounts of pollen were available, higher wind speeds would yield stronger entrainment, hence more airborne pollen. In reality, this is limited by the fact that at a certain point, the flowers will run out of pollen grains. This is not considered in H_{orig}. H_{opt} and S13 take this into account by introducing a threshold wind speed or a function converging to a maximal value that stops further increase of emission.

Short-term pollen emission is driven by current meteorological conditions. All three parameterizations consider these effects using correction terms. H_{orig} and H_{opt} use meteorological correction terms for temperature, relative humidity and wind speed that influence the value of the threshold friction velocity u_{*t}. However, the individual terms are different for both parameterizations (cut-offs at different thresholds etc.). Both, H_{orig} and H_{opt}, consider precipitation through wash-out. S13 considers relative

humidity and precipitation as hindrances for emission if their values are in a certain range. In S13, temperature plays an important role through the seasonal description, short-term effects on emission are not taken into account.

2.3.3   Other features

H_{orig} and H_{opt} use plant-dependent parameters such as the leaf area index (LAI) and the height of the plants that influence the amount of emitted pollen. Their use in the model is reciprocal, leading to higher emissions for small plants and plants with less leaves. The idea behind this is that leaves keep the released pollen grains within the canopy. These parameters are left out in S13.

Resuspension is considered in H_{orig} only.

H_{orig} and S13 use a total amount of pollen that can be produced per season. In S13, this number defines the end of the pollen season. In H_{orig} it can shorten the pollen season if the model runs out of pollen before the prescribed end of the pollen season after 30 days. Since this feature is unwanted, the total amount of pollen has been removed in H_{opt}. The two main problems associated with the total amount of pollen are: (i) the actual number is basically unknown, and (ii) for some plants (such as birch trees) this number varies considerably between years (years with high total amounts of pollen are referred to as 'mast years').

Some plants (such as birch trees) produce less pollen when they grow at higher altitudes (e.g. Sveinbjörnsson et al. 1996; Gehrig and Peeters 2000). To respect this fact in the model, a reducing factor $f_{Q,alt}$ is introduced as a function of altitude in H_{opt}. This factor is plant-specific and must take into account the influence of the changing climatic conditions with altitude on the plant.

2.4   Development of an emission parameterization for pollen grains

The emission process varies from species to species. For example, some grasses need high relative humidities for the opening of their anthers since they have to swell in order to crack. On the contrary, low relative humidities favor the release of birch pollen since its anthers open when they are dry (e.g. Fuckerieder 1976; Puls 1985; Keijzer et al. 1996; Matsui et al. 1999; Dahl et al. 2013). Since all of the emission parameterizations mentioned in Section 2.3 have been developed for tree pollen, the question remains whether they are suitable for herbaceous plants like grasses or ragweed. Since both species are allergenic and responsible for important pollen seasons, it is desirable to have an emission parameterization that is appropriate for these plants as well. Since the model system COSMO-ART is operationally used at the

Federal Office of Meteorology and Climatology in Switzerland (MeteoSwiss), we have looked closer at the two emission parameterizations associated with COSMO-ART (H_{orig} and H_{opt}). The parameterizations show the following disadvantages.

Two plant-dependent parameters in the emission formula are inversely proportional to the emission flux: the leaf area index and the height of the plant. For trees, the variability of these parameters lies in a range where their influence is relatively low. For plants with mean heights of 1 m or less and low leaf area indices, however, these plant-dependent parameters become prominent. Moreover, their use only makes sense if their specific values vary over the model domain or time. Otherwise, they can simply be incorporated into a tuning factor. An important problem in this respect is that the true values of both parameters cannot be known in realtime for the entire model domain. Therefore, they are not suited to be incorporated into the parameterization. Additionally, the sensitivity of the simulated emission flux on the height of the plant shows the undesirable feature that small plants emit more pollen than big plants.

Meteorological influences on the emission flux are incorporated into the parameterization via a threshold friction velocity (see Section 2.3.2). Only if the friction velocity reaches this threshold, emission is allowed in the model. The threshold value is not constant but includes functions of temperature, relative humidity and wind speed. Due to the nature of the parameterization, these functions cannot be determined empirically. In our opinion, one of the main drawbacks of this emission parameterization is the mixing of biological and meteorological factors that influence different aspects of the emission process. This leads to complicated formulations that cannot be easily validated via straight-forward experiments.

Consequently, we have developed a new emission parameterization EMPOL which is based on the biological and physical processes leading to pollen emission. It can easily be adapted to different plant species by adjusting just a few key factors. Plant-dependent values that are variable over the model domain, such as the actual height of plants, are omitted. The meteorological influences are designed in a way that allows simple experimental determination of the corresponding functions.

The description of the pollen season is not part of EMPOL but is taken from the seasonal model developed for H_{opt} (compare Section 2.3.1). It is read into the model as an input parameter.

2.4.1   Basic concepts

Given that the pollen season has started (in other words: plants are ready to release pollen), the emission of pollen can be seen as a two-step process: first, changes in the meteorological conditions lead to a rupture of the pollen sacs (anthesis). Pollen grains are released from the flowers. Second, the pollen grains that are now exposed

to air motions, can be entrained into the atmosphere. We have adopted this view by dividing our emission parameterization into two parts:

1. Depending on biological and meteorological conditions, a certain number of pollen grains are released from the flowers and fill up a pollen reservoir. Botanically, this process is called pollen presentation.

2. If meteorological conditions are favorable, pollen in the reservoir are entrained into the atmosphere.

Figuratively, the pollen reservoir can be seen as a surface where the pollen grains rest after being released from the anthers, e.g. a leaf. Such a process has been described by Bianchi et al. (1959) for ragweed: most of the pollen first fall onto the foliage below the flowers before being entrained into the atmosphere. However, this descriptive view should not be exclusive: if the conditions are favorable, pollen grains can be released from the flowers and entrained into the atmosphere directly. In that case, the reservoir should only be seen as a way to describe the fact that pollen grains have to be made available before they can be carried into the atmosphere.

Conceptually, the parameterization can be described as follows: a constant factor $Q_{\text{pollen,day}}$ gives the maximal daily amount of pollen that could be released at the height of the pollen season on one square meter if the conditions for pollen release and entrainment were perfect. All other factors take values in the range between 0 and 1 and describe resistances to the pollen release. These factors include, e.g., unfavorable meteorological conditions, but also a low plant coverage, or an early or late date in the pollen season.

The reservoir R_{pollen} is made up of the pollen that are released from the flowers at that very time step (ΔR_{pollen}) and the pollen that were left in the reservoir after the previous time step ($R_{\text{pollen,old}}$). We assume that the pollen in the reservoir can be lost due to random processes (such as animals brushing against the plant and causing pollen to fall to the ground). This loss is described in the factor Ψ_{random}. Additionally, rain washes out a specific portion of the reservoir which is described via the function Ψ_{precip}. Combining the factors described above, the content of the reservoir is given by

$$R_{\text{pollen}} = \left(\Psi_{\text{random}} \cdot R_{\text{pollen,old}} + \Delta R_{\text{pollen}} \right) \cdot \Psi_{\text{precip}}. \tag{2.1}$$

The amount of pollen that the flowers release into the reservoir at each time step is given by

$$\Delta R_{\text{pollen}} = \Phi_{\text{plant}} \cdot \Phi_{\text{met}} \cdot \Phi_{\text{biol}}. \tag{2.2}$$

The factor Φ_{plant} combines the plant-specific variables that define the amount of pollen that could be released per time step under perfect meteorological conditions

at a given grid point. It consists of the figure $Q_{\text{pollen},\Delta\text{t}}$ (calculated from $Q_{\text{pollen,day}}$) describing the maximum amount of pollen that could be released per time step and per square meter if the grid box was totally covered with the specific plant in the perfect growing state. This maximum number is reduced by factors describing the percentage of ground actually covered with the specific plant ($f_{\text{Q,cov}}[0,1]$), the course of the pollen season using a mathematical description $f_{\text{Q,seas}}[0,1]$ (see Section 2.3.1), and the influence of the altitude on the productivity of the plants $f_{\text{Q,alt}}[0,1]$ (see Section 2.3.3):

$$\Phi_{\text{plant}} = Q_{\text{pollen},\Delta\text{t}} \cdot f_{\text{Q,cov}} \cdot f_{\text{Q,seas}} \cdot f_{\text{Q,alt}} \tag{2.3}$$

The meteorological influences on pollen release are described via mathematical functions:

$$\Phi_{\text{met}} = f_{\text{R,T}} \cdot f_{\text{R,RH}}. \tag{2.4}$$

They describe the probability that anthesis will happen under the current meteorological conditions. Up to now, only temperature and relative humidity are considered. Since the processes leading to pollen release are slightly different between plant species, these functions are plant-dependent and need to be adapted for the different species.

Additionally, a switch Φ_{biol} is introduced that turns off pollen release as soon as a certain daily amount of released pollen is reached. Under optimal conditions, it can happen that all ripe pollen grains are released before the end of the day. Once the flowers have run out of ripe pollen grains, pollen release will stop despite the continuously good conditions.

The second part of the emission parameterization describes the entrainment of the pollen from the reservoir into the atmosphere. This process is mainly driven by meteorological conditions, namely moistureand turbulence. The pollen flux is given by

$$F_{\text{E,pollen}} = \frac{R_{\text{pollen}}}{\Delta t} \cdot f_{\text{E,TKE}} \cdot f_{\text{E,RH}}. \tag{2.5}$$

With Δt being the time step of the simulation. It is assumed that the pollen are dispersed instantaneously and homogeneously within the grid box. The pollen concentration mainly depends on the amount of turbulence that lifts the pollen into the air. This is considered through the function $f_{\text{E,TKE}}[0,1]$. In moist conditions, entrainment is reduced as pollen grains tend to stick to the surface. The strength of this constraint – $f_{\text{E,RH}}[0,1]$ – is given as a function of the relative humidity. If pollen grains are released from the anthers in an explosive manner (compare Rohwer (1993)) and entrained into the atmosphere regardless of the turbulent kinetic energy and relative humidity, these two functions $f_{\text{E,TKE}}$ and $f_{\text{E,RH}}$ can be set to a fixed value of one. In that case, the pollen reservoir will not be filled, but all pollen released from the anthers will be entrained into the atmosphere directly.

A flowchart in the supplementary materials shows the different steps of the parameterization and the influences for each of these steps. If EMPOL is used for other pollen species, the plant-specific values in the following parameters need to be adapted: $Q_{\text{pollen,day}}$, $Q_{\text{pollen},\Delta t}$, $f_{\text{R,T}}$, $f_{\text{R,RH}}$, $f_{\text{E,TKE}}$, $f_{\text{E,RH}}$, Ψ_{random}, and Ψ_{precip}. Additionally, the following input fields/values need to be provided: $f_{\text{Q,cov}}$, $f_{\text{Q,seas}}$, $f_{\text{Q,alt}}$, the pollen diameter, and the pollen density.

2.4.2 Tuning of the emission parameterization

One of the ideas behind EMPOL is the possibility to deduce the main parameters via dedicated experiments (e.g. Michel et al. 2012). In a laboratory, it should be possible to measure the functions relating the amount of released/entrained pollen and specific environmental conditions (e.g. temperature) while keeping the remaining parameters constant. For lack of such experimental data, we had to formulate the missing functions in the parameterization on the basis of measured pollen concentrations. EMPOL contains several parameters that have to be tuned: $Q_{\text{pollen,day}}$, $Q_{\text{pollen},\Delta t}$, $f_{\text{R,T}}$, $f_{\text{R,RH}}$, $f_{\text{E,TKE}}$, $f_{\text{E,RH}}$, Ψ_{random} and Ψ_{precip}. We used bihourly birch pollen measurements in Switzerland and simulations with COSMO-ART to derive a first guess for each of these parameters. Taking this version of the parameterization, we simulated two months during the birch pollen season (April 2010 and April 2011) to improve this first guess. It should be noted that – using birch pollen measurements as a basis – the formulations and values described here are valid only for birch. It should also be kept in mind that using the full modeling system and measured pollen concentrations at this stage introduces some strong assumptions. The most important of these is that any atmospheric transport and dispersion processes are neglected, i.e. larger pollen concentrations are solely due to larger emissions. The present exercise, therefore, is not more than a 'second guess' and still leaves room for improvement based on a true parameter tuning exercise in which the error is minimized by varying all the parameters which will be performed as soon as corresponding data will be available. The present tuning only attempts to render the resulting emissions in a broadly reasonable range, while attempting to describe the physical and biological overall performance.

The parameter $Q_{\text{pollen,day}}$ reflects the overall level of the pollen flux. It was tuned by calculating the overall bias between measurements and model. Based on these values, $Q_{\text{pollen,day}}$ was set to 2.133×10^9 pollen per square meter and per day. The amount of pollen that can be released per time step is calculated from $Q_{\text{pollen,day}}$ considering the following requirements/assumptions:

- Under optimal conditions for pollen release, the flowers can run out of pollen grains before the end of the day.
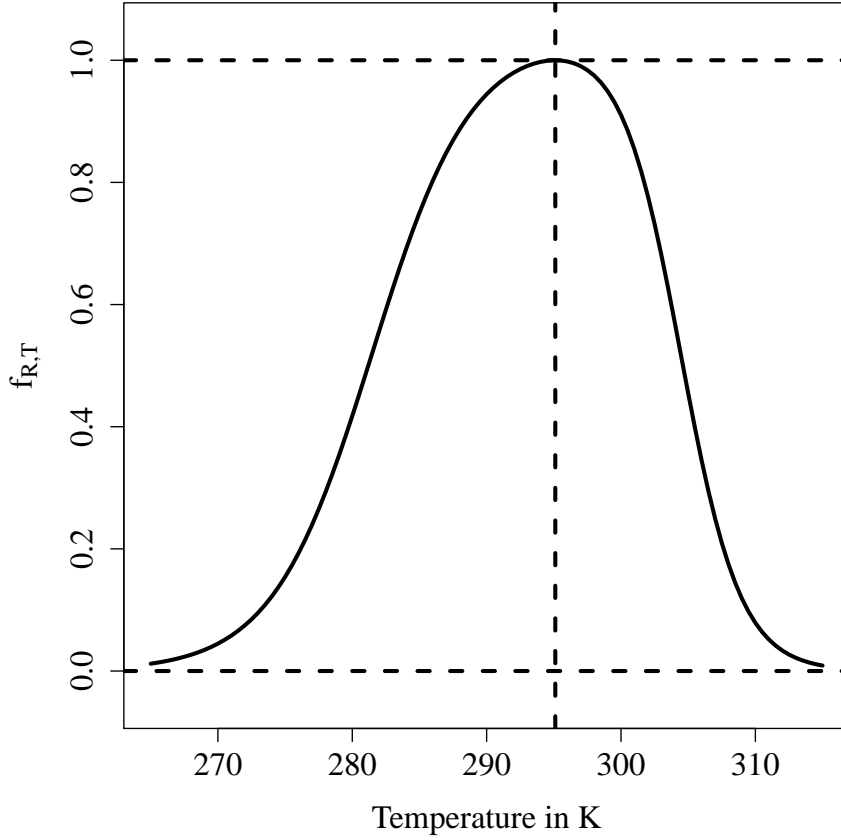
Figure 2.1: Function describing the influence of temperature on the release of birch pollen.

- The daily cycle of pollen release is not prescribed in the model. The amount of released pollen does not depend on the time of the day but results from the functions $f_{R,T}$ and $f_{R,RH}$.

In our implementation, we assume that the flowers will run out of pollen grains after 16 hours of constant pollen release. $Q_{pollen,\Delta t}$ can then be calculated by dividing $Q_{pollen,day}$ by the number of time steps during a 16 hour-period:

$$Q_{pollen,\Delta t} = \frac{Q_{pollen,day} \cdot \Delta t}{16 \cdot 3600}. \tag{2.6}$$

The functions $f_{R,T}$, $f_{R,RH}$ and $f_{E,TKE}$ were tuned by calculating the absolute error between model and measurements for each measuring station. These errors were plotted against the different meteorological variables. These plots were then used to adjust the functions describing the meteorological influences on pollen release/entrainment. The resulting functions are (the corresponding curves can be found in Figs. 2.1, 2.2 and 2.3):

$$f_{R,T} = \frac{1.04}{\left(1 + e^{-0.27T+76}\right) \cdot \left(1 + e^{0.45T-137}\right)} \tag{2.7}$$
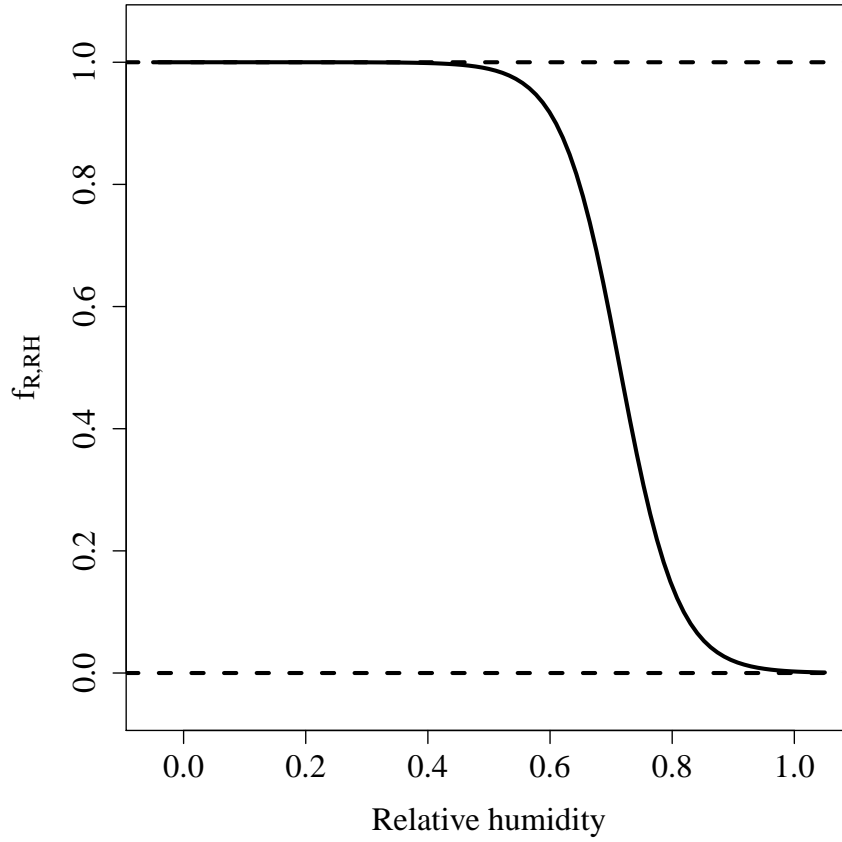
Figure 2.2: Function describing the influence of relative humidity on the release of birch pollen.

$$f_{\text{R,RH}} = \frac{1}{1 + e^{21rh - 15}} \tag{2.8}$$

$$f_{\text{E,TKE}} = \frac{1}{1 + e^{-2.1TKE + 4}} - 0.017. \tag{2.9}$$

In these functions, T denotes temperature, rh the relative humidity and TKE the turbulent kinetic energy on the lowest model level.

The number of pollen that are lost from the reservoir due to random processes is derived by using the concept of a half-life. Under the premise that only the random losses are effective, we assume a continuous removal from the reservoir such that after 12 hours, half of the pollen present in the reservoir is lost. This assumption is used to calculate the percentage of the pollen in the reservoir that are lost per time step due to random processes:

$$\Psi_{\text{random}} = \exp\left\{ \frac{\ln 0.5 \cdot \Delta t}{12 \cdot 3600} \right\}, \tag{2.10}$$
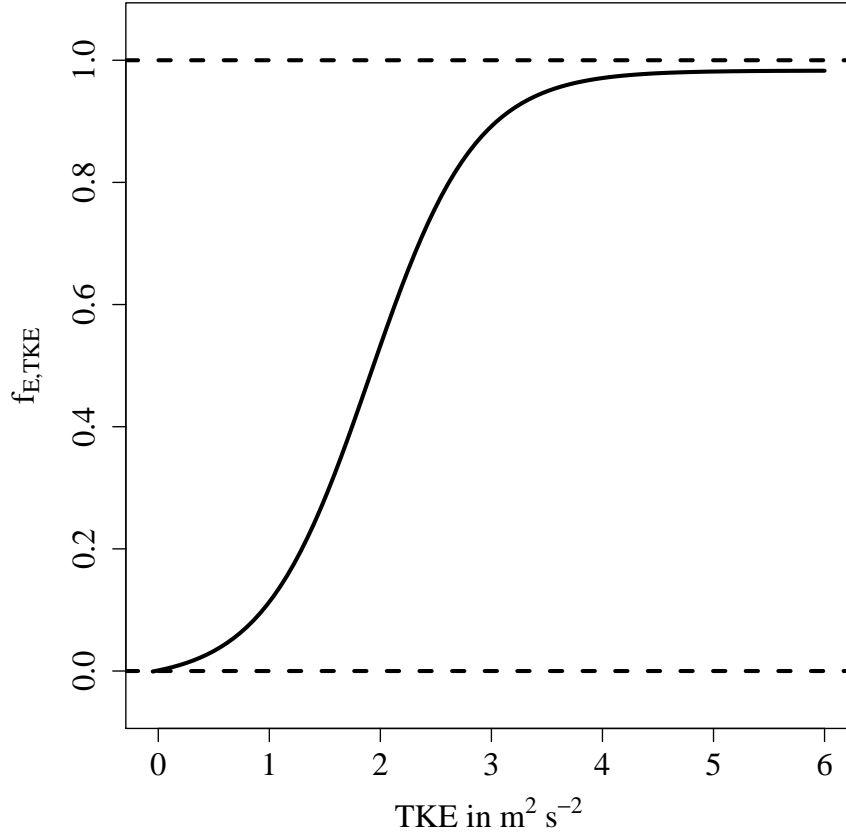
Figure 2.3: Function describing the influence of turbulence on the entrainment of pollen grains into the atmosphere.

where Δt is the time step of the model given in seconds.

The wash-out of the reservoir is given by:

$$\Psi_{\text{precip}} = -2000\,p + 1 \qquad\qquad 0 < p < 0.0005 \qquad\qquad (2.11\text{a})$$

$$\Psi_{\text{precip}} = 0 \qquad\qquad\qquad p \geq 0.0005. \qquad\qquad (2.11\text{b})$$

Wherein p denotes the sum of convective and grid-scale precipitation in the model. It is given in $\text{kg}\,\text{m}^{-2}\,\text{s}^{-1}$.

The tendency of the pollen to stick to the surface under moist conditions is given as a function of the relative humidity rh:

$$f_{\text{E,RH}} = 1 \qquad\qquad\qquad rh \leq 90\,\% \qquad\qquad (2.12\text{a})$$

$$f_{\text{E,RH}} = 0.5 \qquad\qquad 90\,\% < rh \leq 95\,\% \qquad\qquad (2.12\text{b})$$

$$f_{\text{E,RH}} = 0 \qquad\qquad 95\,\% < rh \leq 100\,\%. \qquad\qquad (2.12\text{c})$$

2.5 Testing the new parameterization

After debiasing the model using Swiss pollen data from 2010 and 2011, we have simulated the birch pollen season of 2012 using two model configurations. Both use an identical setup with the emission parameterization being the only difference. First, simulations were carried out using the parameterization H_{opt} (see Section 2.3). Secondly, we have adapted COSMO-ART to run with our newly developed emission parameterization EMPOL.

2.5.1 Setup of the simulations

We have used the COSMO-ART version 2.0 in combination with the COSMO version 4.19. The operational COSMO-ART domain of MeteoSwiss covers a large part of central and western Europe, reaching from Portugal in the West to the Balkans in the East, and from southern Italy in the South to the southern parts of Scandinavia in the North. The model is run at a spatial resolution of $0.06°$ ($\approx 6.6\,\mathrm{km}$) with 60 vertical levels and a time step of $60\,\mathrm{s}$. Our simulations start on 21 March 2012 and end on 16 May 2012, covering the entire birch pollen season in central Europe. Every $72\,\mathrm{h}$, a new run is initialized using updated meteorological boundary and initial conditions from the operational NWP modeling system.

As the map of possible pollen sources, we use the birch distribution dataset that was produced by Pauling et al. (2012). They present a method to create plant distribution datasets using birch as an example. This method combines forest inventory and land use data from Switzerland to derive a distribution map. The transfer to a larger domain (southern and central Europe) is achieved by using the Global Land Cover 2000 dataset in combination with pollen data.

The mathematical description of the pollen season $f_{Q,seas}$ is taken from the phenological model developed for the operational numerical pollen forecasts at MeteoSwiss (compare Section 2.3.1). It is used as an input parameter for the emission parameterization in both model configurations.

2.5.2 Comparison to pollen measurements

The simulated pollen concentrations (mean over 9 grid points) are compared to daily measurements at 34 observational sites throughout Europe for the entire pollen season of 2012. A list of the sites, including their geographical location, can be found in Table 2.1. Pollen grains were sampled using Hirst type traps (Hirst 1952).

The level of the simulated pollen concentrations at the start and end of the pollen season strongly depends on the seasonal description ($f_{Q,seas}$, Section 2.3.1). Since the aim of our exercise is the comparison of the emission parameterizations and explicitly

Table 2.1: Sites of the pollen measurements and their geographical locations, numbers refer to the numbering in the figures and tables of Section 2.6.

	Country	Town	Lon	Lat
1	Austria	Rosalia	16.3033	47.7030
2	Austria	Vienna	16.3561	48.2488
3	Belgium	Brussels	4.3500	50.8333
4	Belgium	Genk	5.5000	50.9500
5	Switzerland	Basel	7.5830	47.5638
6	Switzerland	Bern	7.4211	46.9477
7	Switzerland	Geneva	6.1500	46.2166
8	Switzerland	La-Chaux-de-Fonds	6.8333	47.1144
9	Switzerland	Lausanne	6.6500	46.5333
10	Switzerland	Lucerne	8.2833	47.0500
11	Switzerland	Münsterlingen	9.2333	47.6333
12	Switzerland	Neuchâtel	6.9166	46.9833
13	Switzerland	Zurich	8.5500	47.3833
14	Germany	Berlin	13.4166	52.5333
15	Germany	Delmenhorst	8.6333	53.0500
16	Denmark	Copenhagen	12.5500	55.6833
17	France	Chalon-sur-Saône	4.8369	46.7933
18	France	Chambéry	5.9169	45.5652
19	France	Metz	6.1822	49.0925
20	France	Montluçon	2.6050	46.3400
21	Croatia	Zagreb	15.9833	45.8166
22	Hungary	Györ	17.6000	47.6666
23	Hungary	Kecskemét	19.6666	46.9166
24	Hungary	Budapest	19.0666	47.5000
25	Hungary	Salgótarján	19.9008	48.0455
26	Hungary	Szolnok	20.2000	47.1666
27	Hungary	Tata	18.3180	47.6388
28	Hungary	Veszprém	17.9163	47.1000
29	Italy	Busto Arsizio	8.8541	45.6119
30	Italy	Legnano	8.9088	45.5969
31	Italy	Parma	10.3333	44.7167
32	Poland	Lodz	19.4650	51.7661
33	Poland	Poznan Morasko	16.9166	52.4500
34	Poland	Poznan	16.8833	52.4166

Table 2.2: Pollen classes for birch pollen concentrations (C_{pollen}) used for the operational pollen forecasts at MeteoSwiss (Gehrig et al. 2013).

Pollen class	Pollen concentration in m^{-3}
low pollen load	$C_{\text{pollen}} < 10$
moderate pollen load	$10 \leq C_{\text{pollen}} < 70$
strong pollen load	$70 \leq C_{\text{pollen}} < 300$
very strong pollen load	$300 \leq C_{\text{pollen}}$

Table 2.3: 2×2 contingency table: pairs of measured and simulated values are classified as hits (a), false alarms (b), misses (c) and correct negatives (d).

		Observation	
		yes	no
Forecast	yes	a	b
	no	c	d

not that of the seasonal description, it has to be made sure that the day-to-day differences between modeled and observed pollen concentrations can be accounted mainly to the emission parameterization. Therefore, we exclude days outside the main pollen season from the exercise. The main pollen season is defined as the period between the first and last occurrence of 70 pollen per cubic meter in the observations (daily means). This corresponds to a pollen class of 'strong' (compare Table 2.2). Secondly, we exclude days at the beginning and end of the simulated pollen season since the up- and downswing of the description of the pollen season is not yet very well defined. To ensure that these days are not taken into account, we exclude days where the value of the modeled pollen season $f_{\text{Q,seas}}[0, 1]$ is below 0.3.

The observational data has been checked for outliers. Additionally, we excluded sites that had less than 7 days of observations within the chosen period (see above).

2.6   Performance of the different model versions

2.6.1   Statistical measures

Manual operational pollen forecasts are usually done for pollen classes that reflect more or less the strength of the allergenic symptoms that are induced by the given pollen concentration. These thresholds depend on the sensitization rates and are not constant over regions (Jaeger 2011). Table 2.2 gives the thresholds for birch pollen concentrations used for the operational pollen forecasts at MeteoSwiss (Gehrig et al. 2013). Taking this classification, using a lower and upper limit, the continuous values of pollen concentrations were classified, both for the modeled and the measured values. For each pollen class, a 2×2 contingency table (see Table 2.3) was completed taking the occurrence of the class as an event and the occurrence of any other class as a non-event. Whether the modeled pollen class is higher or lower than the observed one, or the distance between them, cannot be taken into account. Additionally, it has to be noted that the occurrence of any non-event in measurements and simulations is counted as a correct negative. Since a non-event is any pollen class other than the one currently under observation, a correct negative does not necessarily mean that the correct pollen class is forecast.

Additional to this approach based on the usual manner of manual pollen forecasts, we classified the pollen data using single thresholds as it is usually done for precipitation. This reflects the fact that for most allergenic patients, the excess of a certain personal threshold pollen concentration triggers symptoms, and thus necessitates the intake of medication. Whether this threshold is just reached or strongly overpassed is of minor importance.

Based on the four numbers in a 2×2 contingency table (compare Table 2.3), a series of skill scores has been computed (Wilks 2006). Generally, several of these scores should be looked at together in order to present a complete picture of the performance of a model. We have chosen the Threat Score, False Alarm Rate, as well as the Pierce Skill Score.

The Threat Score TS (Eq. 2.13) measures the proportion of correct forecasts without taking into account the correct non-events:

$$\text{TS} = \frac{a}{a + b + c}. \tag{2.13}$$

Usually, this is done for rare events where correct non-events are meaningless. In our case, disregarding the correct non-events is especially wanted since they are not necessarily correct, as described above. TS ranges between 0 and 1, with 1 being a perfect score.

The False Alarm Ratio FAR (Eq. 2.14) gives the fraction of simulated events that were not observed:

$$\text{FAR} = \frac{b}{a+b}. \tag{2.14}$$

FAR takes values between 0 and 1, a perfect score renders a value of 0.

The Pierce Skill Score PSS (Eq. 2.15) is a measure that describes the performance of a model compared to an unbiased random forecast:

$$\text{PSS} = \frac{ad - bc}{(a+c)(b+d)}. \tag{2.15}$$

PSS can take values between -1 and 1. Forecasts worse than a random forecast render negative values. Forecasts with some skill better than random result in positive values. Rare events that are correctly forecast count more than frequent events.

Additionally, we calculated some statistical measures that reflect the pollen concentrations as opposed to pollen classes. This overcomes the problem of classification: values close to the thresholds might lead to a wrong class even though they are not far away from the observed value. Contrary to that, classes that cover a big interval of concentrations lead to correct counts of events even if the real value is several factors wrong. We have calculated the correlation coefficient r^2, the p-value, the root-mean-square-error rmse, the index of agreement d_1, the fraction of predictions within a factor of two of observations FAC2, and the geometric mean bias GMB (GAW Report No. 181 2008).

We have calculated the p-value for r^2. It gives the probability to obtain the observed data if the null hypothesis is true. In our case, the null hypothesis is: 'Observations and modeled simulations do not correlate.' If the p-value falls below a predetermined significance level (we use a value of 0.05), one can assume that the null hypothesis is wrong. It has to be noted that the p-value is not a proof that the alternative hypothesis is correct. However, if the p-value is above the chosen significance level, it is not justified to reject the null hypothesis.

The index of agreement (Willmott et al. 1985) is based on the sums of the absolute values of the errors between observations and modeled values. It can take values between zero and one, with one being a perfect score. It is given by

$$d_1 = 1 - \frac{\sum_{i=1}^{N} |P_i - O_i|}{\sum_{i=1}^{N} \left(\left| P_i - \overline{O} \right| + \left| O_i - \overline{O} \right| \right)}. \tag{2.16}$$

Where P_i denote the simulated values, O_i the observations, $\overline{O}$ the observational mean and N the number of data points.

FAC2 gives the fraction of the predictions that are within a factor of two of the observations. It is calculated as

$$\text{FAC2} = \frac{1}{N} \sum_{i=1}^{N} n_i, \tag{2.17}$$

with $n_i = 1$ if the modeled value lies within a factor of two of the observed value. Otherwise, n_i is zero. A 'perfect' forecast (with respect to the factor of two) renders a score of one.

The geometric mean bias is given as

$$\text{GMB} = \exp\left(\frac{1}{N}\sum_{i=1}^{N}\ln P_i - \frac{1}{N}\sum_{i=1}^{N}\ln O_i\right). \tag{2.18}$$

It has to be noted that GMB is sensitive to the order of magnitude. The difference between 0.1 and 1 is rated equally false as the difference between 10 and 100. In reality, the former is of little importance to allergic people whereas the latter is crucial. Additionally, the measuring systems cannot distinguish between 0.1 and 1 while they are clearly sensitive to the difference between 10 and 100. Furthermore, in the observed pollen concentrations, values of 0 pollen per cubic meter can occur. This obviously results in an error for the logarithm. Hence, the logarithm of pollen concentrations smaller than 20.1 pollen per cubic meter was set to 3.

2.6.2   Results regarding pollen classes

We have studied the ability of the model versions to forecast a certain pollen class using TS and FAR. The results using a double threshold to define a pollen class (upper and lower bound) can be found in Figs. 2.4 and 2.5. Both model versions show that the ability to correctly forecast a pollen class is different for the different pollen classes. Apparently, it is easier to predict higher pollen classes. This is desirable since higher pollen classes induce stronger allergenic symptoms. In any case, the class 'low pollen load' scores worst. This can partly be explained by the fact that the higher pollen classes cover a wider range of pollen concentrations (see Table 2.2): e.g., for the pollen class 'very strong' the concentration needs to be anything above 300 pollen per cubic meter, whereas for the class 'low' the concentration needs to be below 10 pollen per cubic meter. Obviously, the latter is more difficult to hit. It has to be noted, that the class 'low pollen load' is very rare during the main pollen season, both in observations and in the models. The scores are therefore based on only a few data points where the observations fall into this class. Additionally, measurements of small pollen concentrations are uncertain due to the nature of the measuring system. The same scores have also been computed using a single threshold to define a pollen class rather than an upper and lower limit. The results given in Table 2.4 still show strong differences between the classes. However, the conclusion drawn from the exercise is reversed: now, the results indicate that it is easier to forecast the lower pollen classes. This demonstrates that the scores are very sensitive to the way an 'event' or 'non-event' is defined (single or double threshold). Which definition is appropriate depends very much on the question of the study.
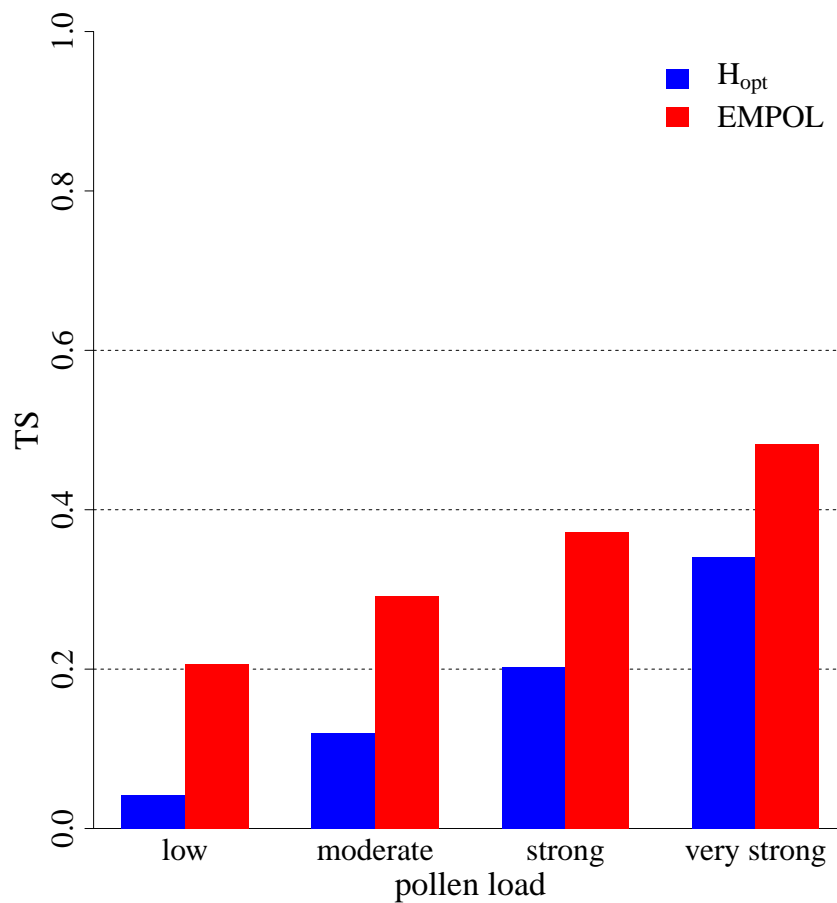
Figure 2.4: Threat Score, based on classes defined by an upper and lower limit.

The PSS using a double threshold is shown in Fig. 2.6. For the three lower pollen classes, the values of PSS are in the order of 0.3 (EMPOL) and less than 0.1 (H_{opt}). The scores for the pollen class 'very strong' are better for both parameterizations: 0.49 and 0.24, respectively. The results indicate that, indeed, the highest pollen class is better predicted than the lower pollen classes. This is true for both emission parameterizations and for both definitions of an 'event' (not shown).

In order to get a feeling for the quality of our results, we have compared the PSS values for pollen to the results obtained for operational COSMO forecasts of precipitation at MeteoSwiss. Since precipitation, in contrast to birch pollen concentrations, is not limited to only one season, the analysis has been done for all four seasons (spring, summer, autumn, winter). For precipitation, 8 different thresholds are used for the classification, starting with $0.1\,\mathrm{kg\,m^{-2}}$ and ending with $50\,\mathrm{kg\,m^{-2}}$. The corresponding values can be found in Table 2.5. In contrary to pollen classes, precipitation is better forecast for the lower thresholds. The best score for pollen classes (EMPOL, class 'very strong', see Fig. 2.6) is in the same order than the best scores for precipitation

Table 2.4: Threat Score (TS) and False Alarm Ratio (FAR) for pollen classes using a single threshold. The threshold is given in pollen per cubic meter.

Score	Threshold	H_{opt}	EMPOL
TS	10	0.91	0.95
TS	70	0.65	0.69
TS	300	0.34	0.48
FAR	10	0.03	0.02
FAR	70	0.27	0.21
FAR	300	0.58	0.29

Table 2.5: Values of the Pierce Skill Score for operational COSMO forecasts of precipitation at MeteoSwiss using different thresholds. The four seasons are evaluated separately.

Threshold in $\mathrm{kg\,m^{-2}}$	Spring	Summer	Autumn	Winter
0.1	0.64	0.60	0.63	0.61
1	0.62	0.54	0.64	0.64
2	0.55	0.47	0.59	0.59
5	0.45	0.38	0.55	0.53
10	0.36	0.28	0.48	0.41
20	0.21	0.21	0.35	0.21
30	0.15	0.16	0.26	0.09
50	0.03	0.05	0.10	0.08
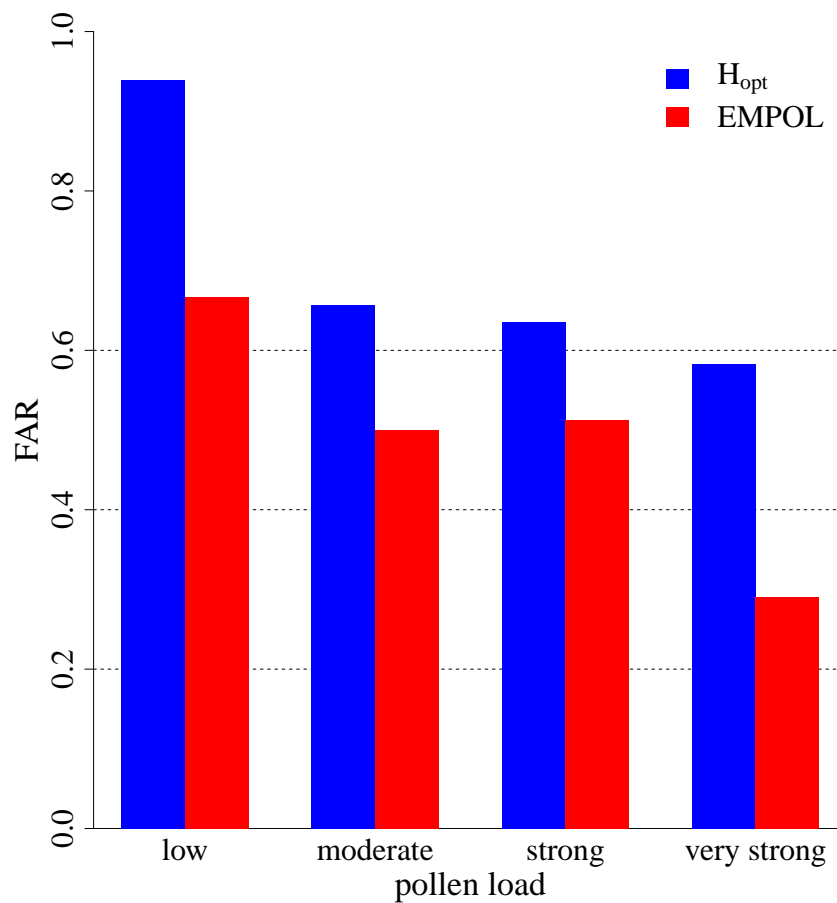
Figure 2.5: False Alarm Ratio, based on classes defined by an upper and lower limit.

(0.6). Likewise, the worst scores for precipitation and pollen (H_{opt}, classes 'low', 'moderate' and 'strong') are in the same range of less than 0.1. Considering that precipitation has already been forecast in NWP models for some decades, this is an encouraging outcome for simulations of pollen concentrations that have been introduced to NWP systems just recently.

Summing up the results, EMPOL scores higher than H_{opt} for any of the pollen classes and for all of the computed skill scores, regardless of the definition of an 'event' (see, e.g., Figs. 2.4 to 2.6).

2.6.3 Results regarding pollen concentrations

The mean correlation coefficient is clearly better for EMPOL than for H_{opt} (see caption of Table 2.6). However, to reject the null hypothesis ('Modeled and observed concentrations are uncorrelated'.), the p-values have to be less than 0.05. Neither the mean p-value of H_{opt} nor that of EMPOL fall below that threshold (see caption of Table 2.6). The picture changes when looking at individual measuring sites (see

Table 2.6: Correlation coefficients (r^2) and their corresponding p-values for the two model configurations at each of the measuring sites. The mean r^2 over all stations is 0.43 for EMPOL and 0.12 for H_{opt}. The corresponding mean p-values are 0.19 for EMPOL and 0.49 for H_{opt}.

| | EMPOL | | H_{opt} | |
Site	r^2	p-value	r^2	p-value
1	0.48	0.03	0.19	0.41
2	0.16	0.54	-0.08	0.76
3	0.80	0.00	0.34	0.21
4	0.35	0.21	0.58	0.02
5	0.74	0.00	0.04	0.87
6	0.76	0.00	0.13	0.59
7	0.85	0.00	0.34	0.22
8	0.41	0.08	0.03	0.90
9	0.72	0.00	0.41	0.13
10	0.86	0.00	-0.02	0.93
11	0.69	0.00	0.20	0.39
12	0.84	0.00	0.17	0.66
13	0.46	0.04	0.25	0.28
14	0.02	0.93	0.03	0.90
15	-0.15	0.69	-0.50	0.17
16	0.88	0.00	0.67	0.02
17	-0.37	0.24	-0.03	0.93
18	0.72	0.01	0.35	0.27
19	0.64	0.06	-0.39	0.29
20	0.43	0.08	0.45	0.06
21	0.16	0.73	-0.27	0.55
22	0.47	0.08	0.38	0.17
23	0.22	0.46	-0.19	0.51
24	0.62	0.01	0.10	0.74
25	-0.29	0.26	-0.05	0.84
26	0.82	0.00	-0.05	0.86
27	0.71	0.08	-0.12	0.79
28	0.31	0.21	0.18	0.47
29	0.66	0.01	0.32	0.27
30	0.67	0.02	0.68	0.01
31	0.39	0.39	0.22	0.64
32	-0.58	0.05	-0.44	0.15
33	0.06	0.84	0.05	0.87
34	0.27	0.34	0.05	0.87
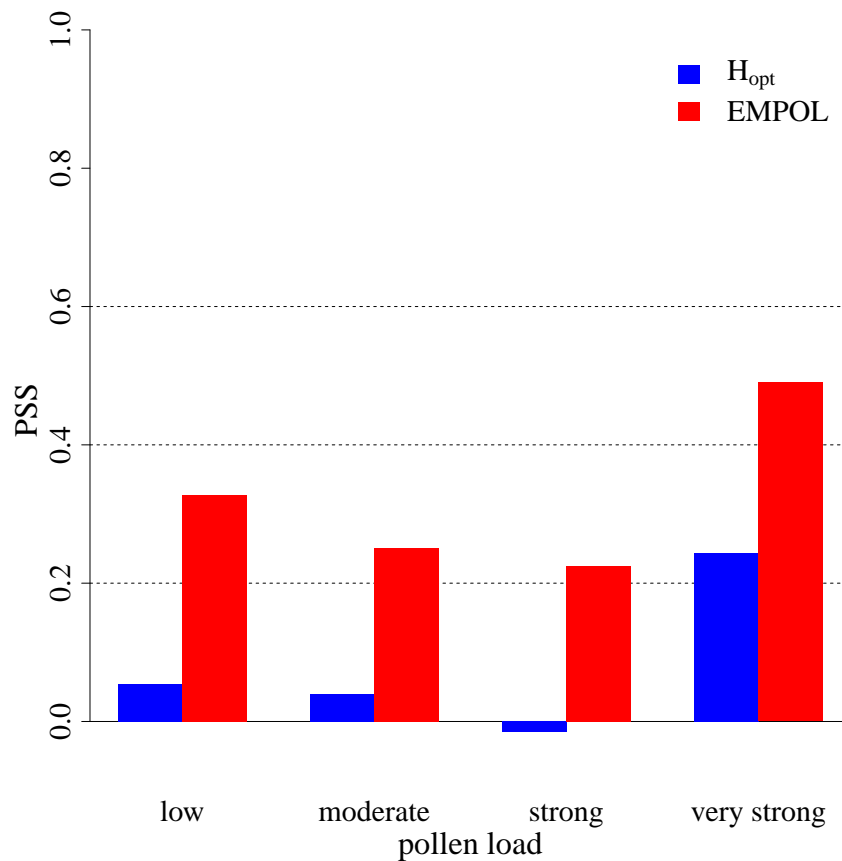
Figure 2.6: Pierce Skill Score, based on classes defined by an upper and lower limit.

Table 2.6). For H_{opt}, the p-values are generally higher, with only three stations below 0.05 (stations 4, 16, and 30). These coincide with the three highest correlation coefficents for H_{opt}. In contrast, EMPOL has p-values of less than 0.05 at 17 stations and only a few stations with very high p-values. Again, the high p-values generally coincide with small correlation coefficients (e.g., stations 2, 14, 15, 21, 23, 33, 34) and vice versa. H_{opt} only performs better at 7 out of the 34 measuring sites. This can be interpreted such that the biological and physical processes are represented better in EMPOL compared to H_{opt}. Both parameterizations have been tuned using Swiss pollen data of the previous years. For EMPOL, this results in better correlation coefficients and very low p-values at most of the Swiss pollen stations (numbers 5 to 13). But apparently, the chosen parameterization also works well for many stations outside of Switzerland (e.g., stations 3, 16, 18, 19, 24, 26, 27, 29, 30). Such a refinement of the results for the stations included in the tuning process cannot be found for H_{opt}.

The model's ability to forecast a concentration in reasonable closeness to the observed value can be measured using FAC2 (see Fig. 2.7). It can be seen that EMPOL
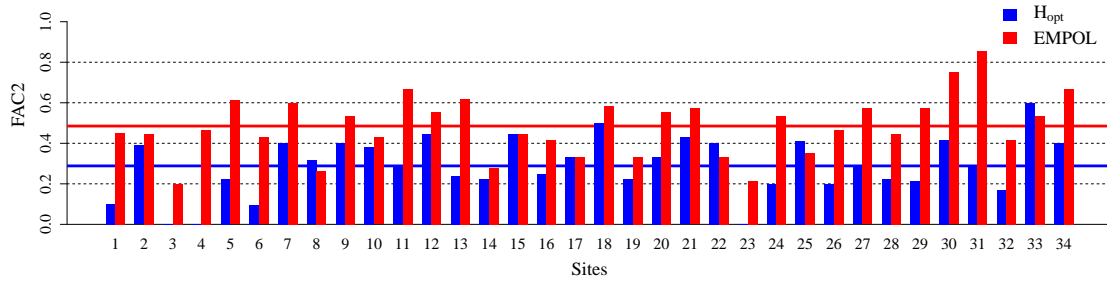
Figure 2.7: Fractions of predictions within a factor of two of observations for the two model configurations at each of the measuring sites. The colored lines denote the mean over all stations.

Table 2.7: Statistical results for the two model configurations based on pollen concentrations. Values are means over all measuring sites. The root-mean-square-error is given in pollen per cubic meter. Figures in the last column give the number of sites where EMPOL scores better than H_{opt}. The total number is 34 sites.

Statistical measure	H_{opt}	EMPOL	#
d_1	0.31	0.46	29
FAC2	0.29	0.49	28
rmse	585	345	32
GMB	2.14	1.18	26
r^2	0.12	0.43	27
p-value	0.49	0.19	28

performs better at 28 of the 34 stations which leads to a considerably higher mean value than for H_{opt}. Overall, about 50 % of the simulated concentrations are within a factor of two of the observed values for EMPOL. For H_{opt}, only about 30 % fall in that range. Similar conclusions can be drawn from d_1 (not shown). Here again, for EMPOL, the results tend to be slightly better at the Swiss stations while H_{opt} does not show this preference (not shown).

The mean rmse is very high for both parameterizations (see Table 2.7). The individual values for different stations are quite diverse (not shown). In many cases, high values of rmse coincide for the two parameterizations. This suggests that the error could have its origin outside the emission parameterizations. Examples of such external factors are the plant distribution or a wrong altitude of Alpine stations in the model due to the low spatial resolution.

A different picture can be found for the GMB (see Fig. 2.8). Here, again, similar values coincide at some of the stations (e.g., sites 12, 19, 20, 25, 26, 33). However, at
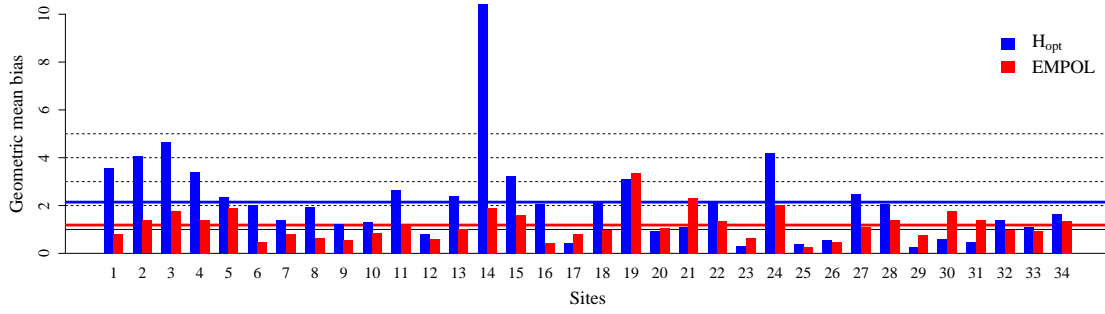
Figure 2.8: Geometric mean biases for the two model configurations at each of the measuring sites. The colored lines denote the mean over all stations.

the majority of stations, one parameterization clearly shows a stronger bias than the other (e.g., sites 1–4, 14, 21, 24). Here, the difference in the error has to originate in the emission parameterizations since the other influencing parameters are the same for both model versions.

2.6.4 Sensitivity to mast years

As mentioned before, birch shows a bi-annual variation of the pollen production (years with high pollen production are referred to as 'mast years'). The overall level of the pollen concentrations in the model is tuned based on simulations and observations of pollen concentrations of a predefined set of years. Usually, such a set of years will contain both mast years and normal years. This will result in a simulated pollen level somewhere between mast years and normal years. Therefore, the occurrence or non-occurrence of a mast year in the period chosen for the experiment will have an influence on the performance of the model for the statistical scores that are sensitive to the overall level of the pollen concentrations (e.g., the fraction of predictions within a factor of 2 of observations). Scores that are not sensitive to the overall level (e.g. the correlation coefficient) will not be influenced by the occurrence of a mast year.

  We tried to identify the mast and normal years in the period used in this study (2010 to 2012) based on the Swiss observational data. Values of the seasonal pollen index SPI (yearly sum of the observed daily pollen concentrations) for the Swiss observational sites is given in Table 2.8. It is not possible to make a clear statement. Four of the Swiss observational sites show the highest SPI in the year 2010, three in the year 2011 and two in the year 2012. The variation between the years can be very small (e.g., sites 5 and 9) or very strong (e.g., sites 6 and 11).

Looking at this data, it is obvious that it is not even possible to make an overall statement for these stations that are relatively close to each other about a certain year being a mast year or not. It is not consistent between the different observational

Table 2.8: Seasonal pollen indices for the Swiss observational sites for the years 2010 to 2012.

Site	2010	2011	2012
5	6304	5484	6052
6	9834	16190	12156
7	6134	3647	4885
8	3131	1413	3418
9	5816	4426	5839
10	7222	3988	5392
11	5336	13842	5038
12	4258	2640	3757
13	10694	12516	10246

sites. Additionally, the difference between mast years and normal years can be strong or very weak, depending on the observational site.

2.7   Summary and conclusions

We have developed an emission parameterization EMPOL for pollen grains for the use in NWP systems. It needs the plant distribution and a description of the pollen season as input parameters. The emission process is separated into two steps: first, the release of the pollen from the flowers into a pollen reservoir (pollen presentation). This is driven by temperature and relative humidity. Second, the entrainment of the pollen from the reservoir into the atmosphere. This is driven by the turbulent kinetic energy. Additional processes that are included: wash-out of the reservoir by precipitation, loss of pollen in the reservoir due to random processes, sticking of the pollen grains in the reservoir in case of high relative humidities. Under favorable conditions, the available pollen grains can be released rapidly. In that case, pollen release is turned off for the rest of the day. The maximum daily amount of available pollen is a function of the progression of the pollen season.

The meteorological functions have been implemented in a way that allows adaptation for different pollen species. This is important since the opening processes of the anthers are different between plant species. Additionally, EMPOL uses individual functions for each of the meteorological parameters. This and the separation of the different steps leading to pollen emission facilitate the design of experiments to determine the different meteorological parameters. Another advantage over the parameterizations based on Helbig et al. (2004) (H_{orig} and H_{opt}) is the avoidance of unknown parameters like LAI that introduce unnecessary uncertainty.

Statistical scores show that the model version using EMPOL performs better than the model version using H_{opt}. This is true both for analyses using continuous values and for analyses based on pollen classes.

TS and FAR show that the performance of the model differs between pollen classes. Using a lower and upper limit to define classes, the higher pollen classes are predicted better than the lower pollen classes. Using a single threshold to discriminate between classes, the lower pollen classes reach better scores. For PSS, the scores of the higher pollen classes are better, both for single and double thresholds. Overall, the scores are comparable to the ones that are reached for operational forecasts of precipitation using the COSMO model. The best score (0.49) is reached for the pollen class 'very strong' and EMPOL. The mean correlation coefficient for H_{opt} is 0.12, whereas for EMPOL it reaches a value of 0.43. The results are quite diverse between the different observational sites. Using EMPOL, 49 % of the simulated values deviate less than a factor of two from the observations (H_{opt}: 29 %).

It has to be noted, however, that this parameterization is not yet fully tuned. The functions in the parameterization work in the timescale of a time step. In our case, these are 60 s. It is hardly possible to tune these functions using daily resolved observations. Only recently, pollen observations with a higher temporal resolution (bihourly values) have started to be registered on an operational basis. Additionally, it would be desirable to conduct laboratory experiments for the explicit determination of the functions that connect the amount of released/entrained pollen to meteorological variables. Taking these exercises into account, EMPOL has a great potential to become considerably better in the future.

For the time being, the functions have only been tested for birch pollen emission. However, during the last months, EMPOL has also been employed for grasses and ragweed using plant-specific constants (e.g. in the functions for temperature, humidity and TKE). First results are very promising (not shown). Further plant species, such as hazel, alder or ash, should follow to enable the operational use of numerical predictions for the main allergenic pollen species.

For the future development of EMPOL, the following paragraph lists some of the possible improvements.

- Conducting field or laboratory experiments to deduce better functions relating meteorological conditions to the different steps of pollen emission.

- Introducing a mechanism that hinders pollen release and/or entrainment for a certain time period after a precipitation event.

- Introducing the influence of rising CO_2 on the pollen production (e.g. Ziska and Caulfield 2000; Rogers et al. 2006)). With respect to the present parameterization this could be done in several ways: (1) $Q_{pollen,day}$ could be transformed

into a variable field (right now, its value is fixed for the entire domain), (2) a new input field could be introduced that reflects the influence of CO_2, e.g. f_{Q,CO_2}, (3) the influence of CO_2 could even be calculated within the model if COSMO-ART is run in a 'full mode' including reactive trace gases.

Acknowledgements

Supplementary materials

EMPOL is an integral part of the NWP model system COSMO-ART. It is written in Fortran. The NWP model system is distributed in two parts: COSMO can be obtained from the German Weather Service (DWD). The ART part (containing EMPOL) can be obtained from the Institute for Meteorology and Climate Research, Karlsruhe Institute of Technology (KIT), Dr. Bernhard Vogel.

Contact COSMO: cosmo-licence@cosmo-model.org
Contact ART: bernhard.vogel@kit.edu

Table 2.9 gives an overview about the necessary input and model fields that have to be provided when implementing the emission parameterization EMPOL into a different NWP model system.

Table 2.10 gives an overview about the differences of the emission parameterizations described in the publication.

The different steps of the pollen emission parameterization EMPOL are displayed in Figure 2.9.

Table 2.9: Parameters and their units used in the emission parameterization EMPOL. The third column indicates the role of the parameters: 'I' - parameter provided as input field, 'M' - parameter taken from the NWP model (at best from the model level that corresponds to the emission height), 'T' - tuning parameter, 'C' - parameter calculated within EMPOL.

Parameter	Unit	Info	Description
$Q_{pollen,day}$	m^{-2}	T	total amount of pollen that can be released per day under perfect conditions
$Q_{pollen,\Delta t}$	m^{-2}	T	amount of pollen that can be released per time step under perfect conditions
R_{pollen}	m^{-2}	C	content of the pollen reservoir, current time step
$R_{pollen,old}$	m^{-2}	C	content of the pollen reservoir, previous time step
$R_{pollen,sum}$	m^{-2}	C	total amount of released pollen since midnight
ΔR_{pollen}	m^{-2}	C	pollen released during the current time step
$F_{E,pollen}$	$m^{-2}\,s^{-1}$	C	emission flux of pollen grains
C_{pollen}	m^{-3}	C	pollen concentration
Ψ_{random}	-	T	loss of pollen from the reservoir due to random processes
Ψ_{precip}	-	T	loss of pollen from the reservoir due to precipitation
Φ_{plant}	-	C	plant-dependent influences on pollen emission
Φ_{met}	-	C	meteorological influences on pollen emission
Φ_{biol}	-	C	biological influences on pollen emission
$f_{R,T}$	-	T	fraction of open flowers as a function of temperature
$f_{R,RH}$	-	T	fraction of open flowers as a function of relative humidity
$f_{E,TKE}$	-	T	fraction of emitted pollen as a function of turbulent kinetic energy
$f_{E,RH}$	-	T	fraction of emitted pollen as a function of relative humidity
$f_{Q,cov}$	-	I	fraction of the grid box covered with the specific plant
$f_{Q,seas}$	-	I	mathematical description of the course of the pollen season
$f_{Q,alt}$	-	I	productivity of the plants as a function of altitude
T	K	M	temperature at the lowest model level
rh	%	M	relative humidity at the lowest model level
TKE	$m^2\,s^{-2}$	M	turbulent kinetic energy at the lowest model level
Δt	s	M	time step of the simulation
p	$kg\,m^{-2}\,s^{-1}$	M	sum of convective and grid-scale precipitation

Table 2.10: Differences between the four parameterizations of pollen emission (see text) that are mentioned in the publication.

Feature	H_{orig}	H_{opt}	S13	EMPOL
Description of the pollen season	Invariable formulation: the pollen season has the shape of a parabola and a fixed length of 30 days.	Use of an external model that describes start, end and course of the pollen season as functions of temperature sums.	Start and course of the pollen season are variable and depend on temperature sums. The end of the season is determined via a pollen reservoir.	Use of an external model that describes start, end and course of the pollen season as functions of temperature sums.
Influence of meteorological parameters on pollen release and entrainment of the pollen into the atmosphere	Pollen release and entrainment are combined: - friction velocity - wind speed - temperature - relative humidity	Pollen release and entrainment are combined: - friction velocity - wind speed - temperature - relative humidity	Pollen release and entrainment are combined: - 10 m wind speed - convective velocity scale - relative humidity - precipitation	Pollen release and pollen reservoir: - temperature - relative humidity - precipitation - random losses Entrainment: - turbulent kinetic energy - relative humidity
Upper limit for emission with high wind speeds?	no	yes	yes	yes
Additional aspects/factors included in the parameterization	- leaf area index - height of the plants - resuspension - maximum value for the sum of emitted pollen grains	- leaf area index - height of the plants - reducing factor for altitude - maximum value for the sum of emitted pollen grains	- maximum value for the sum of emitted pollen grains	- reducing factor for altitude - pollen reservoir - cut-off of the release of pollen if a daily maximum value is reached
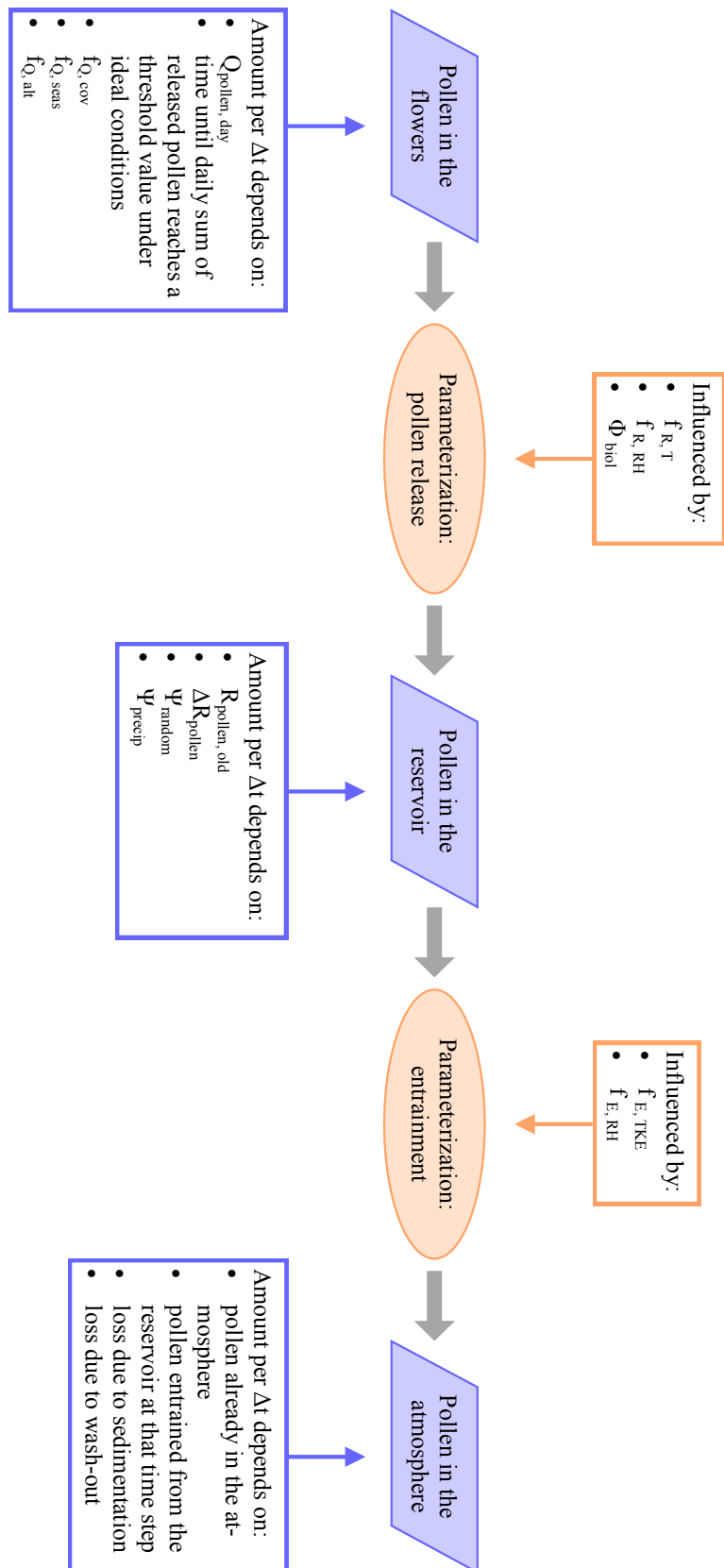
Figure 2.9: Flowchart displaying the different steps and influencing parameters of the emission parameterization EMPOL.

Chapter 3

Using plant inventories to create source maps for pollen emission in numerical weather prediction systems: how detailed need they be?

K. **Zink**[1,2], M. W. **Rotach**[2], P. **Kaufmann**[1], E. **Gentilini**[3], F. **Essl**[4], B. **Petitpierre**[3], O. **Broennimann**[3], A. **Guisan**[3,5], B. **Clot**[1]

[1] *Federal Office of Meteorology and Climatology MeteoSwiss, Switzerland*

[2] *Institute for Meteorology and Geophysics, University of Innsbruck, Austria*

[3] *Department of Ecology & Evolution, University of Lausanne, Switzerland*

[4] *Department of Botany and Biodiversity Research, Division of Conservation, Vegetation and Landscape Ecology, University of Vienna, Austria*

[5] *Institute of Earth Surface Dynamics, University of Lausanne, Switzerland*

Abstract

A detailed map of the pollen sources is one of the key factors in numerical simulations of pollen concentrations. Realistic pollen forecasts require knowledge about both the location and the abundance of the pollen producing plants. However, the degree of detail differs greatly between different plant inventories. The quantitative information can range from mere presence/absence information to exact numbers of plants per population. We conducted a numerical experiment to investigate the influence of different degrees of detail of the distribution map on the skill of a numerical pollen forecast. The setting was chosen to represent a large pollen source of ragweed (*Ambrosia artemisiifolia* L.) in a distance of 100 to 400 km to the area of interest. Ragweed pollen concentrations were simulated with the model system COSMO-ART (**Co**nsortium for **S**mall-scale **Mo**delling - **A**erosols and **R**eactive **T**race Gases) using a set of nine different distribution maps. They were constructed by gradually reducing the quantitative information of the original plant inventory data and the spatial distribution of the maps. The maps were then calibrated using observed pollen concentrations. The ragweed pollen season of 2012 was simulated using each of these distribution maps in turn. The usability of the different distribution maps was studied with statistical scores that were computed using simulated and observed pollen concentrations.

The calibration of the distribution maps was identified as a key factor for the performance of the pollen simulation. We discovered that such a calibration has to be done for each plant inventory separately due to the different nature of the inventories regarding their quantitative information. Provided that pollen observations for the calibration are available, it was found to be beneficiary to only use the presence/absence information of the inventories to create the distribution map. The best results were found for the maps with the highest spatial resolution. The conclusions drawn from our experiment are restricted to areas where the local pollen concentration is dominated by a strong but distant pollen source.

3.1   Introduction

The skill of a numerical pollen forecast is mainly influenced by three aspects: the quality of the map showing the distribution of the pollinating plant, the parameterization of the emission process of the pollen grains, and the transport of the pollen grains within the numerical weather prediction (NWP) model. While emission and transport of the pollen grains in the NWP model depend upon the correct identification and mathematical description of the biological, dynamical and physical processes involved, and thus can be influenced by the model developer, the distribution map has to be

obtained from different sources (e.g. plant inventories or land use data) and the quality of the map is restricted both through the availability and the reliability of the data. Therefore, we studied the sensitivity of the pollen forecast with respect to the quality of the distribution map focusing on ragweed (*Ambrosia artemisiifolia* L.) as an example for herbaceous plants.

The majority of approaches to generate plant distribution maps for numerical pollen modeling found in the literature deal with tree species (e.g., Sofiev et al. 2006; Skjøth et al. 2008; Pauling et al. 2012). These distribution maps usually are based on inventory data (e.g., national forest inventories) and land use data sets (e.g., Corine Land Cover (European Environment Agency 2012)). The main drawback of these approaches is their limitation to forested areas and tree species.

Skjøth et al. (2010) have developed a method to derive a ragweed distribution map based on land use data and observations of airborne pollen concentrations. Considering the typical habitats of ragweed plants, the land use categories suitable for ragweed growth are identified. For each pollen observational site in their study, they calculate a local ragweed infection level based on annual ragweed pollen counts and the percentage of suitable land use categories in the surroundings of the site. The ragweed coverage for the entire domain is then derived using the land use data and interpolations of the local infection levels at the individual pollen observational sites. As indicated by the authors, this approach is limited to highly infested areas where local plants dominate the annual pollen counts. For ragweed, this is true only in three European regions: the Pannonian Plain, the Rhône-Alpes region in France and Northern Italy.

Using land use data sets as a basis becomes critical as soon as we are looking at rare alien species that have not yet reached the limits of their potential distribution. Obviously, the mere existence of a suitable habitat does not mean that the plant has (already) occupied this area. In such a case, collection data of the plant's distribution is essential. Unfortunately, the availability and quality of such inventory data differs greatly between countries or even within countries (Bullock et al. 2012). Ragweed is a prominent representative for such a species: having been introduced to Europe more than a 100 years ago, this plant is present in many European countries but far from occupying all of the possible areas. However, the existence of even a few ragweed plants is relevant since its pollen is highly allergenic. Taking ragweed as an example, typical problems of plant inventories are identified:

- **Currentness of the data:** Often, it is not clear whether the data is up-to-date. Either the year of the finding is missing entirely or only the first encounter of the plant at the specific place is registered. Whether the plant still grows at that place is often not documented. For ragweed, this is problematic (Dullinger et al. 2009): being an annual plant, it is essential for the survival of the population

to produce viable seeds. Additionally, and even more importantly: in many countries, the localized ragweed plants are removed in order to control its spread.

- The **quantitative information** varies between inventories and is usually one of the following three: (1) the exact number of plants per population is given, (2) the quantity is given in classes, and (3) only presence/absence information is given.

- The **spatial resolution** of the data can be very different: usually, either the exact location (longitude and latitude) is given or the data has been assigned to grid cells used, e.g., in floristic mapping projects. But sometimes, the data reflects political boundaries regarding data collection: information is given, e.g., on the basis of counties or districts.

We have studied the influence of different variations of the distribution map on the performance of a pollen forecast. Our focus was set on the influence of a large but distant pollen source when local pollen production is relatively well known but quantitatively negligible. The distribution map used as a reference is derived from plant inventory data and calibrated using measurements of airborne pollen concentrations. This map is resampled several times in order to represent the different levels of detail that can usually be found in inventory data sets regarding the quantitative information. Additionally, the maps are rendered in three different spatial resolutions. Using these distribution maps in turn, the ragweed pollen season of 2012 is simulated several times. The resulting pollen concentrations are statistically compared to measurements in order to derive a ranking of the distribution maps. In a second step, a striking peak pollen concentration in the simulated values is used to further investigate the importance of the calibration that is needed to transform the inventory data into a distribution map.

3.2   Materials

3.2.1   Ragweed inventory data

In order to get a complete picture of the ragweed infestation in Europe, we gathered as many European ragweed distribution data sets as possible. Tables 3.9 and 3.10 in the supplementary materials give an overview of these data sets including the data owners and/or references. Figure 3.1 shows the ragweed populations that are included in these combined data sets. It is apparent from Figure 3.1 that no data is available from northern Italy - despite the fact that it is well known that ragweed is present in this region (e.g., Mandrioli et al. 1998).
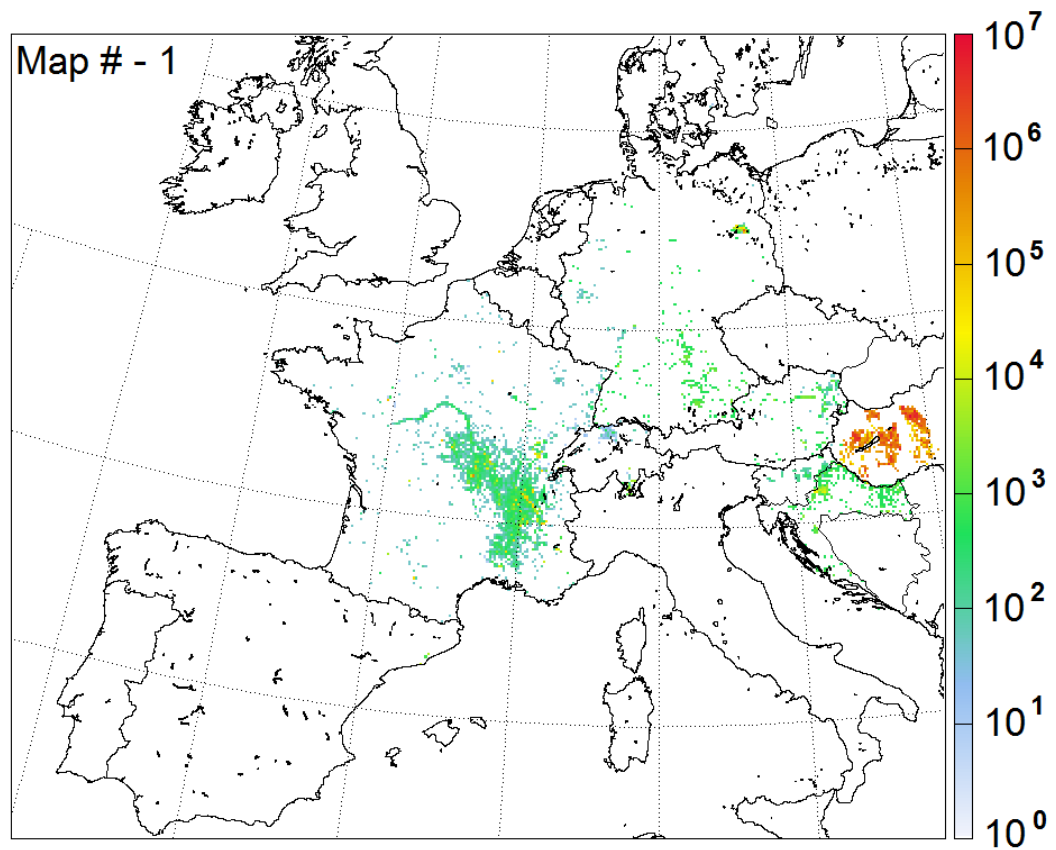
Figure 3.1: The reference map of the ragweed distribution that was derived using all of the quantitative information available. The spatial resolution of the map is approximately 6.6×6.6 km^2. The coloring denotes the number of plants per grid cell.

3.2.2 Observational data

We have used measurements of airborne pollen concentrations in France and Switzerland for the tuning of the emission parameterization in the numerical weather prediction (NWP) model, the calibration of the distribution maps and the verification of the simulated pollen concentrations. French pollen data was provided by the RNSA (Réseau National de Surveillance Aérobiologique) in bi-hourly and daily resolutions for the pollen season of 2012. Swiss pollen data was measured by the Swiss Federal Office for Meteorology and Climatology, MeteoSwiss. A list of the observational sites included in the study can be found in Table 3.11 in the supplementary materials.

3.2.3 The NWP model system COSMO-ART

For our study, we have used the NWP model system COSMO-ART in combination with the emission parameterization EMPOL. COSMO (**Co**nsortium for **S**mall-scale **Mo**delling) has originally been developed by the German weather service (Deutscher Wetterdienst - DWD) and is being used for operational weather forecasts in various countries (Steppeler et al. 2002). At the Karlsruhe Institute of Technology (KIT) in Germany, it has been extended for the simulation of **A**erosols and **R**eactive **T**race Gases to the online-coupled model system COSMO-ART (Vogel et al. 2009). COSMO-ART includes a module describing the emission, transport and deposition of pollen grains. It has been used to simulate the dispersion of birch (Vogel et al. 2008) and ragweed (Zink et al. 2012) pollen using an emission parameterization based on the suggestions of Helbig et al. (2004). Recently, the emission parameterization EMPOL has been developed taking into account that the biological and physical processes leading to pollen emission can be different between plant species (Zink et al. 2013). We used COSMO version 4.19, along with version 2.0 of the ART extension and version 1.1 of the EMPOL emission parameterization in the operational setup for numerical weather forecasts at MeteoSwiss. The domain covers a large part of Central Europe (Figure 3.1). The model is run at a spatial resolution of $0.06°$ ($\approx 6.6\,\text{km}$) and with a time step of 60 seconds. The simulated pollen season is split into 16 runs of 72 hours length each. Every run is initialised using updated boundary and initial conditions of the meteorological fields from the operational NWP modeling system. The simulated pollen concentrations are conserved from one run to the next in order to allow long-distance transport of the pollen grains. The diameter and density of the pollen grains are needed for the calculation of the settling velocity. The diameter of ragweed pollen grains ranges from 18 to 22 µm according to Taramarcaz et al. (2005). In our simulations, we have used a value of 20 µm. The density of dry ragweed pollen grains is set to 830 $\text{kg}\,\text{m}^{-3}$ according to Mandrioli et al. (2003).

The simulated period in 2012 was chosen based on the measured ragweed pollen

concentrations at French and Swiss observational sites. The starting day was taken as the first day when at least two of the measurements showed a strong pollen load (= 10 pollen per cubic meter, Table 3.4). Correspondingly, the ending day was taken as the last day when at least two of the measurements showed a strong pollen load. This led to a simulation period from August, 9th, 2012, to September, 23rd, 2012.

3.3 Methods

3.3.1 Creating synthetical distribution maps

Table 3.1: Overview of the nine different maps used in this study. Quantitative information about the plant populations is given in exact numbers (#), classes or presence/absence information (yes/no). The spatial resolution of the resulting distribution maps is given in grid points (GPs) of the model resolution. 1×1 GP corresponds to a resolution of approximately 6.6×6.6 km^2, 5×5 GPs corresponds to approximately 33×33 km^2, and 10×10 GPs corresponds to approximately 66×66 km^2.

yes/no	yn-1	yn-5	yn-10
classes	cl-1	cl-5	cl-10
#	#-1	#-5	#-10
	1×1 GP	5×5 GPs	10×10 GPs

Quantitative information (row label)

Horizontal resolution

We have used the ragweed inventory data to create different synthetical inventory data sets. They were designed to represent the different degrees of detail regarding the quantitative information that can usually be found in inventory data. Using these synthetical inventory data sets as a basis, we have then created synthetical distribution maps with different spatial resolutions. In both dimensions, we have introduced three quality levels leading to a total of nine distribution maps (Table 3.1). In our study, we distinguish between two regions of interest:

1. The **'source region'**: this region includes the dominant pollen sources. This part of the map is resampled nine times to represent the different types of

distribution maps. The maps were calibrated using observational data in this region.

2. The **'receptor region'**: in this region, pollen sources are relatively well known but scarce. The pollen concentrations are dominated by long-distance transport of pollen from the 'source region'. This part of the map is not resampled and is based on plant inventories of the highest degree of detail that is available. The resolution of this part of the map is 1×1 grid points. Observational data in this region was used to assess the performance of the different simulations.

Regarding the situation in Europe, a domain including Switzerland and the French Rhône-Alpes region (situated west of Switzerland) seems a suitable region for our experiment:

- The Rhône-Alpes region is one of the three regions with major ragweed populations in Europe.

- North of the Alps, Switzerland is fairly free of ragweed plants.

- The Rhône-Alpes region is the main source of ragweed pollen registered at Swiss pollen observational sites (north of the Alps) (Clot et al. 2002).

- The distribution of ragweed plants is relatively well known, both in Switzerland and France. Hence, it is possible to derive a reference state with a high degree of detail.

To simplify the construction of the different distribution maps, the area west of Geneva (the westernmost city of Switzerland) is taken as the source region, while the area east of Geneva is taken as the receptor region. However, we did not want to exclude the biggest source of ragweed pollen in Europe: the Pannonian Plain. We suspected that this source region might have an influence on the local pollen concentrations in Switzerland - even if this influence is only small and episodically. In order to study such an event of long-distance transport, we did not restrict our model domain to the Rhône-Alpes region and Switzerland. Unfortunately, Northern Italy, the third relevant source of ragweed pollen in Europe could not be included in the study due to a lack of inventory data. Since Northern Italy is part of the model domain, we had to limit our investigation to Swiss pollen observational sites that are not influenced by Italian ragweed populations. This led to the exclusion of observational sites in the Ticino region of Switzerland.

The construction of the synthetical distribution maps is done in 4 steps:

1. The original ragweed inventory data is used to create three synthetical inventory data sets that represent different degrees of detail.

Table 3.2: Classification used to reduce the quantitative information of the inventory data set. The range of the population size and the assigned value for each class is given in plants per locality. The population size estimate for large populations was based on exemplary quantitative data from main infestation regions in Europe.

Abundance class	Range	Assigned value
small population	1-100	50
medium population	101-10000	5000
large population	>10000	500000

2. Each of these synthetical inventories is then used to create a distribution map with the highest spatial resolution of 1×1 grid points: maps #-1, cl-1 and yn-1.

3. The maps #-1, cl-1 and yn-1 are used to create the maps with lower spatial resolution: #-5, cl-5, yn-5, #-10, cl-10 and yn-10.

4. The nine distribution maps are calibrated using pairs of measured and simulated pollen concentrations.

Step 1 - creating synthetical inventory data sets   Using the original inventory data from various European countries, we constructed three synthetical inventories representing different degrees of detail regarding the quantitative information: (1) continuous data, (2) classified data, or (3) presence/absence data. First, a 'reference inventory' was created giving the longitude, latitude, and exact number of plants for each plant population. In the cases where the original data sets were not of type (1), we had to assign a typical value according to an 'expert guess'. Any additional information (e.g., ranges of plant density classes or status information like 'established' or 'casual') was used to enhance this 'expert guess'. It has to be noted that the data sets in the two regions of interest (the Rhône-Alpes region and Switzerland) were of type (1) or (2), thus relatively detailed. In a second step, the quantitative information of the 'reference inventory' was then reduced to create the classified inventory according to Table 3.2. For the presence/absence inventory, the quantitative information was additionally reduced by replacing the number of plants per locality with a default value of 1.

Step 2 - creating the maps with the highest spatial resolution   To create the distribution maps #-1, cl-1, and yn-1, the total number of plants per grid cell is calculated by summing up the individual plant populations within the given area. In the maps #-1 and cl-1, the value of each grid point represents the total number of plants in the area. In map yn-1, based on the presence/absence inventory with a

default population size of 1, the value of each grid point represents the number of populations in the area.

Step 3 - reducing the spatial resolution of the maps   Taking maps #-1, cl-1, and yn-1 as a basis, the spatial resolution of the distribution maps is reduced by defining clusters of 5×5 grid cells (and 10×10, accordingly). For each of these clusters, the mean number of plants is calculated. Each grid cell within the cluster is then assigned this mean value. Maps #-5 and #-10 are based on map #-1. Maps cl-5 and cl-10 are based on map cl-1. Maps yn-5 and yn-10 are based on map yn-1.

Step 4 - calibrating the distribution maps   The chosen procedure to construct synthetical distribution maps creates large differences between the maps regarding the total amount of plants in the model domain (as well as in each single grid cell). For example, for the maps based on presence/absence data, the value of each grid point represents the number of plant populations within the grid cell, while for the maps based on classified and numbered data, the value represents the number of plants (with different accuracy). The difference between the values can be of several magnitudes. The overall level of the pollen concentrations in the model (i.e. the EMPOL emission module (Zink et al. 2013)) depends on two parameters: the just mentioned total amount of plants and the tuning factor $Q_{\text{pollen,day}}$ (the maximum number of pollen that can be released per day in the model) in the emission parameterization. Before conducting the experiment, $Q_{\text{pollen,day}}$ was tuned using map #-1 (for details, see Section 3.3.2). Using the same model configuration for each of the distribution maps, the maps then needed to be calibrated in order to simulate meaningful pollen concentrations. To do so, we have simulated the ragweed pollen season of 2012 using the tuned model with the nine uncalibrated distribution maps in turn. Based on the same subset of observations as for the tuning of $Q_{\text{pollen,day}}$, the overall bias between modeled and observed pollen concentrations was calculated for each of the distribution maps. These biases were then used to calibrate the maps. Interestingly, this simple procedure was sufficient to ensure that the total numbers of plants in a given region are of the same magnitude, regardless of the kind of inventory data used or the spatial resolution of the maps. The total amount of plants in the 'source region' is given in Table 3.3 for each of the distribution maps. We are well aware of the fact that such a calibration strongly reduces the differences between the distribution maps and therefore assimilates the results for the different maps. However, leaving this step out would result in inconsistent maps when combining the high quality map of the 'receptor region' and the maps with reduced quality in the 'source region'. The resulting pollen concentrations would be meaningless. Examples

Table 3.3: Total number of plants in the 'source region' for the different distribution maps.

Map	Number of plants
#-1	3333490
cl-1	3156454
yn-1	1203854
#-5	2530237
cl-5	2449936
yn-5	1635872
#10	2310957
cl-10	2453906
yn-10	1949553

of the final distribution maps are shown in Figure 3.2. The supplementary material includes plots of all 9 different maps.

3.3.2 Tuning of the emission parameterization EMPOL

EMPOL contains several parameters that are plant-dependent and need to be tuned when a new pollen emitting species is introduced. One of the main features of this parameterization is the distinction of two steps that represent different processes that take place during pollen emission: (1) the release of pollen grains from the flowers into a reservoir, and (2) the entrainment of pollen from the reservoir into the atmosphere. Please refer to Zink et al. (2013) for a detailed description of the parameterization. The following parameters were specified for the use with ragweed pollen:

- $Q_{\mathrm{pollen,day}}$ - the maximum number of pollen that can be released per day on one square meter if the emission conditions are perfect

- $Q_{\mathrm{pollen,\Delta t}}$ - the maximum number of pollen that can be released per time step on one square meter if the emission conditions are perfect

- $f_{\mathrm{R,T}}$ - pollen release as a function of the temperature

- $f_{\mathrm{R,RH}}$ - pollen release as a function of the relative humidity

- $f_{\mathrm{E,TKE}}$ - entrainment of pollen into the atmosphere as a function of the turbulent kinetic energy

- Ψ_{random} - loss of pollen from the pollen reservoir due to random processes

EMPOL has been designed in a way that allows the tuning of these parameters based on laboratory experiments. For lack of such data, we formulated the parameters based
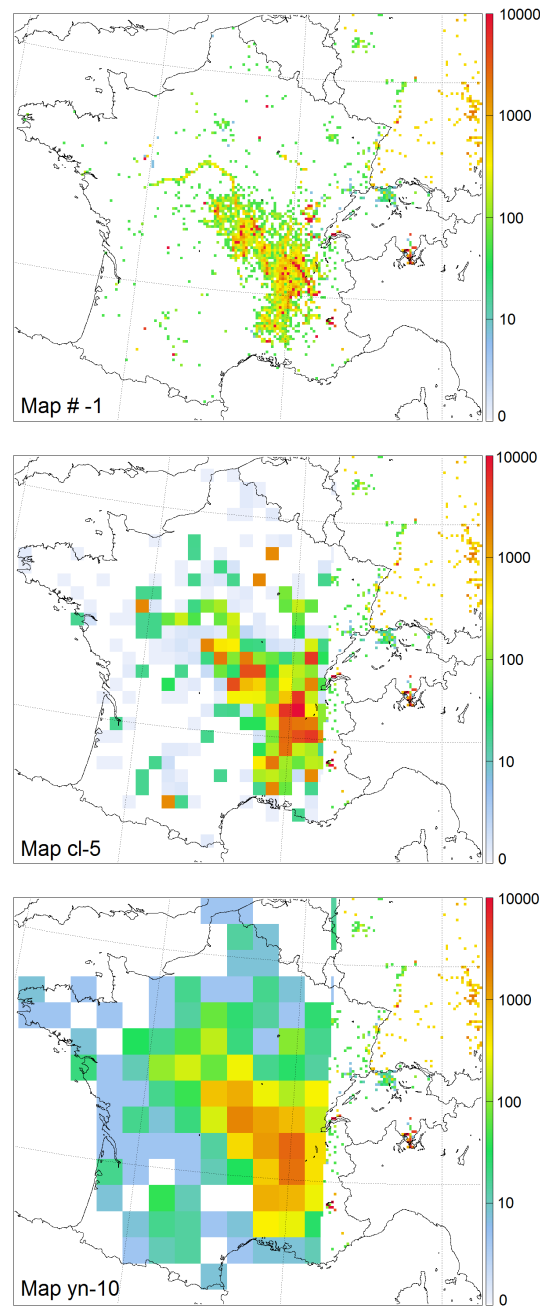
Figure 3.2: Three examples of distribution maps used in this study. The reference map
(#-1) is based on continuous quantitative information on a spatial resolution of 1×1 grid
points. Map cl-5 is based on classified inventory data and has a spatial resolution of 5×5
grid points. Map yn-10 is based on absence/presence inventory data and has a spatial
resolution of 10×10 grid points. The coloring denotes the number of plants per grid cell.
Note that the reduction of resolution/quality is only applied in the 'source region' (i.e. west
of Switzerland). The images only show the part of the distribution maps that includes the
two regions of interest: the Rhône-Alpes region and Switzerland.

on literature and a comparison of measured and simulated pollen concentrations. The simulations used for the tuning of the emission parameterization were carried out for the entire ragweed pollen season of 2012 and based on the reference map.

First, the functions relating the amount of released pollen grains to temperature and relative humidity were formulated on the basis of the description of ragweed pollen emission in Bianchi et al. (1959). In a second step, they were tuned using bi-hourly data at French observational sites. Using only sites close to dominant local sources, we tried to minimize the impact of dispersion processes on the simulated pollen concentrations. The optimized functions are:

$$f_{\text{R,T}} = \frac{1}{1 + e^{-0.2\,T + 60}} \tag{3.1}$$

$$f_{\text{R,RH}} = \frac{1}{1 + e^{20\,rh - 12}} \tag{3.2}$$

Herein, T denotes the temperature in K and rh the relative humidity (dimensionless) on the lowest model level.

The function describing the influence of the turbulent kinetic energy on the amount of entrained pollen grains was based on the function already present for birch pollen emission (see Zink et al. (2013)). It was only slightly adapted using bi-hourly observational data:

$$f_{\text{E,TKE}} = \frac{1}{1 + e^{-2.5\,TKE + 4}} - 0.018. \tag{3.3}$$

TKE denotes the turbulent kinetic energy in m^{2}s^{-2} on the lowest model level.

Assuming that the physical processes leading to a loss of pollen from the reservoir due to random processes are comparable between grass and ragweed, the parameter describing this loss was set equal to the one for grass:

$$\Psi_{\text{random}} = \exp\left\{ \frac{\ln 0.5 \cdot \Delta t}{811s} \right\}, \tag{3.4}$$

where Δt is the timestep of the model given in seconds. This formulation leads to a half-life of the pollen in the reservoir of 811 seconds.

$Q_{\text{pollen,day}}$ was tuned using daily values of measured pollen concentrations in France. From the available observations, we have chosen a subset based on the following reasoning. $Q_{\text{pollen,day}}$ reflects pollen release under perfect conditions: the entire area is covered with ragweed plants, the pollen season is at its climax, and all of the relevant meteorological variables strongly promote pollen emission. Assuming that the concurrence of such favorable conditions should lead to very high pollen concentrations, only days with more than 40 pollen per cubic meter in the measured pollen concentrations were used. This value represents the strongest pollen class with respect to the operational pollen forecasts for allergenic people in Switzerland

Table 3.4: Classification of ragweed pollen concentrations (C_{pollen}) used for the operational pollen forecasts at MeteoSwiss (Gehrig et al. 2013).

Pollen class	Pollen concentration in m^{-3}
low pollen load	$C_{\mathrm{pollen}} < 5$
moderate pollen load	$5 \leq C_{\mathrm{pollen}} < 10$
strong pollen load	$10 \leq C_{\mathrm{pollen}} < 40$
very strong pollen load	$40 \leq C_{\mathrm{pollen}}$

(Table 3.4). Eliminating the overall seasonal bias between modeled and observed mean pollen concentrations, $Q_{\mathrm{pollen,day}}$ was set to $27 \cdot 10^4$ pollen per square meter and per day. The maximum amount of pollen that can be released on one square meter per time step considers the fact that the flowers can run out of ripe pollen grains before the end of the day under ideal conditions. In our setup, the flowers will have released all of their ripe pollen grains after 9 hours of optimal conditions:

$$Q_{\mathrm{pollen,\Delta t}} = \frac{Q_{\mathrm{pollen,day}} \cdot \Delta t}{9 \cdot 3600}. \tag{3.5}$$

In addition to the parameterization described in Zink et al. (2013), we have introduced a 'precipitation memory' to EMPOL. In the original version of the parameterization, pollen entrainment can start directly after the end of a rain event. In reality, pollen will not be released as long as the flowers are wet. Therefore, a certain time lag between the end of precipitation and the start of entrainment should be introduced, accounting for the time that plants need to dry. To describe this process in the model, we have introduced a water reservoir R_{precip}. This reservoir is filled during precipitation events with a maximum content of 1 mm. As soon as precipitation stops, the water in the reservoir starts to evaporate. The evaporation rate is linearly dependent on the relative humidity with a fixed point of zero evaporation at 100% relative humidity. In our implementation, drying of the full reservoir takes 2 hours when the relative humidity is 30%.

Similarly to the explanations in Zink et al. (2013) concerning the parameters and functions for birch, the presented formulations for ragweed should be seen as an 'expert first guess' that ought to be refined using in-situ or laboratory measurements of pollen emission. However, since our study is focused on the relative differences between several simulations, the absolute values of pollen concentrations that depend on the tuning of the emission parameterization are of minor importance.

3.3.3   Description of the pollen season

COSMO-ART and EMPOL require certain input fields such as a mathematical description of the pollen season ($f_{Q,seas}$, see Zink et al. (2013)). In lack of a sophisticated pollen season model, we have developed a simple model based on French pollen data that is functional with respect to our needs: it reduces the maximum number of potentially available pollen grains ($Q_{pollen,day}$) at the beginning and in the end of the pollen season. Basically, it is a climatological curve of the pollen season based on the data in the region of interest (= the source region of our study). Pollen seasons outside of this region (e.g., in Hungary) or year-to-year differences resulting from different weather conditions are disregarded. It should therefore not be used for simulations regarding a wider region or predictions of pollen concentrations. This pollen season model renders a 2D-field of the current pollen potential (a value between 0 and 1) for each day during the pollen season.

The model of the pollen season has been developed using French pollen data from the years 2000 to 2012 (daily mean pollen concentrations). For each observational site, it calculates the mean starting and ending date of the pollen season, defined as the first and last occurence of more than 10 pollen per cubic meter, respectively. These dates are then interpolated onto our model grid. Based on time series of pollen concentrations, the course of the pollen season is assumed to be Gaussian, which leaves two parameters to be fixed: μ gives the position of the peak and σ defines the width of the curve. Using the mean starting and ending dates of the pollen season, these two parameters are set for each grid point. μ is taken as the day in the middle between the starting and ending date. In the Gaussian function, 99.73% of all values lie within the range of $\pm 3\sigma$. Therefore, the length of the pollen season (= ending date - starting date) is taken as 6 σ. In our case, it is important to have a peak value of one and a value of zero at the starting and ending dates of the pollen season. The prefactor for the Gaussian curve was adjusted accordingly.

3.3.4   Statistical measures

The different simulations were validated using several statistical scores based on simulated and observed pollen concentrations. Using France as the main source region and Switzerland as the receptor region, only the Swiss observational sites that are influenced by French ragweed populations were used. This excludes the sites in the Ticino region in southern Switzerland which are mainly influenced by the adjacent Italian ragweed populations. Additionally, the observational site of Visp in the mountainous upper Rhône valley (altitude: 650 m asl) was disregarded. Due to the coarse spatial resolution of the model, the corresponding grid point has an altitude of 1482 m asl, thus the simulated pollen concentrations cannot be compared

to observational data. Since the distribution maps were resampled only in the western part of the domain, only days with a predominant westerly flow were taken into account. Westerly flows were identified using the simulated wind direction of the grid point representing Berne, a town approximately in the center of Switzerland. The wind direction was taken from model level 42 which, in Berne, corresponds to ≈ 3000 m asl. The day was only taken into account when the mean wind direction from 6 to 18 UTC was between 180° and 360°. We have tested different 'definitions' of westerly flows, e.g., different sites or spatial aggregations. This did not yield different results in the statistical measures.

Using measured and simulated pollen concentrations, we have calculated the correlation coefficient r^2 and its corresponding p-value, the root-mean-square-error (in the following: RMSE) and the index of agreement d$_1$ (Willmott et al. 1985):

$$d_1 = 1 - \frac{\sum_{i=1}^{N} |P_i - O_i|}{\sum_{i=1}^{N} \left(|P_i - \overline{O}| + |O_i - \overline{O}| \right)}. \tag{3.6}$$

This score uses the sums of the absolute values of the errors between observations (O_i) and modeled values (P_i). $\overline{O}$ denotes the observational mean and N the number of data points. d$_1$ takes values between zero and one, with one being a perfect score.

While the RMSE and d$_1$ are based on continuous values of pollen concentrations,

Table 3.5: 2×2 contingency table: pairs of measured and simulated values are classified as hits (a), false alarms (b), misses (c) and correct negatives (d).

		Observation	
		yes	no
Forecast	yes	a	b
	no	c	d

the Pierce Skill Score (PSS), Threat Score (TS) and False Alarm Ratio (FAR) are categorical scores (Wilks 2006): the daily values of the pollen concentrations are interpreted as presence/absence information of pollen grains. Any pollen concentration above a certain threshold is taken as an 'event', while the pollen concentrations below this threshold count as a 'non-event'. In order to investigate the sensitivity of the result on the choice of the threshold, we have used two different thresholds. Respecting the fact that ragweed pollen concentrations are very low in Switzerland (they rarely exceed 5 pollen per cubic meter of air), both thresholds are fairly low: First, we

used 1 pollen per cubic meter of air to define a pollen event. This corresponds to a presence/absence information of pollen in the air. Second, we used a threshold of 5 pollen per cubic meter of air. This corresponds to a pollen class of 'moderate' according to Table 3.4. However, a threshold of 5 pollen per cubic meter leads to only a few days being counted as an event: 25 events for the region 'West', 12 events for the region 'Center' and only 2 events for the region 'East' (details regarding these regions can be found in Section 3.4.1). Especially for the region 'East', this leads to highly unreliable statistical results. It has to be noted that measurements of such low pollen concentrations are rather unreliable. With only a few pollen grains in the air, it is incidental how many (or even: if any) pollen grains find their way into the pollen trap and get registered. However, using a threshold of 1 pollen per cubic meter, it is not possible to falsely declare a pollen 'event': as soon as at least one pollen grain is detected in the trap, we can be sure that there are pollen grains in the air. Taking these two 'definitions' of a pollen 'event', the modeled and observed pollen concentrations are sorted into 2x2 contingency tables (Table 3.5). For each of the simulations and thresholds, a separate contingency table is determined. These contingency tables can then be used to calculate the following skill scores.

$$\text{PSS} = \frac{ad - bc}{(a + c)(b + d)}. \tag{3.7}$$

PSS describes the performance of a model compared to an unbiased random forecast. It can take values between -1 and 1. Forecasts worse than a random forecast render negative values. Forecasts with some skill better than random result in positive values. Rare events that are correctly forecast count more than frequent events.

$$\text{TS} = \frac{a}{a + b + c}. \tag{3.8}$$

TS gives the fraction of correct forecasts without taking into account the correct non-events. This score is usually chosen for rare events where the correct prediction of non-events is relatively easy and thus meaningless. For ragweed pollen concentrations, this is the case in Switzerland. TS can take values between zero and one, with one being a perfect score.

$$\text{FAR} = \frac{b}{a + b}. \tag{3.9}$$

FAR gives the fraction of simulated events that were not observed. It takes values between zero and one, a perfect forecast yields a value of 0.

Table 3.6: Allocation of the individual observational stations to the Swiss regions 'West', 'Center' and 'East'. The column 'Distance' gives the approximate distance of the stations in these regions to the main pollen sources in the Rhône-Alpes region (France).

Region	Stations	Distance
West	CHGENE, CHLAUS, CHNEUC, CHLACH	100-200 km
Center	CHBERN, CHBASE CHLUZE, CHZUER	250-350 km
East	CHMUEN, CHBUCH CHDAVO	400 km

3.4   Results

3.4.1   Differences resulting from the distribution maps

Because pollen observations are point values and modeled values represent a bigger region (here: $\approx 6.6 \times 6.6 \text{ km}^2$), statistical scores for individual pollen sites should be interpreted with caution. To improve the reliability of the results, we have averaged the statistical scores of all stations within three regions of Switzerland (Table 3.6). Having the main source of pollen grains situated west of Switzerland in the French Rhône-Alpes region, the regions can be seen as representations of different distances to the pollen source: the western stations are relatively close to the sources, the eastern stations are far away from the sources, while the central stations fall in-between. Table 3.7 shows the regionally averaged statistical scores for each of the distribution maps and the mean values over all of the maps. The best/worst results are highlighted revealing some interesting patterns:

- For the categorical scores using a threshold of one pollen per cubic meter (upper third of the table), the best scores accumulate in the left columns of the colored part of the table: the maps with the highest spatial resolution (#-1, cl-1 and yn-1). The worst results accumulate in the right columns: the maps with the lowest spatial resolution (#-10, cl-10 and yn-10). Comparing the maps with the same spatial resolution, a slight tendency towards the maps with detailed quantitative information can be found. However, the differences are small and inconsistent for the different regions and spatial resolutions.

- For the categorical scores using a threshold of five pollen per cubic meter (middle third of the table) and the scores based on continuous pollen concentrations (lower third of the table), both the best and the worst results accumulate in

Table 3.7: Statistical scores for each of the distribution maps. The third column gives the threshold in pollen per cubic meter of air used to separate events and non-events for the categorical scores. The fourth column gives the mean value of all distribution maps. The individual results for the different maps are given in the columns 5 to 13. In these columns, scores are highlighted in green to indicate the best results and in red to indicate the worst results.

Score	Region	Threshold	Mean	#-1	cl-1	yn-1	#-5	cl-5	yn-5	#-10	cl-10	yn-10
PSS	West	1	0.54	0.54	0.57	0.59	0.57	0.54	0.52	0.50	0.52	0.51
	Center	1	0.57	0.62	0.61	0.45	0.58	0.60	0.60	0.57	0.56	0.57
	East	1	0.62	0.65	0.66	0.59	0.67	0.66	0.56	0.63	0.66	0.53
TS	West	1	0.59	0.60	0.61	0.60	0.61	0.60	0.58	0.58	0.58	0.57
	Center	1	0.42	0.45	0.44	0.36	0.42	0.43	0.44	0.41	0.40	0.41
	East	1	0.30	0.30	0.31	0.31	0.31	0.31	0.29	0.29	0.31	0.27
FAR	West	1	0.31	0.32	0.30	0.24	0.30	0.32	0.30	0.33	0.33	0.32
	Center	1	0.47	0.47	0.47	0.48	0.48	0.48	0.44	0.48	0.49	0.48
	East	1	0.66	0.68	0.66	0.64	0.66	0.66	0.66	0.67	0.66	0.68
PSS	West	5	0.37	0.35	0.34	0.38	0.38	0.38	0.41	0.36	0.36	0.38
	Center	5	0.37	0.56	0.50	0.10	0.42	0.51	0.31	0.28	0.38	0.28
	East	5	0.46	0.43	0.43	0.50	0.46	0.44	0.48	0.46	0.46	0.47
TS	West	5	0.28	0.26	0.25	0.29	0.28	0.28	0.31	0.27	0.27	0.29
	Center	5	0.17	0.22	0.19	0.08	0.18	0.21	0.19	0.14	0.16	0.14
	East	5	0.18	0.12	0.12	0.50	0.12	0.12	0.25	0.12	0.12	0.16
FAR	West	5	0.64	0.66	0.67	0.58	0.64	0.65	0.61	0.66	0.67	0.64
	Center	5	0.74	0.74	0.77	0.58	0.74	0.73	0.71	0.80	0.79	0.80
	East	5	0.67	0.88	0.88	0.00	0.75	0.88	0.50	0.75	0.75	0.67
d_1	West		0.45	0.39	0.38	0.52	0.44	0.43	0.50	0.45	0.42	0.48
	Center		0.54	0.52	0.52	0.56	0.55	0.54	0.55	0.55	0.54	0.55
	East		0.52	0.46	0.47	0.57	0.51	0.50	0.56	0.54	0.52	0.55
RMSE	West		9.98	12.91	13.82	5.91	10.07	11.28	7.18	9.25	11.24	8.17
	Center		3.22	4.28	4.34	2.45	3.23	3.47	2.56	2.82	3.17	2.69
	East		1.64	2.21	2.22	1.14	1.73	1.83	1.25	1.45	1.62	1.35
r^2	West		0.40	0.35	0.34	0.40	0.39	0.37	0.42	0.44	0.43	0.43
	Center		0.45	0.41	0.40	0.49	0.46	0.43	0.48	0.46	0.43	0.48
	East		0.44	0.37	0.37	0.54	0.42	0.40	0.50	0.46	0.43	0.48
p-value	West		0.04	0.07	0.08	0.03	0.04	0.04	0.02	0.03	0.03	0.02
	Center		0.04	0.08	0.08	0.02	0.03	0.05	0.02	0.02	0.04	0.02
	East		0.04	0.06	0.06	0.01	0.04	0.04	0.02	0.03	0.03	0.03

Table 3.8: Observed (obs) and simulated (mod) daily mean pollen concentrations on September 5th, 2012, at the Swiss observational sites. The simulation was done using the reference map #-1. Concentrations are given in pollen per cubic meter of air.

Station	obs	mod
CHBASE	4	433
CHBERN	0	877
CHBUCH	24	239
CHDAVO	2	104
CHGENE	6	443
CHLACH	2	1125
CHLAUS	2	345
CHLUZE	8	752
CHMUEN	6	746
CHNEUC	4	697
CHZUER	6	1124

the left columns of the colored part of the table (maps #-1, cl-1 and yn-1). A clear ranking of the distribution maps can be derived from this pattern: the best results are achieved when using map yn-1, the worst results are achieved for the maps #-1 and cl-1. All the maps with lower resolutions are in-between. Apparently, when using continuous or classified inventory data as a basis, maps with lower spatial resolution should be prefered. When using presence/absence inventory data it is the opposite: the maps with higher spatial resolution lead to better results. However, when looking at the maps with the same spatial resolution, a clear preference for the presence/absence maps can be seen.

The distance between source and receptor region does not have a clear influence on the results (compare the column 'Mean' in Table 3.7): some of the scores are degrading with increasing distance (e.g., TS), some are ameliorating with increasing distance (e.g., RMSE), while others are neither degrading nor ameliorating (e.g., d_1). The spread between the different maps also shows no clear dependance on the distance to the main source.

3.4.2   Long-distance transport from Hungary

The importance of a comprehensive calibration of the distribution map can be seen when looking at a case of long-distance transport from the Pannonian Plain. For a visual review of the data, we have plotted time series of the measured and simulated pollen concentrations at each of the observational sites (examples of such time series
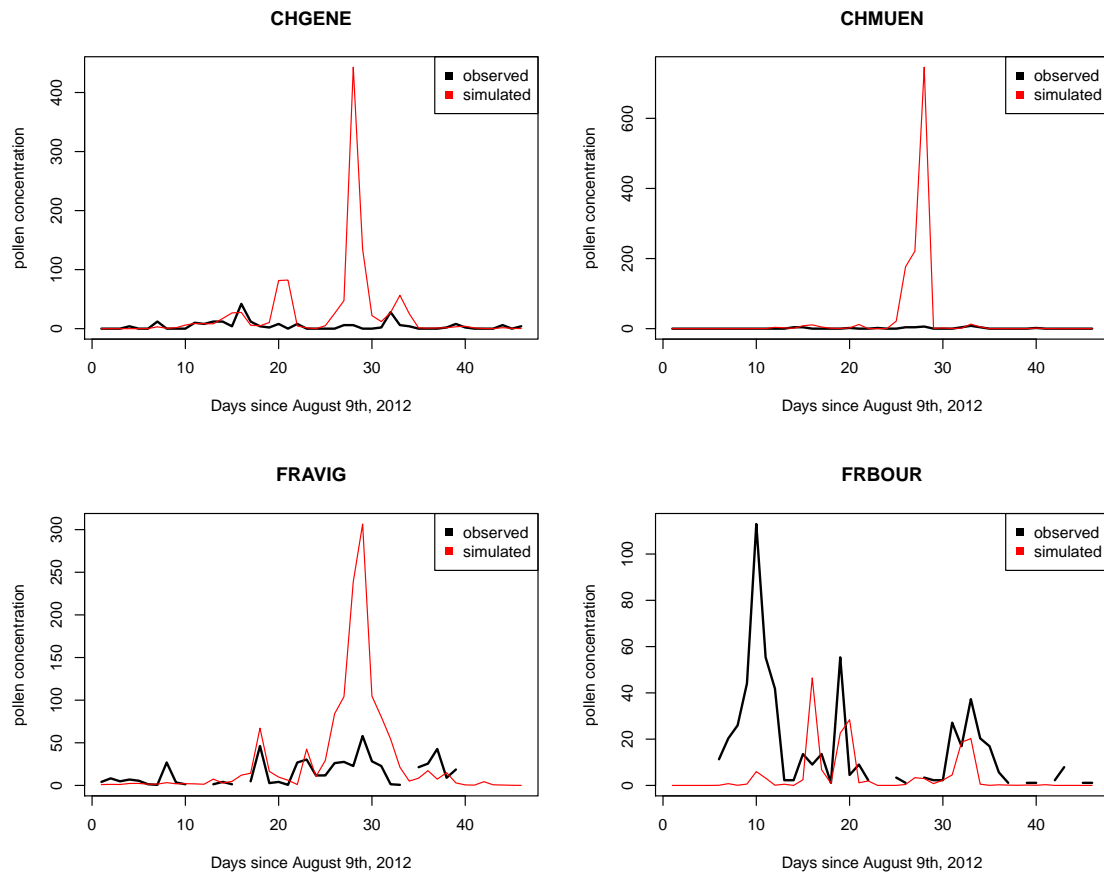
Figure 3.3: Time series of pollen concentrations (daily mean values given in pollen per cubic meter of air) at four observational sites. The reference map #-1 has been used as the plant distribution map in the simulation. A peak pollen concentration can be observed at the Swiss sites and some of the French sites (here: CHGENE, CHMUEN and FRAVIG) in the simulated values. It is absent in the observations and cannot be observed at some of the French sites (here: FRBOUR). Note the different vertical scales.
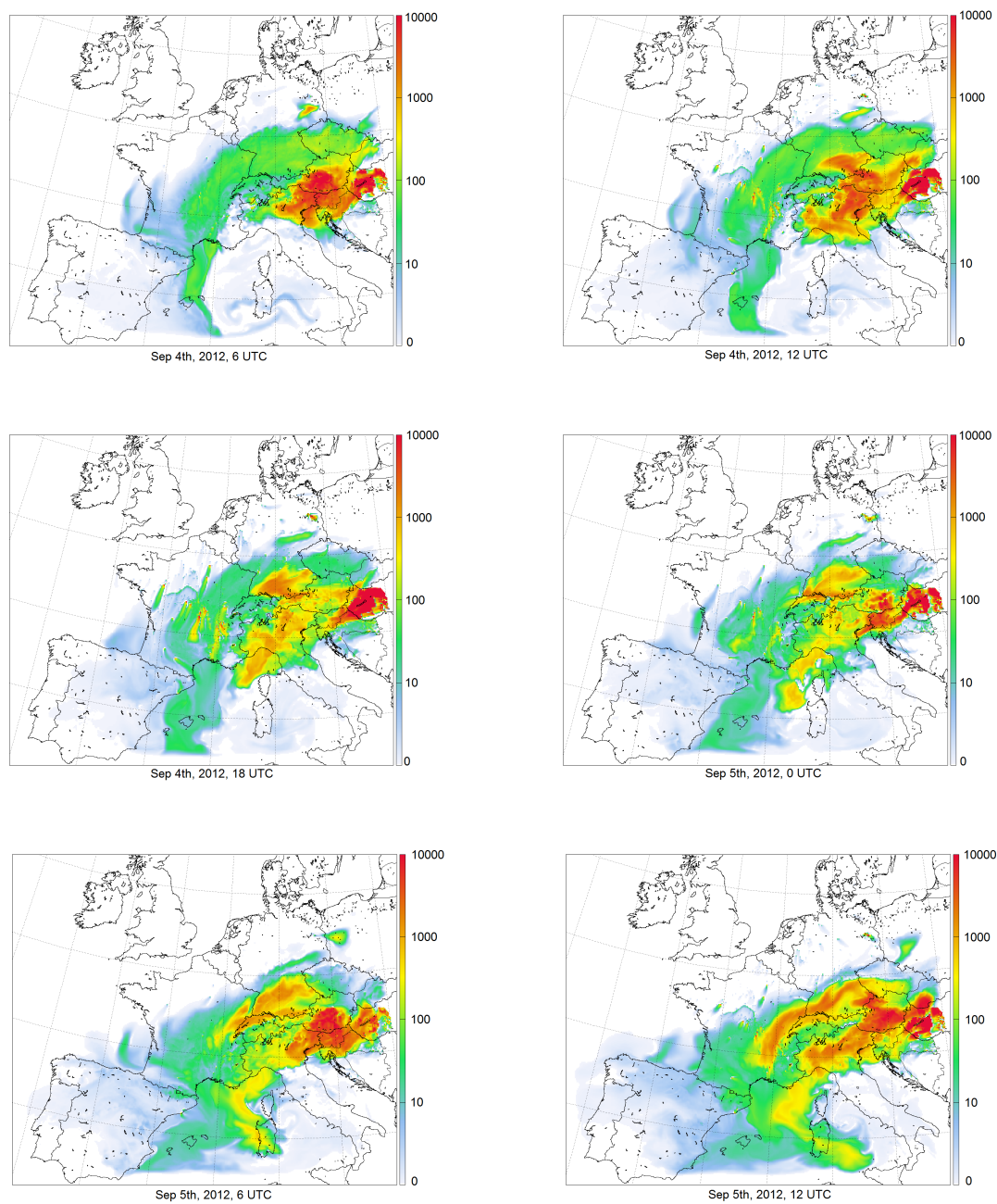
Figure 3.4: Spatial distribution of the pollen concentration from Sep 4th, 6 UTC, to Sep 5th, 12 UTC, in 6-hourly steps. The coloring denotes the pollen concentration in pollen per cubic meter of air (current value at that time step, no temporal averaging). The plots show a pollen cloud originating in the Pannonian Plain on its way to France passing over Italy, Austria, Germany and Switzerland.

are shown in Figure 3.3). Looking at these time series, a striking peak pollen concentration on September 5th, 2012, in the simulated values attracts notice. This simulated peak is present in any of the simulations regardless of the distribution map. It exhibits pollen concentrations of up to 1125 pollen per cubic meter of air (daily mean value). Interestingly, this peak is strongly visible in the simulations for the Swiss stations and to a lesser extent at many of the French stations. The measurements at the corresponding observational sites show values between 0 and 24 pollen per cubic meter of air (Table 3.8). Since pollen sources are scarce in the proximity of most of the Swiss observational sites, we suspected an episode of increased long-distance transport to be the cause of this intense peak. 2D-plots of the pollen concentration at several points in time before the peak support this assessment: the pollen grains causing this peak in the modeled concentrations originate in the Pannonian Plain (Figure 3.4). Note that this day apparently has a large-scale easterly wind direction - and therefore was not part of the sample yielding the statistics in Section 3.4.1. Knowing that ragweed is very abundant in the Pannonian Plain, long-distance transport of measurable amounts of pollen from this region is plausible (see also Zink et al. (2012) where such an episode of long-distance transport from Hungary to Germany has been studied). However, in our case the amount of pollen grains appears to be largely overestimated. The cause was found in the distribution map. Combining inventory data from different sources into one distribution map is based on the assumption that the collection of data is done in a similar manner for all of these inventories. In other words: a field of 1000 plants should render the same amount of plants registered in any of the inventories. However, due to the nature of the different inventories (absence/presence data, classified data, continuous data), this is not the case. It is not even true within one type of inventory (e.g. classified data) since the methods to gross up the count data (e.g. from ten square meters where the plants are actually counted to the entire size of the field) can be different for different inventories. Additionally, the range of classes do not have to coincide for different inventories. Therefore, combining different inventories in a single distribution map poses the danger of generating inconsistent values.

In order to produce reasonable pollen concentrations in the model, the distribution map has to be calibrated (as described in Section 3.3.1). If this calibration factor is calculated based on paired series of measured and simulated pollen concentrations (as it is the case here), it greatly depends on the choice of observational sites. Since our exercise is aimed at the plant localities in France and their influence on Swiss observational sites, we calibrated the distribution maps based on French observational sites only. Looking at observational sites in the Pannonian Plain, a different calibration factor would have been found. This explains why the pollen concentration in the Pannonian Plain is greatly overestimated: the plant abundance in the map would be

smaller if we would have used the Pannonian Plain as the tuning region (based on a rough estimate of the calibration factor derived for the Pannonian Plain). In our exercise, we are not primarily interested in the pollen concentrations of the Pannonian Plain and can therefore disregard the tuning of this part of the distribution map. However, in an application where the modeling system is meant to be used in a wider region, it is not possible to use a single tuning factor for the entire map. It is essential to conduct a seperate tuning for each of the included inventories. Since we did not do this, our distribution maps are only suitable for the regions that are primarily influenced by the French Rhône-Alpes region.

3.5   Summary and conclusions

One of the key factors of successful numerical pollen forecasts is a sophisticated map of the pollen sources. Since the degree of detail of the data used to construct such distribution maps varies greatly, we have conducted an experiment to study the influence of different maps on the performance of a pollen forecast. Our study concentrates on a special setting: a 'receptor region' whose local pollen production is fairly low and a 'source region' with a high number of pollen producing plants. The pollen concentrations in the receptor region are mainly produced in the source region. We have used the French Rhône-Alpes region as the source region and Switzerland as the receptor region. For the source region, several different distribution maps were designed representing the different levels of the quantitative information included in plant inventory data and different spatial resolutions of the distribution maps. In both directions, we have introduced three levels of detail leading to a total of nine different distribution maps. For the map in the receptor region, all available information has been used. Please note that all of the results presented here are only valid for this specified setting.

Using these different distribution maps, the ragweed pollen season of 2012 has been simulated. For each of the maps, statistical scores have been computed using observed and simulated pollen concentrations at 11 Swiss observational sites. These sites are sorted into three regions 'West', 'Center', and 'East' that represent different distances to the main pollen source in order to show whether the proximity to the source has an impact on the spread and mean values of the calculated scores.

We have found that neither the spread between the scores for the different distribution maps nor the mean values of the scores clearly decrease with increasing distance to the main pollen source. Apparently, the pollen sources in the Rhône-Alpes region are intense enough to have an impact on the pollen concentrations throughout northern Switzerland. Based on the observational sites in the study with distances of 100 km to 400 km to the main source, it is not possible to give a minimal distance at

which differences in the distribution map become irrelevant. That is to say, main sources that are within a radius of at least 400 km can clearly affect local pollen concentrations and can therefore not be ignored.

Looking separately at the different types of scores used (the categorical scores with two different thresholds and the scores based on continuous pollen concentrations), two different statements can be made. The categorical scores (threshold 1 pollen per cubic meter of air) are relatively insensitive to the quantitative information of the inventory data. But they highlight the importance of a high spatial resolution of the distribution map. On the contrary, the scores based on continuous pollen concentrations and the categorical scores using a threshold of 5 pollen per cubic meter do not show a clear tendency regarding the spatial resolution. But looking at the maps with the same spatial resolution, these scores clearly favor the maps based on presence/absence inventory data. Combining these two results, we conclude that the best results are obtained when using presence/absence data to construct a distribution map with a high spatial resolution. This rather unexpected result regarding the quantitative information may be explained by the nature of the inventories: the quantitative information found in plant inventories is a snapshot taken at the moment of the inventory-taking. Usually, there is no information about the further development of the population: whether the number of plants is increasing or decreasing. Additionally, the absolute numbers given in the inventories are extrapolations that are not necessarily based on the same assumptions in different inventories. Usually, the accuracy of estimations of population sizes is worse for large populations. All things considered, it seems that using the quantitative information found in the inventories adds uncertainty to the data rather than providing additional value.

A day with very high simulated pollen concentrations in a majority of stations has been used to further investigate the impact of a calibration factor. It has been found that it is very important to carry out a separate calibration for each of the inventory data sets used to construct the distribution map. This is due to the different nature of the inventories regarding the quantitative information. Since many of the inventories lack detailed information about the abundance of plants, this figure has to be derived by tuning the distribution map using pollen observations. Interestingly, using such a tuning, the final number of plants is in the same order of magnitude for all of the nine distribution maps regardless of the kind of inventory that has been used and regardless of the spatial resolution of the map.

Considering all of the results mentioned above, we conclude that knowledge about the location of plants is more important than their abundance provided that pollen observations in the given region are available to derive a local calibration factor. Apparently, presence/absence inventories are sufficient to construct satisfactory distribution maps when studying long-distance transport. Moreover, it may prove

useful to leave out available quantitative information and concentrate on the locations only. On the other hand, a high spatial resolution of the distributon map should be sought.

A future study could investigate how the calibration should be done regarding, e.g., the (1) subset of observations used for the calculation of a calibration factor, (2) the minimum/maximum size of the regions the same factor can be used for, or (3) differences regarding main source regions and regions with only a few small plant populations. It would also be interesting to investigate how different types of distribution maps (e.g., based on inventory data, based on land use data sets, based on maps of potential distributions) may be combined into a single distribution map.

Acknowledgements

Supplementary materials

Content:

Table 3.9 gives an overview about the ragweed inventory data sets of various European countries that were used in this study.

Table 3.10 gives an overview about the Swiss ragweed inventory data sets that were used in this study.

Table 3.11 shows the pollen observationals sites used in this study.

Figures 3.5, 3.6 and 3.7 show the nine different distribution maps used in the exercise.

Table 3.9: Overview of the ragweed inventory data sets of various European countries used in this study. The third column gives the type of the inventory data regarding the quantitative information: (1) numbered data, (2) classified data, and (3) presence/absence data.

Country	Data owner/reference/homepage	Type
Austria	Umweltbundesamt	3
	www.umweltbundesamt.at	
Bavaria	Projektgruppe Biodiversität und Landschaftsökologie	2
	Nawrath and Alberternst (2011)	
Croatia	Flora Croatica Database	3
	Faculty of Science	
	University of Zagreb	
	Nikolić (2011)	
Denmark	The Danish Nature Agency	1
	www.naturstyrelsen.dk/Naturbeskyttelse/invasivearter/Indberetning/	
France	Fédération des conservatoires botaniques nationaux	2
	Petermann (2011)	
Germany	Berliner Aktionsprogramm gegen Ambrosia	1
	Freie Universität Berlin	
	Institut für Meteorologie	
Hungary	Institute of Geodesy, Cartography and Remote Sensing	2
Liechtenstein	Amt für Umwelt	3
	Abteilung Landwirtschaft	
	www.lwa.llv.li	
Slovenia	Umweltbundesamt (Austria)	3
Spain	Departament de Biologia Animal, Biologia Vegetal i Ecologia	1
	Universitat Autònoma de Barcelona	
	Fernández-Llamazares et al. (2012)	

Table 3.10: Overview of the Swiss ragweed inventory data used in this study. The Swiss data is not available at a national basis but is gathered by the different cantons. The third column gives the type of the inventory data regarding the quantitative information: (1) numbered data, (2) classified data, and (3) presence/absence data.

Swiss canton	Data owner/reference/homepage	Type
Aargau)	Landwirtschaftliches Zentrum Liebegg Pflanzenschutzdienst/Projekte www.liebegg.ch	2
Appenzell Ausserrhoden	Departement Volks- und Landwirtschaft Landwirtschaftsamt Zentralstelle für Pflanzenschutz und Obstbau www.ar.ch/lwa	1
Berne	Amt für Landwirtschaft und Natur Fachstelle Pflanzenschutz Turolla et al. (2008)	2
Jura	Station Phytosanitaire du Canton du Jura http://geoportail.jura.ch/	2
Neuchâtel	GRINE - groupe espèces invasives de Neuchâtel Service de l'agriculture www.ne.ch/grine	1
Obwalden	Amt für Landwirtschaft und Umwelt Obwalden www.ow.ch/de/verwaltung/aemter/?amt_id=166	3
Schaffhausen	Landwirtschaftsamt	1
Schwyz	Amt für Landwirtschaft Abt. Beratung und Weiterbildung (Pflanzenschutz)	3
Solothurn	Bildungszentrum Wallierhof www.wallierhof.ch	3
St Gallen	Volkswirtschaftsdepartement Landwirtschaftliches Zentrum SG	2
Thurgau	Bildungs- und Beratungszentrum Arenenberg Pflanzenschutzdienst	3
Ticino	Phytosanitary Service of the Canton of Ticino Ferrario (2010)	2
Uri	Amt für Umweltschutz	3
Valais	Service des forêts et du paysage Section nature et paysage	3
Vaud	Département de l'économie et du sport Service de l'agriculture Agrilogie Grange-Verney	2
Zug	Kantonaler Pflanzenschutzdienst Zug LBBZ Schluechthof	3

Table 3.11: Observational sites for pollen measurements in France (FR...) and Switzerland (CH...) used in the present study. Longitude (Lon), latitude (Lat) and altitude (Alt) of the observational sites and the parameters of their corresponding grid points in the model (mod). Altitudes are given in m above sea level.

Station code	Town	Lon	Lat	Alt	Lon (mod)	Lat (mod)	Alt (mod)
CHBASE	Basel	7.5830	47.5638	273	7.598	47.575	286.4
CHBERN	Bern	7.4211	46.9477	570	7.362	46.970	586.7
CHBUCH	Buchs	9.4738	47.1744	445	9.559	47.179	832.2
CHDAVO	Davos	9.8555	46.8294	1600	9.824	46.880	1742.0
CHGENE	Geneva	6.1500	46.2166	380	6.097	46.213	373.2
CHLACH	La-Chaux-de-Fonds	6.8333	47.1144	1040	6.915	47.079	1037.6
CHLAUS	Lausanne	6.6500	46.5333	570	6.685	46.532	593.6
CHLUZE	Lucerne	8.2833	47.0500	460	8.325	47.108	478.5
CHMUEN	Münsterlingen	9.2333	47.6333	410	9.198	47.657	437.1
CHNEUC	Neuchâtel	6.9166	46.9833	490	7.014	46.901	443.0
CHZUER	Zurich	8.5500	47.3833	556	8.494	47.350	520.4
FRAIXP	Aix-en-Provence	5.4500	43.3700	180	5.385	43.361	176.7
FRAMBE	Ambérieu-en-Bugey	5.3589	45.9578	270	5.333	46.003	291.2
FRAVIG	Avignon	4.8102	43.9536	25	4.837	43.937	30.1
FRBAGN	Bagnols-sur-Cèze	4.6164	44.1549	51	4.649	44.169	76.9
FRBOUB	Bourg-en-Bresse	5.2269	46.1977	233	5.226	46.239	232.6
FRBOUJ	Bourgoin	6.2744	45.5917	240	6.229	45.556	647.5
FRBOUR	Bourges	2.3965	47.0829	13	2.319	47.104	138.3
FRCHAL	Chalon-sur-Saône	4.8369	46.7933	183	4.829	46.763	182.9
FRDIJO	Dijon	5.0350	47.3216	248	5.046	47.254	241.7
FRGENA	Genas	4.9966	45.7330	220	4.930	45.685	220.5
FRGREN	Grenoble	5.7363	45.1941	216	5.744	45.179	309.2
FRLYON	Lyon	4.8566	45.7633	173	4.839	45.741	196.0
FRNEVE	Nevers	3.1602	46.9861	180	3.132	46.975	189.2
FRROUS	Roussillon	4.8136	45.3727	208	4.788	45.378	209.3
FRVALE	Valence	4.8931	44.9347	125	4.917	44.903	130.0
FRVICH	Vichy	3.4219	46.1238	260	3.411	46.148	310.4
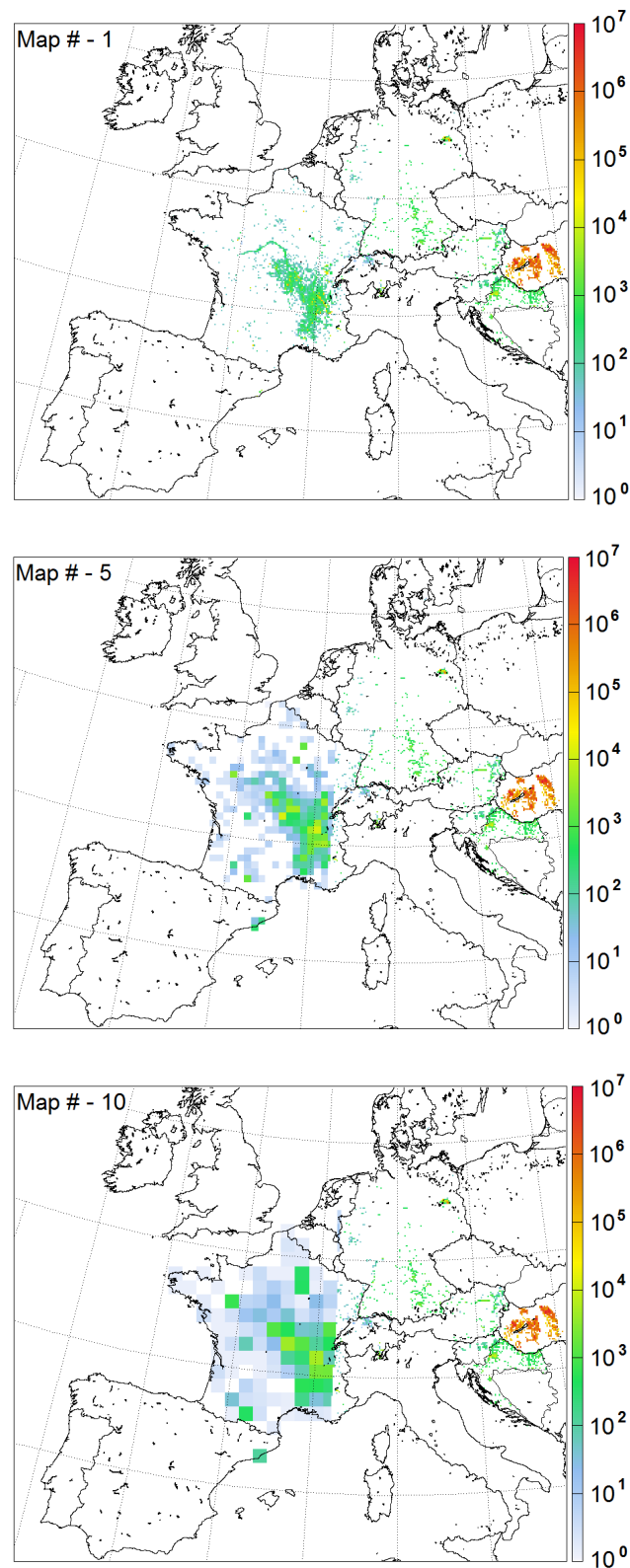
Figure 3.5: The three distribution maps based on continuous inventory data used in the exercise. The reduction of quality has been applied to the region west of Geneva only. The distribution map in the left panel (map #-1) has a horizontal resolution of 1×1 grid points. The map in the middle panel (map #-5) has a resolution of 5×5 grid points. The map in the right panel (map #-10) has a resolution of 10×10 grid points.
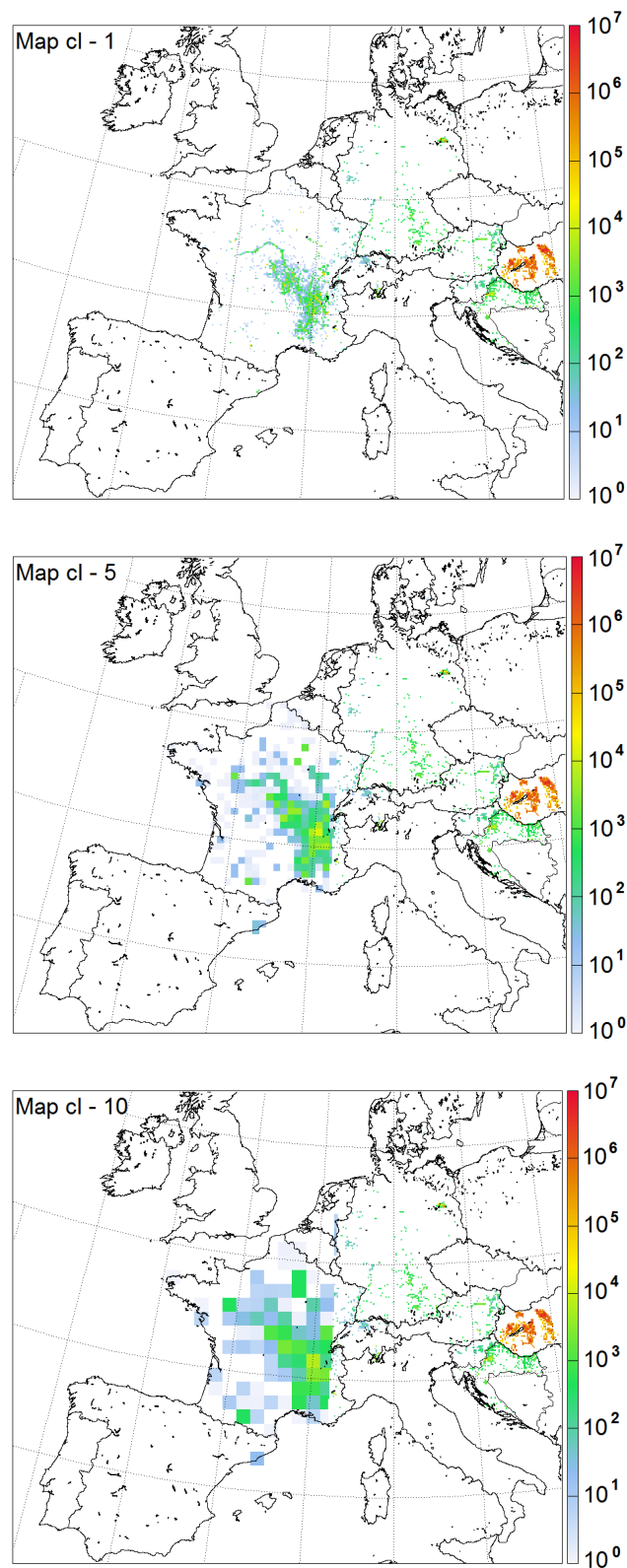
Figure 3.6: The three distribution maps based on classified inventory data used in the exercise. The reduction of quality has been applied to the region west of Geneva only. The distribution map in the left panel (map cl-1) has a horizontal resolution of 1×1 grid points. The map in the middle panel (map cl-5) has a resolution of 5×5 grid points. The map in the right panel (map cl-10) has a resolution of 10×10 grid points.
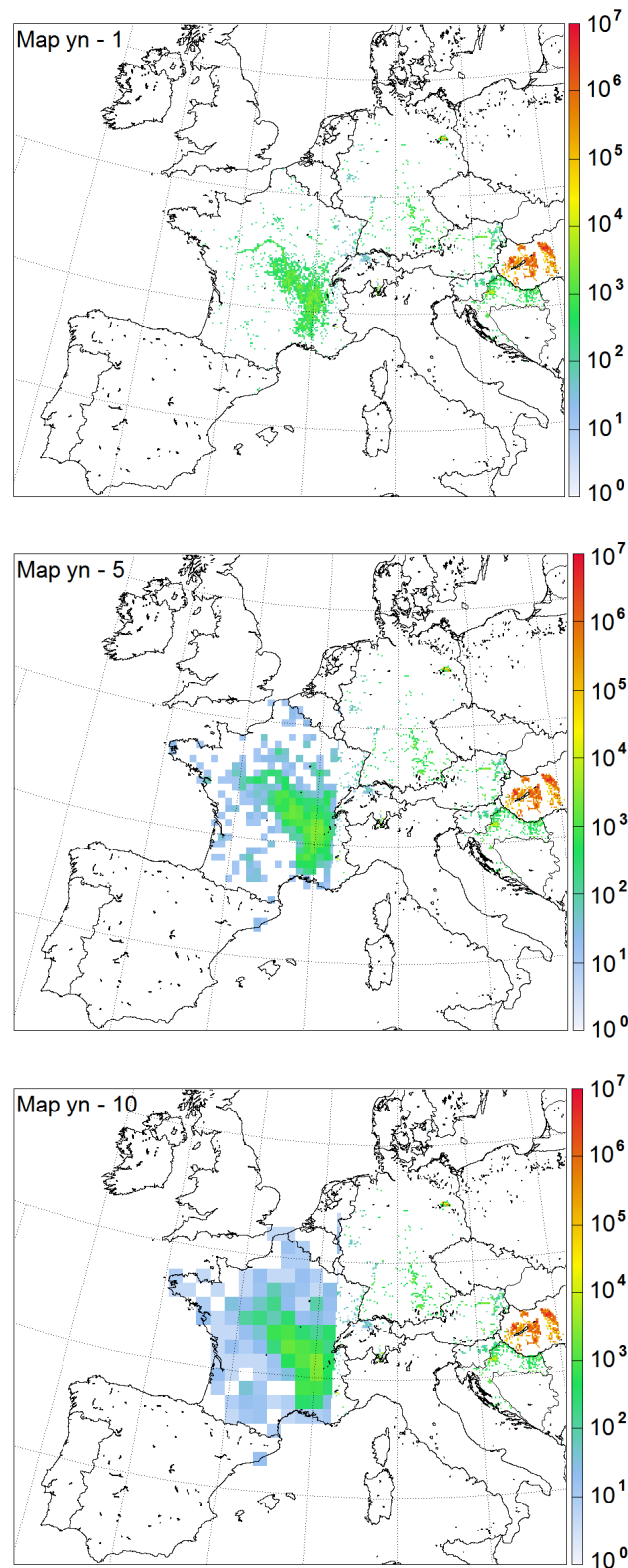
Figure 3.7: The three distribution maps based on presence/absence inventory data used in the exercise. The reduction of quality has been applied to the region west of Geneva only. The distribution map in the left panel (map yn-1) has a horizontal resolution of 1×1 grid points. The map in the middle panel (map yn-5) has a resolution of 5×5 grid points. The map in the right panel (map yn-10) has a resolution of 10×10 grid points.

Chapter 4

Numerical ragweed pollen forecasts using different source maps: a comparison for France

K. **Zink**[1], P. **Kaufmann**[2], B. **Petitpierre**[3], O. **Broennimann**[3], A. **Guisan**[3,4], E. **Gentilini**[3], M. W. **Rotach**[1]

[1] *Institute for Meteorology and Geophysics, University of Innsbruck, Austria*

[2] *Federal Office of Meteorology and Climatology MeteoSwiss, Switzerland*

[3] *Department of Ecology & Evolution, University of Lausanne, Switzerland*

[4] *Institute of Earth Surface Dynamics, University of Lausanne, Switzerland*

Abstract

One of the key input parameters for numerical pollen forecasts is the distribution of pollen sources. Generally, three different methodologies exist to assemble such distribution maps: (1) plant inventories, (2) land use data in combination with annual pollen counts, and (3) ecological modeling. We have used six exemplary maps for all of these methodologies to study their applicability and usefulness in numerical pollen forecasts. The ragweed pollen season of 2012 in France has been simulated with the numerical weather prediction model COSMO-ART using each of the distribution maps in turn. The simulated pollen concentrations were statistically compared to measured values to derive a ranking of the maps with respect to their performance. It is shown that potential maps resulting from ecological modeling that does not include a sophisticated estimation of the plant density have rather poor results. For inventory maps and the maps based on land use data and pollen counts, the results depend very much on the observational site. The use of pollen counts to calibrate the map enhances the performance of the model considerably.

4.1   Introduction

Airborne pollen grains can lead to allergenic reactions (such as rhinitis or asthma) in sensitized persons. Even though medication is possible, avoidance of the allergens is the best way to avoid symptoms (van Moerbeke 1997). Therefore, spatially and temporally highly resolved pollen forecasts are needed to help allergy sufferers to plan their outdoor activities. Traditional pollen forecasts are issued manually, taking into account measured pollen concentrations of the previous days, climatological knowledge about the typical course of the pollen season and current weather forecasts. In recent years, numerical weather prediction (NWP) models have been extended to simulate the dispersion of pollen grains (e.g., Vogel et al. 2008; Sofiev et al. 2006; Efstathiou et al. 2011; Zhang et al. 2014). One of the major sources of uncertainty in these models is the distribution of pollen sources (Sofiev et al. 2006; Skjøth et al. 2010).

Different ways to map the distribution of pollen sources have been described in the literature. The first methodology relies on inventory data displaying the occurence of the allergenic plant. This has been applied to trees (e.g., Sofiev et al. 2006; Skjøth et al. 2008) and ragweed (Bullock et al. 2012; Zink et al. 2012). The main obstacle of this approach is the limited availability, completeness, comparability and timeliness of such data. For example, forest inventories only cover forested areas even though trees can also grow outside of forests. Additionally, the quantitative information of inventories varies strongly regarding the degree of detail and the accuracy.

A second methodology combines land use data and observed annual pollen counts to derive a plant distribution (e.g., Skjøth et al. 2010; Thibaudon et al. 2014). In addition to land use and pollen counts, Pauling et al. (2012) take into account forest inventory data. This methodology assumes that the same land use class is equally suitable for the plant in question throughout the entire domain. The limitations of this method are the availability of pollen measurements, the spatial resolution, timeliness and the detailedness of the classification of the land use data set. Using annual pollen counts for the local calibration of the map, this method cannot be applied to regions whose annual pollen counts are dominated by transported pollen grains.

A third methodology is based on ecological modeling: taking into account biological, climatological, geographical and anthropogenic factors, the spread of the plant is simulated (e.g., Bullock et al. 2012; Prank et al. 2013). In Prank et al. (2013), the simulated plant distribution is calibrated using a numerical dispersion model: the pollen concentrations are modeled using the original map as input for the dispersion model. The simulated pollen concentrations are then compared to observed ones and the deviations are used to tune the map. This calibration procedure is repeated until the differences between the simulated and observed concentrations fall below a certain threshold. The limitations of the ecological modeling are related to the underlying assumptions and availability, completeness and quality of data that is used during the building-process of the model (e.g., plant inventories). Additionally, anthropogenic influences can only be taken into account stochastically, hence, the resulting map always is only one out of many possible solutions. The calibration process using a dispersion model relates all the differences between measured and simulated pollen concentrations to the source map, neglecting the uncertainties coming from the parameterization of pollen emission (Zink et al. 2013) or the simulation of transport processes. Additionally, it assumes that both measured and simulated pollen concentrations are mainly influenced by local pollen emission. Hence, this procedure is of limited use in areas that are mainly influenced by transported pollen. Our study uses exemplary maps for all three methodologies to simulate the ragweed (*Ambrosia artemisiifolia* L.) pollen season of 2012. We have chosen France as the region of study since maps of all three types were available for this area. A total of six different distribution maps has been used to run the NWP system COSMO-ART (**Co**nsortium for **S**mall-scale **Mo**delling - **A**erosols and **R**eactive **T**race Gases, details can be found in Section 4.2.4) and simulate ragweed pollen concentrations. These are then statistically compared to observed pollen concentrations. The results are used to assess the suitability of the different maps in numerical pollen forecasts. A ranking of the maps is derived according to the skill of the different forecasts. Finally, a

recommendation is given on how to generate a distribution map for numerical pollen forecasts.

4.2   Materials and methods

4.2.1   Two distribution maps based on inventory data

We have used a ragweed distribution data set from France to create a source map for pollen emission. The data has been collected by the Fédération des conservatoires botaniques nationaux (FCBN) and has been published in Petermann (2011). The data gives the location and classified quantitative information for each plant stand. The inventory data was used to generate two distribution maps (see upper two images in the left column of Fig. 4.1):

- The full information given in the inventory was used to generate map 'INV-#' (**inv**entory, numbered (#) quantitative information). The distribution map was created by counting all plants recorded within each grid cell of the model domain.

- According to Zink et al. (submitted), the quantitative information given in the plant inventories does not promote the skill of a numerical pollen forecast (under certain circumstances). Because of this, we disregarded the quantitative information given in the inventory to generate a second distribution map 'INV-yn' (**inv**entory, **y**es-**n**o information). Here, the map to be used in the NWP model is generated by counting the number of plant localities within each grid cell of the model domain.

4.2.2   A distribution map based on land use data

Thibaudon et al. (2014) have published a ragweed distribution map for France based on land use data and observations of airborne pollen concentrations. The method involves the following steps:

1. Based on ecological knowledge, the different classes of a land use data set are divided into two categories: suitable and unsuitable for ragweed growth.

2. For each grid cell of the distribution map, the percentage of the area suitable for ragweed growth is calculated based on the land use data set (which has a finer resolution than the distribution map).

3. For each observational site of pollen concentrations in the study area, the local ragweed density is calculated taking into account the percentage of suitable
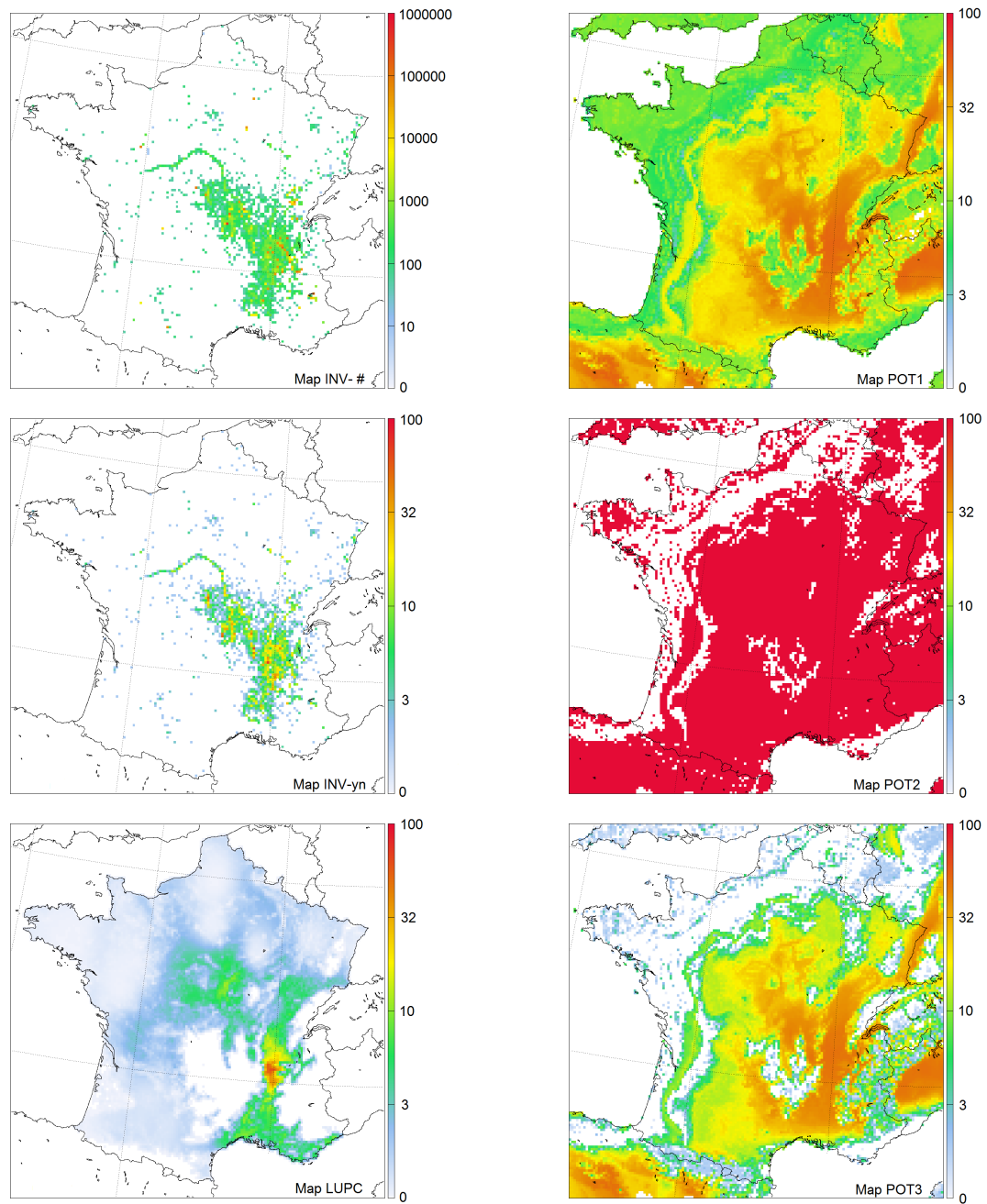
Figure 4.1: The six different ragweed distributions for France. The colors denote the quantity: for map INV-# the number of plants per grid cell, for map INV-yn the numbers of populations per grid cell, for map LUPC the plant density in %, for the potential maps (POT1, POT2, POT3) the suitability of the grid cell transformed into a plant density in %. The images show the original maps before they were calibrated using part of the NWP simulations.

land use classes within a radius of 30 km and the mean Seasonal Pollen Index of the site (SPI, the total number of pollen measured during one year).

4. These local ragweed densities are interpolated onto the suitable land use areas using inverse distance weighting.

5. Grid cells above a certain altitude are set to zero plants, assuming that ragweed populations cannot reproduce at higher altitudes.

This map is called 'LUPC' (**l**and **u**se and **p**ollen **c**ounts) in the following (see lower image in the left column of Fig. 4.1).

4.2.3   Three potential distribution maps

Species distribution models (SDMs, Guisan and Thuiller 2005, more information is available in the supplementary materials) were calibrated using occurrences of ragweed from various herbarium and environmental agencies in France and neighboring countries (e.g., Switzerland, Germany, Austria, Slovenia and Croatia) where ragweed can accomplish a full reproduction cycle (Storkey et al. 2014). Within the boundaries of these countries, 10.000 points were randomly sampled to depict the climatological conditions of the regions where ragweed is not present. The occurrences (and the randomly sampled non-occurences) were attached to 6 climate variables known to be important for the delineation of the potential distribution of ragweed: maximum temperature of the warmest month, annual temperature range, mean temperature of the coldest quarter, precipitation of the driest quarter, precipitation of the warmest quarter and aridity. Different modeling techniques were used: generalized linear models (GLM), generalized boosted regression models (GBM) and the maximum enthropy method (Maxent). The predictions of these models were averaged following an ensemble approach (Thuiller et al. 2009). Modeling was achieved using the R package 'biomod2' (Thuiller et al. 2009), keeping the default set of parameters. Models were calibrated on 70% of the data and evaluated with the remaining 30% of the data. The modeling procedure was replicated 10 times and the final results consist in an average of the 10 replicates. We further performed a Multivariate Environmental Similarity Surfaces analysis (MESS, Elith et al. 2010) to identify climates 'non-analog' to the calibration dataset. In this context, 'non-analog' means that the specific climate might be suitable for ragweed, however, it does not exist in the calibration data set. Finally, we derived three potential distribution maps from the raw predictions of the ensemble model (see right column of Fig. 4.1):

- POT1: continuous predictions of the ensemble model over the study area, with grid cells where at least one variable is non-analog according to the MESS analysis and grid cells without predictions (i.e. in water bodies) set to zero.

The raw output of the model gives the suitability of the grid cell for ragweed growth on a scale between 0 and 1000. With the assumption that the actual plant density is linearly correlated with the suitability, the output of the model was transformed into densities by rescaling the values between 0% and 100%. This leads to a maximum density of 55.3% in the model domain.

- POT2: binary predictions derived from POT1 using a threshold set to ensure that 95% of presences are predicted correctly. The assumption here is that below this threshold ragweed cannot grow and the density of ragweed at the corresponding grid cells is 0%. At the grid cells suitable for ragweed, the density is set to 100%.

- POT3: same as POT1 but with grid cells set to zero where POT2 is zero. In order to avoid strong gradients of the ragweed density at the borders of the regions that are set to zero, the remaining non-zero values of POT3 were linearly rescaled such that the maximum possible value (suitability of 1000) is set to 100% and the lowest occuring value in POT3 (suitability of 82) is set to 0%. This procedure leads to a maximum density of 51.3% in the model domain.

4.2.4 Simulations using the model COSMO-ART

The purpose of generating these distribution maps is to use them in numerical pollen forecasts. Therefore, in addition to comparing the maps themselves, we used the maps as input fields in the emission parameterization of the NWP system COSMO-ART to simulate the ragweed pollen season of 2012 in France. COSMO is a NWP model that has been initially developed at the German weather service DWD (Steppeler et al. 2002)). The extension ART (**A**erosols and **R**eactive **T**race Gases, Vogel et al. (2009)) is coupled to COSMO in order to allow the simulation of airborne substances/particles and their feedback on the weather system. The emission of pollen grains is parameterized according to Zink et al. (2013). The setup of the simulations is taken from Zink et al. (submitted).

4.2.5 Observational data of pollen concentrations

The simulated ragweed pollen concentrations were compared to measured values at French pollen observational sites (Table 4.1 and Figure 4.2). The pollen data were recorded at the RNSA (Réseau National de Surveillance Aérobiologique). The measured pollen concentrations are available in a daily resolution for the entire pollen season of 2012.
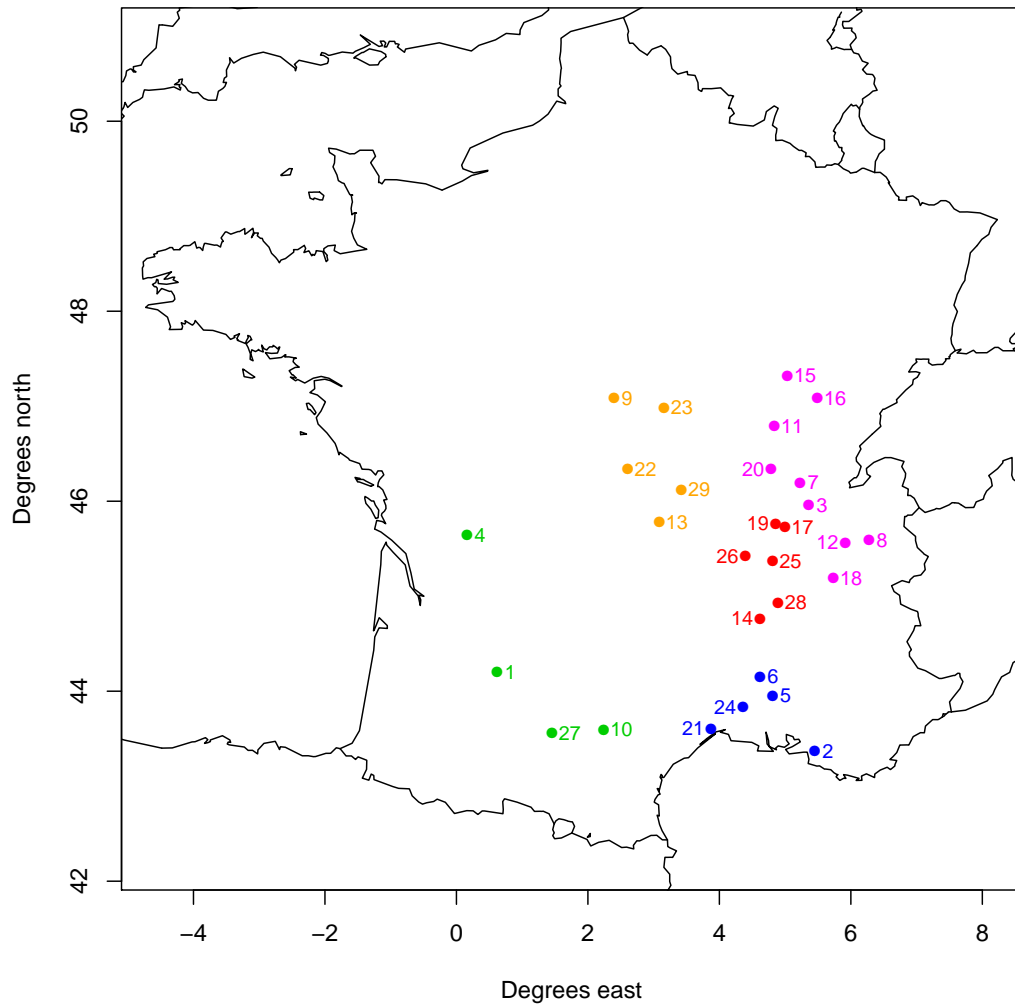
Figure 4.2: Sites where pollen concentrations are recorded. The numbers refer to the numbering in Table 4.1. The coloring denotes the regions that are introduced during the analysis of the results: sites in region A are colored in red, sites in region B are colored in blue, sites in region C are colored in green, sites in region D are colored in orange, sites in region E are colored in pink.

Table 4.1: Observational sites for pollen measurements in France. Longitude (Lon) and latitude (Lat) of the each observational site are given.

#	Station	Town	Lon	Lat
1	FRAGEN	Agen	0.6200	44.2000
2	FRAIXP	Aix-en-Provence	5.4500	43.3700
3	FRAMBE	Ambérieu-en-Bugey	5.3589	45.9578
4	FRANGO	Angoulême	0.1611	45.6483
5	FRAVIG	Avignon	4.8102	43.9536
6	FRBAGN	Bagnols-sur-Cèze	4.6164	44.1549
7	FRBOUB	Bourg-en-Bresse	5.2269	46.1977
8	FRBOUJ	Bourgoin	6.2744	45.5917
9	FRBOUR	Bourges	2.3965	47.0829
10	FRCAST	Castres	2.2419	43.5950
11	FRCHAL	Chalon-sur-Saône	4.8369	46.7933
12	FRCHAM	Chambéry	5.9169	45.5652
13	FRCLER	Clermont-Ferrand	3.0850	45.7783
14	FRCOUX	Coux	4.6181	44.7667
15	FRDIJO	Dijon	5.0350	47.3216
16	FRDOLE	Dole	5.4908	47.0881
17	FRGENA	Genas	4.9966	45.7330
18	FRGREN	Grenoble	5.7363	45.1941
19	FRLYON	Lyon	4.8566	45.7633
20	FRMACO	Mâcon	4.7858	46.3383
21	FRMONP	Montpellier	3.8733	43.6083
22	FRMONT	Montluçon	2.6050	46.3400
23	FRNEVE	Nevers	3.1602	46.9861
24	FRNIME	Nîmes	4.3600	43.8383
25	FRROUS	Roussillon	4.8136	45.3727
26	FRSTET	Saint-Étienne	4.3950	45.4227
27	FRTOUS	Toulouse	1.4530	43.5594
28	FRVALE	Valence	4.8931	44.9347
29	FRVICH	Vichy	3.4219	46.1238

4.2.6   Calibration of the maps

The different approaches to generate the pollen source map lead to different descriptors of pollen amount: the map INV-# contains the number of plants per grid cell, the map INV-yn shows the number of plant locations per grid cell while the map LUPC gives the plant density of the grid cell with respect to the maximum density observed in Europe (around Kecskemét, Skjøth et al. (2010); Thibaudon et al. (2014)). Likewise, the potential maps give a plant density in %, however it is a derived value based on the climatic suitability of the grid cell regarding ragweed growth. This was done in three different ways, hence the resulting densities are not directly related to each other. Using the same configuration of the emission parameterization for all maps, it is clear that the raw numbers of the maps have to be calibrated in order to produce meaningful pollen concentrations in the NWP model. The calibration includes the following steps for each of the maps separately:

1. Simulation of the entire pollen season of 2012 using the uncalibrated maps.

2. Comparison of the simulated and measured mean daily pollen concentrations: The overall level of the distribution map should reproduce the pollen level under ideal conditions (e.g., during the height of the pollen season, optimal emission conditions, ...). Assuming that such ideal conditions should lead to very high pollen concentrations, only days with at least 40 pollen per cubic meter (daily mean) are used for the calibration. Taking this subset of simulated and measured pollen concentrations, the ratio between simulated and observed values is calculated.

3. The uncalibrated maps are then calibrated by multiplication with this ratio.

4.2.7   Comparison of simulated and observed pollen concentrations

The simulated daily mean pollen concentrations resulting from the different maps were statistically compared to measured concentrations in France. For each of the maps and each of the observational sites, we calculated the following categorical scores based on 2×2 contingency tables using two different thresholds (5 and 20 pollen per cubic meter of air, representing low and strong pollen concentrations, respectively) to define a pollen event: Pierce Skill Score (PSS), Threat Score (TS), False Alarm Ratio (FAR). Additionally, we computed the correlation coefficient r and its corresponding p-value, the root-mean-square-error (rmse), the fractional bias (FB) and the index of agreement d_1. Table 4.2 gives an overview about these scores. For a more detailed description, please refer to Zink et al. (2013), Zink et al. (submitted), Wilks (2006) and GAW Report No. 181 (2008).

Table 4.2: Overview about the statistical scores used in this study.

Score	Range	Interpretation
PSS	-1 to 1	best: 1 random: 0 worst: -1
TS	0 to 1	best: 1 worst: 0
FAR	0 to 1	best: 0 worst: 1
r	-1 to 1	perfect correlation: 1 no correlation: 0 perfect anti-correlation: -1
p-value	0 to 1	significant result: < 0.05
d_1	0 to 1	best: 1 worst: 0
FB	not restricted	best: 0
rmse	not restricted	best: 0

4.3 Results

4.3.1 Visual comparison of the maps

Since the human eye is still one of the best devices to compare different images, we have first conducted a visual comparison of the uncalibrated maps. The maps have been plotted using a logarithmic scale (Figure 4.1). This was done since ragweed shows very inhomogeneous plant densities across France: in some areas (e.g., the western part of Rhône-Alpes, red sites in Figure 4.2) the densities/numbers of plants are very high, while in other areas (e.g., northwestern France) the densities/numbers of plants are very low. Map POT2 only gives presence/absence information and thus the quantitative information of this map cannot be compared to the other five maps. Since the spatial extent of the ragweed distribution in POT2 equals the one in POT3, we will refrain from describing map POT2 at all. The visual comparison of the remaining five maps yields the following findings:

- The western part of the region of Rhône-Alpes is one of the major ragweed pollen sources in Europe (Thibaudon et al. 2014). This feature is reproduced

in all of the maps, however, the details differ largely. In map LUPC, the area of maximum plant density is rather small, centering around the cities of Lyon/Roussillon (sites 19/25). The gradient in plant density between this highly infested area and the surroundings is relatively strong. In maps INV-# and INV-yn, the highly populated area is larger, reaching further south than in map LUPC and additionally covering a large region northwest of Lyon. The gradients within this area are smaller than in map LUPC: Especially, the region northwest of Lyon displays ragweed populations nearly as large and numerous as close to the main area (near sites 14, 17, 19, 25, 26 and 28) itself. In the potential maps POT1 and POT3, this western part of Rhône-Alpes is also very strongly populated with ragweed. However, the area is a lot larger, stretching from the Mediterranean coast to the borders of Germany and including large areas in southern and central France. The gradients within the highly populated area are not as strong as in map LUPC.

- The Mediterranean coast is nearly free of ragweed plants in the maps INV-# and INV-yn, while in map LUPC, it displays a continuous ragweed density of up to 10%. In map POT1, the Mediterranean coast is even more strongly populated: ranging from about 10% ragweed density east of Marseille (south of site 2) and west of Montpellier (site 21) to about 30% on the coast between these cities. Map POT3 also displays a dense ragweed growth between Marseille and Montpellier, however, the high densities of up to 30% do not totally reach the coastline. East of Marseille, the coast is nearly free of ragweed plants. West of Montpellier, only smaller densities of up to 10% exist. This visual impression is reflected in the time series of simulated and observed pollen concentrations for 2012 (compare Figure 4.3): In Montpellier, maps LUPC, POT1, POT2 and POT3 strongly overestimate the pollen concentrations while maps INV-# and INV-yn underestimate the concentrations. Further north (e.g., site 6), all six maps overestimate the observed pollen concentrations.

- A region in central France (close to the cities Bourges and Nevers, sites 9 and 23) is moderately populated in maps INV-#, INV-yn and LUPC. However, the exact position does not match: it is slightly shifted to the north for map LUPC. In the maps POT1 and POT3, this region belongs to the highly infested areas with densities of up to 30% (in map LUPC, the density reaches values of $\approx$ 10%).

- In maps INV-# and INV-yn, the river Loire can easily be identified as a line source of ragweed pollen. A small part of the river (from Nevers northwestwards) is also captured as a ragweed pollen source in maps LUPC, POT1 and POT3.

- While in the maps INV-# and INV-yn, the greater part of France is free of ragweed plants, these regions display a low plant density in map LUPC. The densities only rarely exceed 3% and are below 1% for most of the area. Map POT1 does not display areas free of ragweed at all: minimum values range around 3%, but the majority of areas that are free in the inventory maps display a ragweed density of 10% or even more in map POT1. Map POT3 shows larger areas with no or only small ragweed populations (densities of up to 3%). The gradient between these ragweed free areas to the neighboring populated areas is rather strong going from 0 to more than 10% within only a few grid cells. The time series of pollen concentrations at site 10 (FRCAST, Figure 4.3) reflects this impression: while the inventory maps display rather low pollen concentrations, map LUPC shows moderate overestimation and the potential maps show very strong overestimations.

- A comparison between the maps INV-# and INV-yn is rather corollary: obviously, the spatial range of ragweed populations coincide since the maps are based on the same plant locations. Using only presence/absence information (map INV-yn) assimilates the gradients within this spatial range.

Overall, the coarse distribution (big populations in western Rhône-Alpes and none or only very small populations in northern and northwestern France) is reflected in all of the maps. However, when looking at smaller scales, both the spatial patterns and the plant densities in certain areas vary considerably between the different maps.

4.3.2 Linear correlation of the three maps displaying the current distribution

In order to give a more objective assessment of the difference between the maps, we also compared the map LUPC to both inventory maps (INV-# and INV-yn) statistically by calculating the correlation coefficient r. The correlation coefficients r between the map LUPC and the inventory maps proved to be poor. Since map LUPC is smoothed due to the methodology (interpolation of point values), we decided to reduce the spatial resolution of the inventory maps to also smooth their distribution. This was done by averaging the values of clusters of 5×5 grid cells which renders artificial 'grid cells' of about 33 km edge length. This grid cell size corresponds roughly to the radius of 30 km around each observational site that was taken as the area of influence in Thibaudon et al. (2014). Averaging maps INV-# and INV-yn enhanced the correlation between the inventory maps and map LUPC. The best result was achieved for the averaged presence/absence map. However, the values of r were still quite low (not even reaching 0.65) showing that the inventory maps (in whatever version) do not very well match map LUPC.

4.3.3   Statistical analysis of simulated pollen concentrations

The statistical analysis of the simulated pollen concentrations has been done for each observational site separately. The result is rather divers: it depends both on the score and on the site whether a specific map performs well or not. In order to enhance the representativity of the results, we have grouped the observational sites into five regions. This was done because simulated pollen concentrations represent the mean areal values while observations are point values. Region A represents the main pollen source region in France including the observational sites 14, 17, 19, 25, 26 and 28 (red dots in Figure 4.2). Region B is the area south of the main source stretching to the Mediterranean coast (observational sites 2, 5, 6, 21 and 24; blue dots in Figure 4.2) which displays different levels of ragweed infestation depending on the map. Region C are the observational sites 1, 4, 10, and 27, located to the west and southwest of the main source and fairly free of ragweed plants (green dots in Figure 4.2). Region D are the observational sites 9, 13, 22, 23 and 29 that are located to the northwest of the main source and display an intermediate level of ragweed infestation (orange dots in Figure 4.2). Region E is located to the north and northeast of the main source and displays inhomogeneous ragweed infestation depending on the map (observational sites 3, 7, 8, 11, 12, 15, 16, 18, 20; pink dots in Figure 4.2). The statistical results of the individual sites were averaged to get regional values. The exact values for each score and region (Tables 4.4 to 4.8) and the mean values over all sites (Table 4.9) can be found in the supplementary materials.

The Threat Score (TS) and the False Alarm Ratio (FAR) always have to be seen together: only if both scores show good results, the simulation can really be regarded as good. This is because a simulation that always exceeds the threshold concentration will lead to a perfect TS, even though the usefulness of the forecast is strongly limited if it is not able to forecast low pollen concentrations. This feature can be found in all of the maps: in many cases, the TS values are quite good, largely exceeding 0.5 (e.g., Tables 4.4 and 4.7). However, FAR values that even reach the worst possible value of 1.0 (Table 4.6) show that all simulations strongly overestimate the observed pollen concentrations. This is also reflected in the results for the Pierce Skill Score (PSS) that are rather poor with a maximum of about 0.5 and values down to about 0.1. For most of the maps, the PSS using a threshold of 20 pollen per cubic meter of air is clearly better than the PSS using a threshold of 5 pollen per cubic meter of air. This shows that it is especially difficult to forecast the low pollen concentrations. The potential maps (POT1, POT2, POT3) strongly overestimate the pollen concentrations: the fractional bias (FB) reaches values of up to 1.78 for these maps (Table 4.6). This is also true for the LUPC map except for region D (Table 4.7) where the level of the simulated pollen concentrations is rather close to the observations. Map INV-yn shows varying results: for some regions, the pollen

concentrations are estimated relatively well while in other regions they are over- or underestimated. Map INV-# clearly displays the best results for FB. For most regions it underestimates the pollen concentrations. However, the underestimation is rather small and in some regions negligible. The correlation between measured and simulated pollen concentrations differs strongly between the regions: for example, in region C (Table 4.6) the correlations are very poor while in region B (Table 4.5) they are rather good. However, the p-values of the correlation coefficients denote that only the results for the regions A and B are significant (Tables 4.4 and 4.5). Within the regions, the differences regarding the correlations are rather small between the six maps. We conclude that the temporal evolution of the pollen concentrations depends rather on the pollen emission (which is parameterized equally for all maps) than on the source map.

Altogether, it seems difficult to deduce a ranking of the maps using the raw values of the statistical scores. Often, the results of several maps are rather close, thus taking the best score as an indication would be rather unfair to the maps that are nearly as good. Therefore, we have determined the actual range of values for each score and site/region. This range is divided into three equally sized parts that are used to assess the distribution maps: if the result of a specific map falls into the best third of the range, the map scores one point. If it falls into the worst third of the range, one point is taken from the map. If it falls into the middle third, the points do not change. Sometimes all six maps have very similar scores (e.g., 0.52, 0.53 and 0.54 for a score that can take values between 0 and 1). In such a case, the division of the actual range of values results in very small ranges for each third and a rather coincidental assignment of points. To avoid this, a score was not taken into account if the actual range of values stretches over less than 5% of the maximum possible range of values. For example, for the score TS, that can take values between 0 and 1, points were only rewarded (or taken) if the difference between the actual maximum and minimum values is more than 0.05. The points have been assigned twice: (1) for the statistical results of each individual observational site, and (2) for the regional mean values of the statistical scores. This provides a somewhat objective ranking of the distribution maps for the individual sites and for the five regions: the more points the better. Figure 4.4 shows the number of points at each site for the six distribution maps. The regional ranking can be found in the first 5 rows of Table 4.3. Finally, two overall rankings are derived by summing up the points for (1) the 29 observational sites, and (2) the five regions for each map separately. The result is displayed in the two last rows of Table 4.3 ('Total sites' and 'Total regions').

The ranking of each map for the individual observational sites is displayed in Figure 4.4. The first impression of the plots leads to a division of the maps into two groups: maps INV-# and LUPC display all possible results (colors ranging from red to
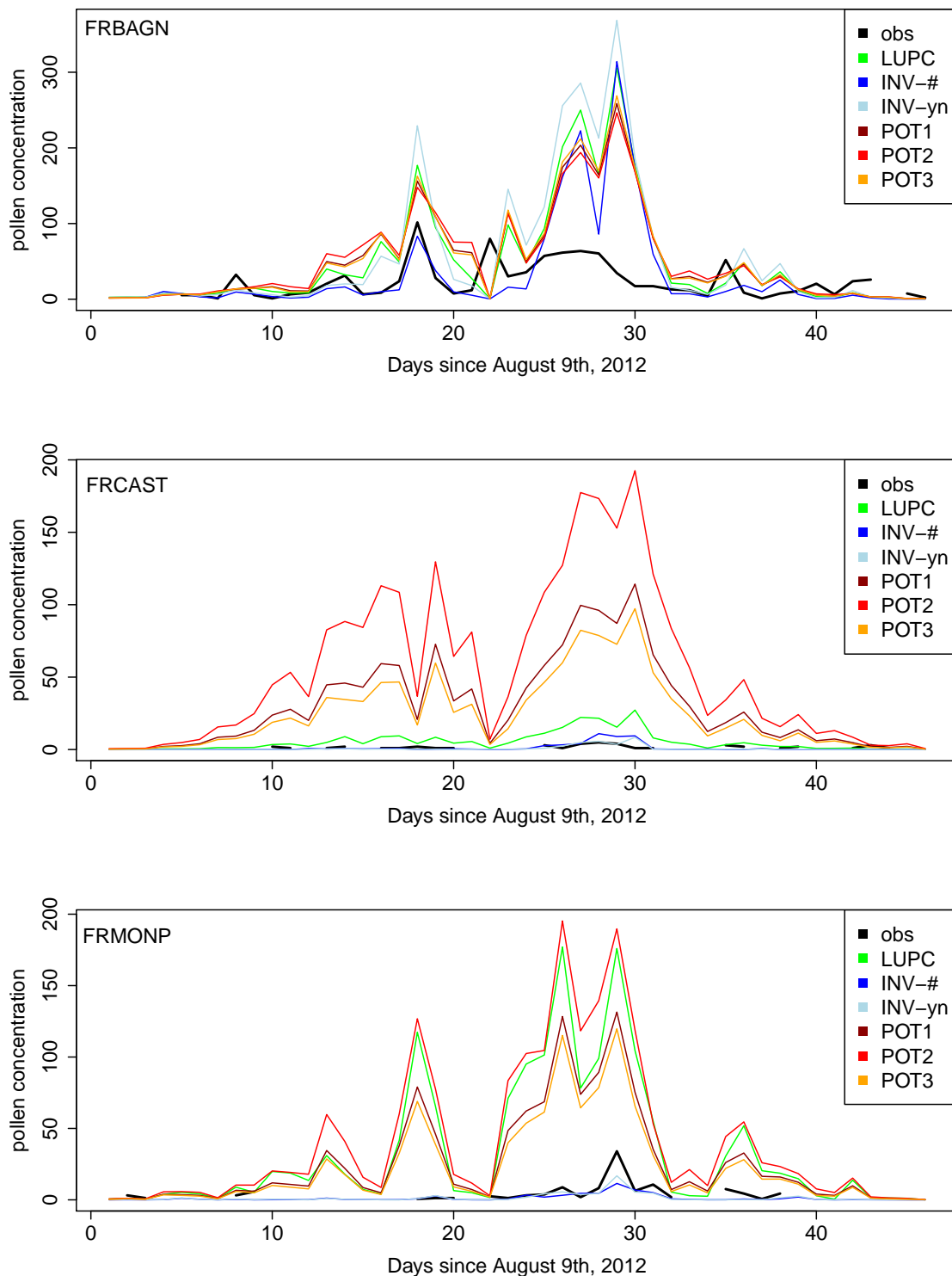
Figure 4.3: Time series of observed and simulated pollen concentrations at exemplary observational sites. The concentrations are given as daily mean values in pollen per cubic meter of air.
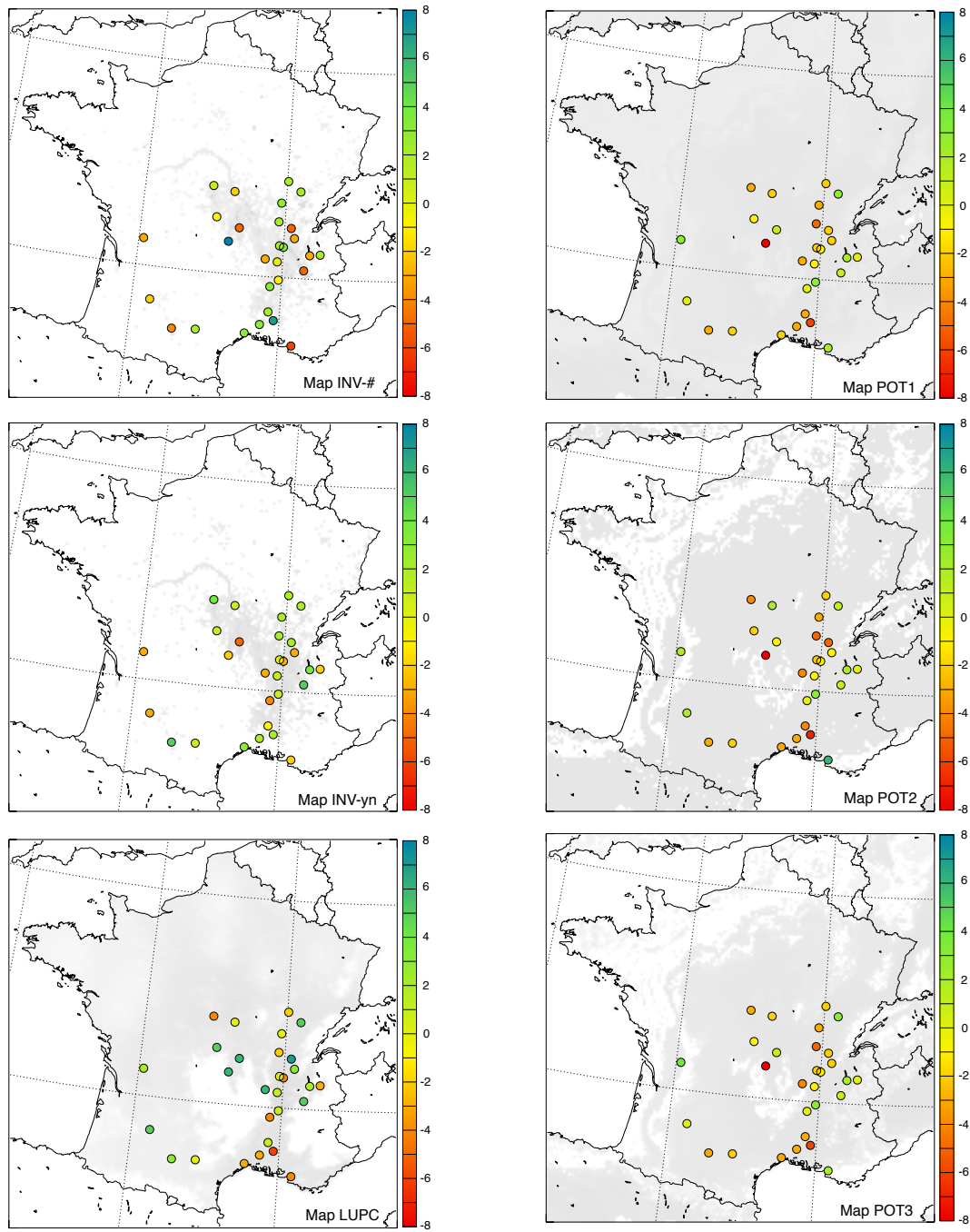
Figure 4.4: Sums of points representing the goodness of each map (see explanations in Chapter 4.3.3). Good results are displayed in green colors, bad results in red colors. The scale gives the number of points that each map scores at each observational site. The background shading in grey represents the distribution map.

dark green/blue with practically all colors in-between) while the other four maps show a tendency to be somewhat intermediate with colors ranging from red to light green. Especially, the good scores (dark green colors) concentrate largely on the maps INV-# and LUPC. Overall, the plots are quite scattered and it is difficult to give clear statements. Only in a few regions, the plots are quite clear: in region B, INV-# scores best except for site FRAIXP which is best in map POT2. Region C and the three southern sites of region D are best in map LUPC. For the remaining sites, the ranking of the different maps varies between the sites.

Looking at the regional ranking (Table 4.3), map LUPC performs very inhomogeneously: in the regions C and D it has by far the best rank. In region B it has the worst result of all maps while in the other two regions it is intermediate. The potential maps clearly score worst: they never have the highest number of points and in almost all cases one (or more) of the potential maps has the lowest number of points. Within the potential maps, map POT2 shows the worst results. The two inventory maps display rather similar results in the regions C, D and E with a maximum difference of one point per region. In region E, both maps have the same best result of all maps. In the regions A and B, map INV-# has the best score of all six maps while map INV-yn is equally bad as the potential maps in region A and intermediate in region B. In region C, map INV-# scores worst while INV-yn is intermediate.

Calculating the overall ranking in two different ways (based on individual results - 'Total sites' - and based on regional mean values - 'Total regions', Table 4.3) reveals an interesting fact: the order of the maps is similar (LUPC being the best map, then the two inventory based maps follow, and finally the potential maps), however, the details differ largely. Looking at 'Total region', the maps LUPC and INV-# nearly have the same score, with map LUPC being only slightly better. Looking at 'Total sites', map LUPC has by far the best result. Additionally, for 'Total region', map INV-yn is clearly inferior to map INV-#. In contrast, when looking at 'Total sites', map INV-yn is considerably better than map INV-#. This is in accordance to the result of Zink et al. (submitted) who have found that precise quantitative information in the inventory does not necessarily add value to the pollen forecast. In both rankings, the three potential maps have very similar poor results with map POT2 being the worst. However, one time POT1 is better than POT3, and the other time it is the other way round.

4.4   Discussion and conclusions

Regarding the statistical results for the individual sites and for the five study regions, the first conclusion is that it is not possible to declare one of the maps as being the best for all cases. Which of the maps scores best depends on the region, and even

Table 4.3: Ranking of the different distribution maps based on the statistical scores calculated for five French regions. For each region, the best map (or maps if several maps have the same rank) is highlighted with green , the worst map/maps is/are highlighted with red . The total ranking of the maps is calculated twice: 'Total regions' based on mean statistical scores for each region and 'Total sites' based on the individual results at each observational site.

Region	LUPC	INV-#	INV-yn	POT1	POT2	POT3
A	-1	1	-3	-3	-3	-3
B	-4	1	-1	-2	-3	-2
C	3	-2	-1	-1	-1	0
D	4	0	-1	-6	-6	-5
E	0	1	1	-3	-4	-3
Total regions	2	1	-5	-15	-17	-13
Total sites	23	3	9	-39	-42	-40

on the site within the same region. However, in nearly all cases, the three potential maps (POT1, POT2, POT3) exhibit the lowest scores. This was expected given the fact that they represent model predictions whereas INV-#, INV-yn and LUPC reflect more directly the observed densities. Except for some of the sites in regions with big ragweed populations, the potential maps largely overestimate the plant density. This is, of course, due to the methodology that renders the climatic potential for ragweed growth following unlimited dispersal and no-eradication. It is not restricted by land use or soil properties.

Assigning points according to the scores of the specific map relative to the scores of the other maps leads to a ranking: LUPC is the best map, followed by the two inventory maps, followed by the three potential maps. However, only in one of the two versions to compute the ranking, the LUPC map is clearly on the lead. Using the regional mean values, map INV-# is almost as good as LUPC.

Looking at the ranking for the different regions, it seems that the 'best map' would be a combination of the maps INV-# and LUPC. For example, taking map INV-# for regions A, B and E, and map LUPC for regions C and D. Such a semi-manual approach, however, is not feasible: how would the maps be merged? Therefore, it is mandatory to select the method that can produce a comprehensive map by itself. Even though map INV-# shows very good results for many regions, this kind of map is rather impractical: It depends on a domain-wide and up-to-date assessment of the plant populations. Additionally, the size of the plant populations needs to be estimated. For annual plants such as ragweed all this is critical. As a consequence of

this and the very good results of map LUPC, we would rather recommend using a theoretically derived map as the source distribution in a NWP model. Map LUPC is, in effect, a very simple potential map (taking into account land use only) tuned with mean SPIs. Apparently, the introduction of SPIs in the methodology of map LUPC has a very positive influence on the simulated pollen concentrations. The maps POT1, POT2 and POT3 take into account climatic information to derive the potential distribution of ragweed. We expect that using an extended potential map (considering both land use and climatic information) as a basis and tuning it with SPIs would probably render a map that is considerably better than any of the maps used in this study. The main drawback of using SPIs for the tuning of a distribution map is the fact that they are influenced not only by locally emitted pollen but also by transported pollen. In addition to that, the observational network for pollen concentrations is rather coarse, hence the measured values have to be interpolated over large distances. A similar approach has been described by Bullock et al. (2012); Prank et al. (2013, see introduction), using simulated and observed pollen concentrations to calibrate a map based on ecological modeling. The main difference to our suggestion is the additional step using a dispersion model during the calibration procedure which introduces additional uncertainty.

Finally, ragweed is an annual plant that is spreading on the one hand and being eradicated on the other hand. Because of this, the distinct distribution and densities can vary largely from year to year. Consequently, numerical pollen forecasts would presumably profit from the use of an assimilation cycle that could respond to annual variations rapidly.

Acknowledgements

Supplementary materials

Content:

A detailed description of the species distribution models used to generate the potential maps.

Table 4.4 gives the statistical results for region A.

Table 4.5 gives the statistical results for region B.

Table 4.6 gives the statistical results for region C.

Table 4.7 gives the statistical results for region D.

Table 4.8 gives the statistical results for region E.

Table 4.9 gives the statistical results averaged over all regions.

Species distribution models - SDMs

Species distribution models (SDMs) were calibrated using occurrences of ragweed from various herbarium and environmental agencies in France and neighboring countries (Switzerland, Germany, Austria, Slovenia and Croatia) where ragweed can accomplish a full reproduction cycle (Storkey et al. 2014). Within the boundaries of these countries, 10.000 points were randomly sampled to depict the climatological conditions of the regions where ragweed is not present. After disaggregation of the data by keeping a minimal distance of 10 km between each pair of occurrences (i.e. to decrease sampling bias and spatial autocorrelation; Verbruggen et al. (2013)), the 1570 occurrences left were attached to 6 climate variables known to be important for the delineation of the potential distribution of ragweed (Gentilini 2010): maximum temperature of the warmest month, annual temperature range, mean temperature of the coldest quarter, precipitation of the driest quarter, precipitation of the warmest quarter and aridity. Climate data were downloaded at a 30 arc second resolution from the Worldclim database (Hijmans et al. 2005) and aridity data was taken from Trabucco et al. (2008). Different modeling techniques were used: generalized linear models (GLM, with second order polynomial coefficient and stepwise selection using the Bayesian information criteria, McCullagh and Nelder 1983)), generalized boosted regression models (GBM, Friedman et al. 2000) and the maximum enthropy method (Maxent, Phillips et al. 2006). The predictions of these models were averaged following an ensemble approach (Thuiller et al. 2009). Modeling was achieved using the R package 'biomod2' (Thuiller et al. 2009), keeping the default set of parameters. Models were calibrated on 70% of the data and evaluated with the remaining 30% of the data. The modeling procedure was replicated 10 times and the final results consist in an average of the 10 replicates.

The contributions of the different variables were estimated by assessing the impact of

variable randomizations on the predictions (Thuiller et al. 2009). The most important variables in the models are (in the order of decreasing contribution): maximum temperature of the warmest month (drop contribution = 0.56, for explanations see Thuiller et al. (2009)), annual temperature range (0.20), mean temperature of the coldest quarter (0.13), aridity (0.08), precipitation of the driest quarter (0.07) and precipitation of the warmest quarter (0.07).

The SDMs were evaluated with the Area Under the Curve of a Receiver Operating Characteristics (AUC, ROC, Zweig and Campbell 1993) and the True Skill Statistic (TSS, Allouche et al. 2006). AUC varies between 0 (meaning: complete counter predictions of the model) and 1 (perfect fit with the observed distribution), 0.5 being random predictions. TSS varies as a correlation coefficient between -1 and 1, with -1 meaning counter-prediction, 0 random prediction, and 1 perfect prediction. With a mean AUC of 0.803 +/- 0.009 and a mean value of TSS value of 0.481 +/- 0.017, the predictions of the models can be considered as 'good' (Swets 1988).

Table 4.4: Statistical results of the simulations using different ragweed distribution maps for region A. Region A is the main pollen source region in France including the observational sites 14, 17, 19, 25, 26 and 28.

Score	Threshold	LUPC	INV-#	INV-yn	POT1	POT2	POT3
PSS	5	0.13	0.32	0.19	0.22	0.23	0.22
TS	5	0.74	0.68	0.72	0.71	0.72	0.71
FAR	5	0.19	0.17	0.20	0.20	0.20	0.20
PSS	20	0.52	0.47	0.52	0.49	0.49	0.49
TS	20	0.56	0.48	0.51	0.46	0.46	0.46
FAR	20	0.36	0.31	0.37	0.37	0.37	0.37
rmse		144.32	59.46	115.39	60.30	59.85	61.12
FB		0.74	0.08	0.64	0.38	0.34	0.40
r		0.48	0.42	0.42	0.44	0.43	0.44
p-value		0.01	0.08	0.02	0.04	0.04	0.04
d_1		0.38	0.48	0.38	0.41	0.41	0.40

Table 4.5: Statistical results of the simulations using different ragweed distribution maps for region B. Region B is the area between the main source (region A) and the Mediterranean coast (observational sites 2, 5, 6, 21 and 24) which displays different levels of ragweed infestation depending on the map.

Score	Threshold	LUPC	INV-#	INV-yn	POT1	POT2	POT3
PSS	5	0.18	0.38	0.22	0.21	0.21	0.15
TS	5	0.55	0.49	0.47	0.55	0.56	0.51
FAR	5	0.41	0.19	0.22	0.39	0.39	0.41
PSS	20	0.33	0.26	0.24	0.34	0.32	0.38
TS	20	0.24	0.22	0.23	0.26	0.26	0.28
FAR	20	0.72	0.50	0.44	0.69	0.68	0.64
rmse		74.33	26.99	32.04	55.65	64.65	53.87
FB		1.21	-0.21	-0.09	1.01	1.04	0.84
r		0.56	0.56	0.65	0.56	0.56	0.58
p-value		0.00	0.01	0.01	0.00	0.00	0.00
d_1		0.19	0.47	0.44	0.25	0.24	0.27

Table 4.6: Statistical results of the simulations using different ragweed distribution maps for region C. Region C are the observational sites 1, 4, 10, and 27, located to the west and southwest of the main source and fairly free of ragweed plants.

Score	Threshold	LUPC	INV-#	INV-yn	POT1	POT2	POT3
PSS	5	0.42	0.12	0.25	0.12	0.10	0.14
TS	5	0.18	0.02	0.06	0.14	0.15	0.15
FAR	5	0.78	0.98	0.94	0.85	0.85	0.84
PSS	20	NA	NA	NA	NA	NA	NA
TS	20	0.00	0.00	NA	0.00	0.00	0.00
FAR	20	1.00	1.00	NA	1.00	1.00	1.00
rmse		9.73	30.29	3.60	41.00	81.99	30.97
FB		0.68	-0.36	-1.07	1.57	1.78	1.40
r		0.16	0.10	0.10	0.18	0.18	0.17
p-value		0.53	0.51	0.43	0.40	0.41	0.42
d_1		0.23	0.29	0.37	0.06	0.03	0.10

Table 4.7: Statistical results of the simulations using different ragweed distribution maps. Region D are the observational sites 9, 13, 22, 23 and 29 that are located to the northwest of the main source and display an intermediate level of ragweed infestation.

Score	Threshold	LUPC	INV-#	INV-yn	POT1	POT2	POT3
PSS	5	0.33	0.38	0.33	0.28	0.25	0.28
TS	5	0.53	0.52	0.52	0.54	0.54	0.54
FAR	5	0.29	0.21	0.27	0.33	0.34	0.33
PSS	20	0.43	0.29	0.31	0.33	0.33	0.34
TS	20	0.36	0.25	0.26	0.25	0.28	0.26
FAR	20	0.54	0.62	0.51	0.67	0.66	0.67
rmse	20	22.60	39.87	46.94	38.28	49.02	36.09
FB		-0.05	-0.19	0.22	0.60	0.82	0.52
r		0.39	0.35	0.44	0.39	0.39	0.40
p-value		0.33	0.22	0.15	0.31	0.34	0.27
d_1		0.50	0.45	0.39	0.33	0.29	0.35

Table 4.8: Statistical results of the simulations using different ragweed distribution maps for region E. Region E is located to the north and northeast of the main source and displays inhomogeneous ragweed infestation depending on the map (observational sites 3, 7, 8, 11, 12, 15, 16, 18, 20).

Score	Threshold	LUPC	INV-#	INV-yn	POT1	POT2	POT3
PSS	5	0.16	0.25	0.21	0.17	0.17	0.19
TS	5	0.50	0.45	0.45	0.51	0.52	0.52
FAR	5	0.35	0.29	0.30	0.35	0.35	0.34
PSS	20	0.43	0.19	0.24	0.34	0.31	0.34
TS	20	0.27	0.21	0.22	0.24	0.23	0.24
FAR	20	0.66	0.53	0.45	0.72	0.73	0.72
rmse		30.94	37.93	29.84	39.52	42.90	39.45
FB		0.41	-0.03	-0.18	0.75	0.83	0.74
r		0.30	0.37	0.39	0.22	0.21	0.21
p-value		0.28	0.18	0.18	0.47	0.48	0.47
d_1		0.36	0.42	0.43	0.29	0.28	0.29

Table 4.9: Statistical results of the simulations using different ragweed distribution maps. The scores obtained for the different regions (compare Tables 4.4 to 4.8) are averaged to give the mean value for all of France.

Score	Threshold	LUPC	INV-#	INV-yn	POT1	POT2	POT3
PSS	5	0.22	0.30	0.23	0.20	0.19	0.20
TS	5	0.52	0.46	0.47	0.52	0.52	0.51
FAR	5	0.38	0.33	0.35	0.39	0.39	0.39
PSS	20	0.43	0.29	0.32	0.37	0.36	0.38
TS	20	0.30	0.28	0.30	0.26	0.26	0.26
FAR	20	0.63	0.51	0.44	0.67	0.67	0.66
rmse		57.52	39.78	47.25	46.59	56.60	44.67
FB		0.57	-0.11	-0.05	0.80	0.89	0.74
r		0.38	0.37	0.41	0.35	0.34	0.35
p-value		0.22	0.18	0.15	0.26	0.27	0.26
d_1		0.34	0.43	0.41	0.28	0.27	0.29

Chapter 5

Conclusions and recommendations

In this thesis, pollen concentrations were simulated within a NWP model. Emission, transport, diffusion and removal processes were described using an additional balance equation analog to the equations for aerosols. However, the source term in this equation contains several pollen specific elements that have to be addressed. Three basic questions are answered by the source term: (1) When are pollen grains emitted?, (2) Where are pollen grains emitted? and (3) How many pollen grains are emitted? In this thesis, a new parameterization was developed that takes into account the phenological course of the pollen season, the release of the pollen grains from the flowers and their entrainment into the atmosphere. Furthermore the impact of different distribution maps was investigated. To achieve this goal, different methods were employed to generate distribution maps. The findings can be used to set up numerical pollen forecasts for different species and models. This last chapter of the thesis discusses the main results and presents instructions on how to set up numerical forecasts for a new pollen species.

5.1   A parameterization of pollen emission

5.1.1   Seasonal variations

The growing state of the plants determines the amount of pollen currently available for emission. A mathematical description of the ragweed pollen season is presented in Chapter 3. A rather similar approach has been published by Prank et al. (2013). Both approaches use a Gaussian function to describe the shape of the pollen season. The length of the pollen season is set to 6 σ (this study) or 4 σ (Prank et al. 2013). The main difference concerns the starting and ending dates of the pollen season: while in our study climatological dates are used, Prank et al. (2013) introduce a model that uses temperature sums, photo period and the occurence of low temperatures to predict the starting and ending dates of the pollen season. If used for operational

pollen forecasts, climatological dates for the start and end of the pollen season are not sufficiently accurate. In such a case, I would therefore recommend to use the parameterization of Prank et al. (2013). However, the phenological model for ragweed based on climatological dates presented here is not meant to be used for operational pollen forecasts. It was designed for the use in two studies regarding distribution maps (Chapters 3 and 4). The correct identification of the starting and ending dates of the pollen season were of minor interest in these studies. Therefore, it was sufficient to use a climatological model.

Recommendations for the development of a phenological model

Since the phenological model was not the main scope of this thesis and therefore was not studied in detail, I can only give general recommendations for the development of a mathematical description of the pollen season for a new species. As a first step, I would identify the parameters that determine the start and the end of the pollen season. For many pollen species (especially for the species that are flowering in spring), these are temperature sums. For some species, photoperiod or the occurence of frost are more important. An example for such a species is ragweed. Using these parameters, a predictive model for the starting and ending dates of the pollen season should then be developed.

Knowing the starting and ending dates, the course of the season between these dates has to be mathematically described. I would recommend to use generalized (averaged over several years and many different observational sites) and normalized timeseries to identify the typical course of the season for the given species.

If the simulations of the pollen concentrations are done in hindcast-mode only, a phenological model is not mandatory: the starting and ending dates of the pollen season can simply be extracted from the measurements. The typical course of the pollen season can then be distributed between these two dates.

5.1.2 Daily variations

If ripe pollen grains are available, the daily variations in pollen emission are primarily related to the current meteorological conditions. In Chapter 2, a new parameterization of pollen emission is described. It is designed in a way that allows a simple expansion to other pollen species. Pollen emission is treated as a two-step process. The first step (pollen release from the flowers into a pollen reservoir) is influenced by temperature and relative humidity. The second step (pollen entrainment from the reservoir into the atmosphere) is mainly influenced by the turbulent kinetic energy. Additional processes are considered, e.g., wash-out of the reservoir during precipitation events, reduced entrainment under moist conditions, random effects leading to a (partial)

emptying of the reservoir. In Chapter 3, an additional feature is implemented: after a precipitation event, emission is suppressed for a certain span of time.

At MeteoSwiss, this parameterization has been used operationally for the forecasts of birch and grass pollen concentrations, and pre-operationally for the forecasts of ragweed pollen concentrations. Despite their operational use, the functions and parameters for birch, grass and ragweed can still be enhanced. They have been set up using descriptions in the literature. Comparisons between measured and simulated time series of the pollen concentration were used for a basic tuning of the functions. However, the functions in the parameterization actually do not simulate the pollen concentration but the pollen emission. It would therefore be beneficial to set up experiments to quantitatively measure the factors that influence the pollen emission rate. The first functions to be mentioned are $f_{R,T}$ and $f_{R,RH}$ that describe the influences of temperature and relative humidity on the release of the pollen from the flowers into the reservoir. A major improvement would be to set up an experiment to measure the pollen release rates (for each plant species separately) as a function of temperature and relative humidity. The third function to be improved is $f_{E,TKE}$, the emission rate in relation to turbulent kinetic energy (TKE). A promising experiment would therefore be to measure emission rates as a function of TKE in a wind tunnel. The function that suppresses emission after an event of rainfall currently only depends on the amount of precipitation and the relative humidity after the rainfall. It could be enhanced by explicitly simulating the interception and the evaporation of the intercepted water.

An additional feature that could be implemented for grasses is the cutting of the fields. In measured time series, it can be seen that pollen concentrations are reduced considerably after a certain time (despite the still on-going pollen season). This can be related to the meadows being cut. While it is certainly not possible to implement the cutting of each individual grass land (due to lack of data), it might still be possible (and rewarding) to acknowledge the cutting randomly.

Finally, there are several functions whose impact on the final emission rate is small as compared to the other functions, e.g., the emptying of the pollen reservoir due to random processes. Obviously, these functions can also be enhanced by dedicated experiments. However, I would not focus on them in favor of the more important functions and parameters mentioned above.

Instructions on how to adapt the parameterization for new pollen species

The following pollen specific parameters and functions need to be adapted when the parameterization presented in Chapter 2 shall be used for a new pollen species (they are approximately ordered in decreasing importance):

- the distribution of the plant $f_{Q,cov}$ needs to be provided as an input field (see below for instructions on the generation of distribution maps)

- the daily output of a phenological model $f_{Q,seas}$ (ranging between 0 and 1) needs to be provided as an input field

- the density of the pollen grains

- the diameter of the humid pollen grain, the diameter of the dry pollen grain, the minor and the major principal diameter (for round pollen grains, these are the same)

- the functions describing the influence of temperature and relative humidity on the pollen release rate ($f_{R,T}$ and $f_{R,RH}$)

- the duration (during one day) of emission under ideal conditions (this defines the amount of pollen that can be released per time step $Q_{pollen,\Delta t}$)

- maximum number of pollen that can be produced on one square meter per day $Q_{pollen,day}$ (if unknown, this parameter can be used as a tuning factor when comparing the measured and simulated mean pollen concentrations)

- if the productivity of the plant species depends on the altitude, the field $f_{Q,alt}$ has to be provided, otherwise it is homogeneously set to a value of 1

- the function $f_{E,TKE}$ describing the influence of TKE on the emission rate

- the rate Ψ_{random} at which pollen are lost from the reservoir randomly

- the function $f_{E,RH}$ describing the influence of relative humidity on the emission rate

- the function Ψ_{precip} describing the washout of the pollen from the reservoir by precipitation

For some of these functions/parameters, the values of birch, grass or ragweed can be used as a first guess (e.g., for $f_{E,TKE}$, $f_{E,RH}$, Ψ_{random} or Ψ_{precip}). For others, the specific values of the new pollen species are indispensable (e.g., plant distribution, phenological model, density and different diameters of the pollen grains).

5.2   Generating distribution maps

Naturally, pollen can only be emitted where the plant in question is present. Theoretically, inventory data should give a realistic image of the plant's spatial distribution.

However, inventory data is bound to be incomplete and out-dated since it is simply not possible to monitor every square meter of the land surface at all times. Therefore, alternative methods to generate distribution maps have been developed (see Section 1.3). In summary, these methods make use of different types of data or models to derive some sort of potential plant distribution that is then calibrated using some kind of weighting factors. Due to the different limitations and assumptions, all of these methods lack accuracy. It is therefore necessary to assess which distribution map leads to the most useful pollen forecast.

5.2.1   Maps based on inventory data

In addition to the presence/absence information, the abundance of the pollen (i.e. plants) needs to be estimated in order to produce meaningful pollen concentrations in the model. The most obvious approach to derive quantitative distribution maps is the allocation of inventory data that includes quantitative information. This thesis investigates the requirements that inventory data has to fulfill in order to be useful in the field of numerical pollen forecasts (Chapter 3 and parts of Chapter 4).

Chapter 3 focuses on a very specific setting: a large but distant pollen source while local pollen sources are negligible. It is found that the quantitative information in the source region (e.g., number of plants per population or classified population sizes) does not necessarily enhance the pollen forecast in the receptor region. In the studied case, it was sufficient to know the locations of plant populations. It should be noted that this already includes a certain quantitative information: counting the number of plant populations within each grid cell results in a distribution map that can distinguish between regions with a high plant density and regions with only a few populations. Additionally, the spatial resolution of the distribution maps in this study is reduced twice to investigate the sensitivity of the pollen forecast to the exact position of the pollen sources. It is shown that a high spatial resolution is needed, hence a good knowledge about the locations of the plant populations.

The setting of this investigation might seem rather limited, however, it is based on the situation in Switzerland: being fairly free from ragweed plants itself, the majority of ragweed pollen grains is transported to Switzerland from the Rhône-Alpes region in France and from northern Italy. While in France the ragweed distribution is known fairly well (and thus this region as source region is perfectly suited for a study in Switzerland), the ragweed distribution is practically unknown in Italy. The setting was chosen in order to give hints for the construction of a ragweed distribution map for northern Italy. Knowing that the quantitative information of the inventory is dispensable, it is now easier to find useful data that can be used for the generation of a ragweed distribution map in northern Italy. Despite the restrictive setting, the

findings of this investigation might still help to create ragweed distribution maps
in many countries: being abundant only in three European regions (the Pannonian
Plain, the Rhône-Alpes region in France, and northern Italy), this setting applies to
many regions in Europe. Additionally, it can be applied to any plant species with a
similarly patchy pattern.

In the second study focusing on distribution maps (Chapter 4), the perspective is
shifted from the receptor region to the source region and from methods using inventory
data only to several different methods to produce distribution maps. Focussing on
France as the area of study, different types of ragweed distribution maps are used
to simulate the ragweed pollen season of 2012. The simulated pollen concentrations
are statistically compared to measured values at French pollen observational sites.
Using these statistical scores, a ranking of the different maps is derived. Here, only
the maps based on inventory data are discussed. The other methods are addressed
later in Chapter 5.2.2.

In contrast to the previous study, it is found that it is beneficial to make use of the
quantitative information of the inventory data if the pollen forecast shall be issued
for the source region itself. This indicates that the detailed information about the
abundance of sources is lost during the process of transportation. Hence, in regions
with only weak local emission where the transported pollen dominates the pollen
concentrations, this information can be left out from the beginning. In regions that
are mainly influenced by local pollen emission, the quantitative information should
be as detailed as possible.

In all cases, the overall level of pollen concentrations in the model needs to be
adjusted to measured concentrations. This is because the distribution maps all
display different units, e.g., some give the number of plants per grid cell, others the
number of populations per grid cell. Since the same model configuration is used for
all of the maps, a tuning factor is essential. If the distribution map is generated
from data of different plant inventories, a separate tuning factor has to be derived
for each inventory (see case study 'long-distance transport from Hungary' in Section
3.4.2). This is due to the different nature of the inventories that leads to inconsistent
quantitative information (e.g., numbered or classified information). In Chapter 3, it
is shown that such a tuning is sufficient to make sure that the total number of plants
is in the same order of magnitude for all of the different maps in the corresponding
study.

Conceptually, it is problematic to use measured pollen concentrations to enhance the
accordance between simulated and measured pollen concentrations. However, due
to lack of data, there is no other way of calibrating the model. Neither the plant
distribution nor the emission flux can be verified. Using pollen concentrations to
approach this difficulty has been frequently described in the literature (e.g., Prank

et al. 2013; Duhl et al. 2013; Zhang et al. 2014). The problem can be resolved or at least diminished by using different data sets (e.g., different years or a certain subset of the observational sites) for the tuning and validating processes.

Comments on the use of inventory data for the generation of distribution maps

If a highly resolved, complete and up-to-date inventory including detailed quantitative information is at hand, using this inventory as a basis should be the method of choice to produce a distribution map (both in the source and the receptor region). If the data is of high quality, this method is the most reliable since it does not have any underlying assumptions. If the inventory data does not include quantitative information, it might still be used to create a distribution map for remote pollen sources. For each inventory that is included in the map, a separate calibration factor needs to be computed.

5.2.2 Comparing different methods to generate distribution maps

Chapter 4 describes a study in which distribution maps that are derived using different methods are compared to each other. Taking France as an example, two maps based on inventory data, one map based on land use data and pollen counts, and three maps based on ecological modeling are used to simulate the ragweed pollen season of 2012. The performance of the different simulations is evaluated statistically to derive a ranking of the distribution maps: which map produces the best pollen forecast?

In the main source region of France (called region A in this study), the map based on quantitative inventory data (INV-#) clearly renders the best results. However, looking at the overall result for all of France, the map based on land use data and pollen counts (LUPC) is as good as or even better than INV-#. Map LUPC can be seen as a very simple form of a potential map (considering land use only) being weighted with annual pollen counts to respect local differences. Regarding the more sophisticated potential maps (taking into account different climatic factors but without any account of actual occurence) that all perform rather poorly, it seems that this weighting process is the essential step to produce a reliable and differentiated distribution. Particularly, such a weighting makes sure that the plant's distribution is not overestimated in regions that are potentially suitable for but not (yet) invaded by the plant. Therefore, it is assumed that the combination of the more sophisticated potential maps with annual pollen count data would yield maps that are better than any of the maps used in this study. Since France comprises both regions with large ragweed populations and regions that are fairly free of ragweed, this result is not

limited to a certain setting.

The study on distribution maps has been conducted on the example of ragweed which is - in Europe - an invasive plant. Therefore, the question arises whether the conclusions drawn from these studies can also be applied to other species - especially to species that are native in Europe. In other words: are the underlying assumptions valid for both invasive and native plants?

1. The first assumption is that most inventory data is incomplete, out-dated and not highly resolved and should therefore not be used. Whether this assumption is justified depends mainly on the plant in question and on the size of the domain. For example, as trees are multi-annual plants, the currentness of the inventory is of minor concern. In contrast, for an annual plant like ragweed (which is also being eradicated) old data is of no use. Additionally, the coverage of inventories differs strongly between countries/states. Therefore, this first assumption has to be checked for each species and region separately.

2. The second assumption is that the same land use class displays the same suitability for the development of the plant wherever it appears in the domain. If this assumption is valid for invasive plants, it should also be valid for native plants that are adapted to the regional climate and soil types. For large domains, this assumption is problematic, both for native and invasive species.

3. The third assumption is that a map based on ecological modeling renders a better estimate of the potential distribution than a map that is solely based on land use categories. Whether this assumption is justified or not depends on the skill of the ecological model rather than on the species. Of course, the skill of a certain ecological model might itself depend on the plant species - but this question is out of scope for this thesis.

4. The fourth assumption is that the annual pollen counts reflect the local plant level and thus can be used for the weighting of the potential distribution map. This assumption is justified if only a small proportion of the pollen is transported over large distances (Sofiev et al. 2013a, and references herein). In Skjøth et al. (2010) it is assumed that the annual pollen counts reflect the amount of plants within a distance of about 30 km. There is no indication that the validity of this assumption depends on the plant being native or invasive.

As can be seen, the assumptions are equally valid for native and invasive species. Thus, the recommendations drawn from these studies can be applied to any wind-pollinated plant.

Instructions for the generation of distribution maps based on potential distributions

In most cases, inventory data of high quality (as described in Chapter 5.2.1) is not available for the entire domain. However, in order to produce operational pollen forecasts, a domain-wide distribution map is essential. Therefore, in the absence of high quality inventory data, the following procedure is recommended:

1. A map of the potential distribution of the plant in question should be generated: this can be based on ecological modeling taking into account, e.g., climatic factors, soil type and/or land use. If an ecological model is not at hand, a simple potential distribution can also be derived from a land use data set by dividing the land use classes into 'suitable' and 'not suitable' for the given species. The percentage of suitable area within each grid cell gives a rough estimation of the potential distribution.

2. This 'raw' potential distribution should then be calibrated using annual pollen counts. One possibility to do this is to average the annual pollen counts over several years. These averaged site-based values should then be interpolated onto the grid of the model. The final distribution map is generated by multiplying the potential distribution map with the interpolated annual pollen counts.

3. The first two steps of the procedure described here render a map that shows the relative differences in plant density for the different grid cells. It does not give absolute values, such as a number of plants per grid cell or the percentage of the grid cell that is covered with the plant. Therefore, as described above, the final step in producing a usable distribution map is a calibration using simulated and measured pollen concentrations.

A slightly different procedure is described in Thibaudon et al. (2014) where a site-based plant level is calculated using the fraction of suitable land use classes in the vicinity of the site and the averaged annual pollen counts of the site itself. The interpolation to the grid of the model is then conducted using the site-based plant levels. It has not been tested which of these two procedures renders the better result or if the results are very similar.

5.3   Concluding remarks

Looking at the results of this thesis, it is clear that numerical pollen forecasts are still subject to a lot of uncertainties and assumptions. They can be found in all of the different elements that are necessary to issue a numerical pollen forecast: the

distribution map, the parameterization of pollen emission, and the handling of the pollen grains within the NWP model. The question arises which of these uncertainties is the largest?

Looking at time series of pollen concentrations at different observational sites, it seems that the overall level of the concentration is mainly a matter of the distribution map. If the simulated pollen concentration overestimates the measured one, it usually does so throughout the entire time series. The same is true for underestimations. This leads to a second conclusion: the simulated pollen concentration is dominated by local sources. This is consolidated by the fact that time series of the simulated emission flux and time series of the simulated pollen concentrations are fairly parallel regarding their up- and downswings. Obviously, observational sites that do not have local sources do not show this feature.

The second feature that can be identified in time series is the importance of the phenological model at the beginning and end of the pollen season. During the first and last days of the pollen season, the overall pollen level is largely controlled by the phenological model. If the pollen forecasts shall be issued on an operational basis, it is therefore of great importance to implement a sophisticated model of the pollen season. During the main pollen season, the influence of the phenological model is small. At the end of the pollen season, the simulated pollen concentrations also depend strongly on the phenological model. However, the exact ending date of the pollen season is of minor importance to the patients as compared to the beginning. Without having done a thorough investigation of this, I assume that the distribution map is the biggest uncertainty of numerical pollen forecasts. If I had to set up a forecast for a new species, I would therefore focus on the generation of a distribution map. Secondly, I would build a sophisticated model for the prediction of the start of flowering. The prediction of the end of flowering and the course of the season in-between have to be implemented also. However, I feel that these are not as crucial as the prediction of the start of flowering. In a third step, I would calibrate the functions within the parameterization of pollen emission. In lack of measured emission fluxes, I would try to calibrate the functions such that the resulting pollen concentration at grid cells with high plant densities resemble the measured daily cycle of pollen concentrations. Of course, the functions have to be kept within the range of values that are biologically sound.

As a conclusion, it can be said that this thesis can be taken as a guideline to set up operational pollen forecasts for new species or domains. It provides a parameterization of pollen emission that can be adapted for the species in question and gives advice on the generation of distribution maps.

Bibliography

Alberternst, B., S. Nawrath, and F. Klingenstein, 2006: Biologie, Verbreitung und Einschleppungswege von Ambrosia artemisiifolia in Deutschland und Bewertung aus Naturschutzsicht. *Nachrichtenblatt des Deutschen Pflanzenschutzdienstes*, **58(11)**, 279–285.

Allouche, O., A. Tsoar, and R. Kadmon, 2006: Assessing the accuracy of species distribution models: prevalence, kappa and the true skill statistic (TSS). *Journal of Applied Ecology*, **43 (6)**, 1223–1232.

Bianchi, D. E., D. J. Schwemmin, and W. H. Wagner (Jr.), 1959: Pollen Release in the Common Ragweed (Ambrosia artemisiifolia). *Botanical Gazette*, **120 (4)**, 235–243.

Bullock, J., D. Chapman, S. Schaffer, D. Roy, M. Girardello, T. Haynes, S. Beal, B. Wheeler, I. Dickie, Z. Phang, R. Tinch, K. Civic, B. Delbaere, L. Jones-Walters, A. Hilbert, A. Schrauwen, M. Prank, M. Sofiev, S. Niemelä, P. Räisänen, B. Lees, M. Skinner, S. Finch, and C. Brough, 2012: Assessing and controlling the spread and the effects of common ragweed in Europe (env.b2/etu/2010/0037). Tech. rep., NERC Centre for Ecology & Hydrology.

Chuine, I., P. Cour, and D. D. Rousseau, 1998: Fitting models predicting dates of flowering of temperate-zone trees using simulated annealing. *Plant, Cell & Environment*, **21**, 455–466.

Clot, B., R. Gehrig, A. Peeters, D. Schneiter, P. Tercier, and M. Thibaudon, 2002: Pollen d'ambroisie en Suisse: production locale ou transport? *Allergie et Immunologie*, **34**, 126 – 128.

Dahl, Å., C. Galán, L. Hajkova, A. Pauling, B. Šikoparija, M. Smith, and D. Vokou, 2013: The Onset, Course and Intensity of the Pollen Season. *Allergenic Pollen: A Review of the Production, Release, Distribution and Health Impacts*, M. Sofiev and K.-C. Bergmann, Eds., Springer Science+Business Media, chap. 3, 29 – 70.

Doms, G., J. Förstner, E. Heise, H.-J. Herzog, D. Mironov, M. Raschendorfer, T. Reinhardt, B. Ritter, R. Schrodin, J.-P. Schulz, and G. Vogel, 2011: A Description of

the Nonhydrostatic Regional COSMO Model. Part II: Physical Parameterization. Documentation, Consortium for Small-Scale Modelling.

Duhl, T. R., R. Zhang, A. Guenther, S. H. Chung, M. T. Salam, J. M. House, R. C. Flagan, E. L. Avol, F. D. Gilliland, B. K. Lamb, T. M. VanReken, Y. Zhang, and E. Salathé, 2013: The Simulator of the Timing and Magnitude of Pollen Season (STaMPS) model: a pollen production model for regional emission and transport modeling. *Geoscientific Model Development Discussions*, **6 (2)**, 2325–2368, doi: 10.5194/gmdd-6-2325-2013, URL `http://www.geosci-model-dev-discuss.net/6/2325/2013/`.

Dullinger, S., I. Kleinbauer, J. Peterseil, M. Smolik, and F. Essl, 2009: Niche based distribution modelling of an invasive alien plant: effects of population status, propagule pressure and invasion history. *Biological Invasions*, **11 (10)**, 2401–2414.

Efstathiou, C., S. Isukapalli, and P. Georgopoulos, 2011: A mechanistic modeling system for estimating large-scale emissions and transport of pollen and co-allergens. *Atmospheric Environment*, **45 (13)**, 2260 – 2276, doi:http://dx.doi.org/10.1016/j.atmosenv.2010.12.008, URL `http://www.sciencedirect.com/science/article/pii/S1352231010010332`.

Elith, J., M. Kearney, and A. S. Phillips, 2010: The art of modelling range-shifting species. *Methods in Ecology and Evolution*, 1–13.

European Comission, 2003: Global Land Cover 2000 database. URL `http://bioval.jrc.ec.europa.eu/products/glc2000/glc2000.php`.

European Environment Agency, 2012: Corine Land Cover 2006 raster data. URL `http://www.eea.europa.eu/data-and-maps/data/corine-land-cover-2006-raster-2`.

Fernández-Llamazares, Á., J. Belmonte, M. Alarcón, and M. López-Pacheco, 2012: Ambrosia L. in Catalonia (NE Spain): expansion and aerobiology of a new bioinvader. *Aerobiologia*, **28 (4)**, 435–451.

Ferrario, M., 2010: Presenza di Ambrosia artemisiifolia e Heracleum mantegazzianum in Ticino - rapporto 2010. Tech. rep., Phytosanitary Service Cantone Ticino.

Friedlander, S. K., 1977: *Smoke, Dust and Haze.* John Wiley and Sons, New York.

Friedman, J. H., T. J. Hastie, and R. Tibshirani, 2000: Additive logistic regression: a statistical view of boosting. *Annals of Statistics*, **28**, 337–374.

Fuchs, N. A., 1964: *The Mechanics of Aerosols.* Pergamon Press, Oxford.

Fuckerieder, K., 1976: Der Graspollengehalt der Luft in Mitteleuropa. Ph.D. thesis, Auswertestelle Aerobiologie des Umweltbundesamtes und Botanisches Institut der Technischen Universität München.

Galán, C., M. J. Fuillerat, P. Comtois, and E. Dominguez, 1998: A predictive study of Cupressaceae pollen season onset, severity, maximum value and maximum value date. *Aerobiologia*, **14**, 195–199.

García-Mozo, H., C. Galán, J. Belmonte, D. Bermejo, P. Candau, C. Díaz de la Guardia, B. Elvira, M. Gutiérrez, V. Jato, I. Silva, M. M. Trigo, R. Valencia, and I. Chuine, 2009: Predicting the start and peak dates of the Poaceae pollen season in Spain using process-based models. *Agricultural and Forest Meteorology*, **149**, 256 – 262.

GAW Report No. 181, 2008: Joint Report of COST Action 728 and GURME - Overview of Tools and Methods for Meteorological and Air Pollution Mesoscale Model Evaluation and User Training.

Gehrig, R. and A. G. Peeters, 2000: Pollen distribution at elevations above 1000 m in Switzerland. *Aerobiologia*, **16 (1)**, 69–74.

Gehrig, R., B. Pietragalla-Köhler, B. Clot, T. Herren, M.-J. Graber, M. Hauser, M. Moersen, and C. Sallin, 2013: Luftpollengehalt in der Schweiz 2012. Tech. Rep. 20, MeteoSchweiz, 21 pp.

Gentilini, E., 2010: Modelling the distribution and spread of Common Ragweed (Ambrosia artemisiifolia) at multiple scales. M.S. thesis, University of Lausanne.

Grewling, Ł., B. Jackowiak, M. Nowak, A. Uruska, and M. Smith, 2012: Variations and trends of birch pollen seasons during 15 years (1996–2010) in relation to weather conditions in Poznań (western Poland). *Grana*, **51 (4)**, 280–292.

Guisan, A. and W. Thuiller, 2005: Predicting species distribution: offering more than simple habitat models. *Ecology Letters*, **8 (9)**, 993–1009.

Helbig, N., B. Vogel, H. Vogel, and F. Fiedler, 2004: Numerical modelling of pollen dispersion on the regional scale. *Aerobiologia*, **3**, 3–19.

Hijmans, R. J., S. E. Cameron, J. L. Parra, P. G. Jones, and A. Jarvis, 2005: Very high resolution interpolated climate surfaces for global land areas. *International Journal of Climatology*, **25**, 1965–1978.

Hirst, J. M., 1952: An automatic volumetric spore trap. *Annals of Applied Biology*, **39 (2)**, 257–265, doi:10.1111/j.1744-7348.1952.tb00904.x, URL `http://dx.doi.org/10.1111/j.1744-7348.1952.tb00904.x`.

Jaeger, S., 2011: The trouble with threshold values for allergy forecasts. *Aerobiological Monographs. Towards a comprehensive vision*, B. Clot, P. Comtois, and B. Escamilla-Garcia, Eds., MeteoSwiss (CH) and University of Montreal (CA), 233–245.

Keijzer, C. J., H. B. Leferink-Ten Klooster, and M. C. Reinders, 1996: The mechanics of the grass flower: Anther dehiscence and pollen shedding in maize. *Annals of Botany*, **78 (1)**, 15–21, doi:10.1006/anbo.1996.0089, URL http://aob.oxfordjournals.org/content/78/1/15.abstract, http://aob.oxfordjournals.org/content/78/1/15.full.pdf+html.

Laaidi, M., M. Thibaudon, and J.-P. Besancenot, 2003: Two statistical approaches to forecasting the start and duration of the pollen season of Ambrosia in the area of Lyon (France). *International Journal of Biometeorology*, **48**, 65–73.

Makra, L., I. Matyasovszky, M. Thibaudon, and M. Bonini, 2011: Forecasting ragweed pollen characteristics with nonparametric regression methods over the most polluted areas in Europe. *International Journal of Biometeorology*, **55 (3)**, 361–371.

Mandrioli, P., G. Caneva, and C. Sabbioni, (Eds.) , 2003: *Cultural Heritage and Aerobiology: Methods and Measurement Techniques for Biodeterioration Monitoring.* Kluwer Academic Publishers, 113.

Mandrioli, P., M. D. Cecco, and G. Andina, 1998: Ragweed pollen: The aeroallergen is spreading in Italy. *Aerobiologia*, **14**, 13–20.

Marceau, A., B. Loubet, B. Andrieu, B. Durand, X. Foueillassar, and L. Huber, 2011: Modelling diurnal and seasonal patterns of maize pollen emission in relation to meteorological factors. *Agricultural and Forest Meteorology*, **151 (1)**, 11 – 21, doi:10.1016/j.agrformet.2010.08.012, URL http://www.sciencedirect.com/science/article/pii/S0168192310002261.

Martin, M. D., M. Chamecki, and G. S. Brush, 2010: Anthesis synchronization and floral morphology determine diurnal patterns of ragweed pollen dispersal. *Agricultural and Forest Meteorology*, **150**, 1307–1317, doi:10.1016/j.agrformet.2010.06.001.

Matsui, T., K. Omasa, and T. Horie, 1999: Mechanism of Anther Dehiscence in Rice (Oryza sativa L.). *Annals of Botany*, **84 (4)**, 501–506, doi:10.1006/anbo.1999.0943, URL http://aob.oxfordjournals.org/content/84/4/501.abstract, http://aob.oxfordjournals.org/content/84/4/501.full.pdf+html.

McCullagh, P. and J. A. Nelder, 1983: *Generalized Linear Models.* 1st ed., Monographs on Statistics and Applied Probability, Springer US, doi:10.1007/978-1-4899-3244-0.

Menut, L., B. Bessagnet, D. Khvorostyanov, M. Beekmann, N. Blond, A. Colette, I. Coll, G. Curci, G. Foret, A. Hodzic, S. Mailler, F. Meleux, J.-L. Monge, I. Pison, G. Siour, S. Turquety, M. Valari, R. Vautard, and M. G. Vivanco, 2013: Chimere 2013: a model for regional atmospheric composition modelling. *Geoscientific Model Development*, **6 (4)**, 981–1028, doi:10.5194/gmd-6-981-2013, URL `http://www.geosci-model-dev.net/6/981/2013/`.

Michel, D., M. W. Rotach, R. Gehrig, and R. Vogt, 2012: On the efficiency and correction of vertically oriented blunt bioaerosol samplers in moving air. *International Journal of Biometeorology*, **56 (6)**, 1113–1121, doi:10.1007/s00484-012-0526-x.

Nawrath, S. and B. Alberternst, 2011: Verzeichnis großer Ambrosia-Bestände (>100 Pflanzen) in Bayern, In: Forschungsvorhaben Beifuß-Ambrosie FOBAB I-Studie. Unveröff. Gutachten im Auftrag des Bayerischen Staatsministeriums für Umwelt und Gesundheit.

Nikolić, T., 2011: Flora Croatica Database. Faculty of Science, University of Zagreb, URL `http://hirc.botanic.hr/fcd/`.

Pasken, R. and J. A. Pietrowicz, 2005: Using dispersion and mesoscale meteorological models to forecast pollen concentrations. *Atmospheric Environment*, **39**, 7689–7701.

Pauling, A., R. Gehrig, and B. Clot, 2014: Toward optimized temperature sum parameterizations for forecasting the start of the pollen season. *Aerobiologia*, **30 (1)**, 45–57.

Pauling, A., M. W. Rotach, R. Gehrig, B. Clot, and Contributors to the European Aeroallergen Network (EAN), 2012: A method to derive vegetation distribution maps for pollen dispersion models using birch as an example. *International Journal of Biometeorology*, **56**, 949–958, doi:10.1007/s00484-011-0505-7, URL `http://dx.doi.org/10.1007/s00484-011-0505-7`.

Pawankar, R., C. E. Baena-Cagnani, J. Bousquet, G. W. Canonica, A. A. Cruz, M. A. Kaliner, and B. Q. Lanier, 2008: State of world allergy report 2008: allergy and chronic respiratory diseases. *The World Allergy Organization Journal*, **1 (6 Suppl)**, S4–S17.

Petermann, A., 2011: Première Cartographie Nationale de l'Ambroisie (Ambrosia artemisiifolia L.). Etude réalisée pour le Ministère du Travail, de l'Emploi et de la Santé. Tech. rep., Fédération des conservatoires botaniques nationaux (FCBN).

Phillips, S. J., R. P. Anderson, and R. E. Schapire, 2006: Maximum entropy modeling of species geographic distributions. *Ecological Modelling*, **190 (3)**, 231–259.

Prank, M., D. S. Chapman, J. M. Bullock, J. Belmonte, U. Berger, A. Dahl, S. Jäger, I. Kovtunenko, D. Magyar, S. Niemelä, et al., 2013: An operational model for forecasting ragweed pollen release and dispersion in Europe. *Agricultural and Forest Meteorology*, **182**, 43–53.

Puls, K. E., 1985: Scheitert die Pollenflugvorhersage an der Wetterprognose? *Allergologie*, **8 (1)**, 21–25.

Réaumur, R.-A. F. d., 1735: Observations du thermomètres, faites à Paris pendant l'année 1735, comparées avec celles qui ont été faites sous la ligne, à l'isle de France, à Alger et quelques unes de nos isles de l'Amérique. *Académie des Sciences de Paris*, **545**.

Reinhardt, F., M. Herle, F. Bastiansen, and B. Streit, 2003: Ökonomische Folgen der Ausbreitung von Neobiota. Forschungsbericht 201 686 211, Umweltbundesamt. Umweltforschungsplan des Bundesministeriums für Umwelt, Naturschutz und Reaktorsicherheit. UBA-FB 000441. Seiten 23-29.

Rinke, R., 2008: Parametrisierung des Auswaschens von Aerosolpartikeln durch Niederschlag. Ph.D. thesis, Universität Karlsruhe, Institut für Meteorologie und Klimaforschung.

Rogers, C. A., P. M. Wayne, E. A. Macklin, M. L. Muilenberg, C. J. Wagner, P. R. Epstein, and F. A. Bazzaz, 2006: Interaction of the Onset of Spring and Elevated Atmospheric CO2 on Ragweed (Ambrosia artemisiifolia L.) Pollen Production. *Environmental Health Perspectives*, **114 (6)**, 865–869.

Rohwer, J. G., 1993: Moraceae. *Flowering Plants. Dicotyledons: Magnoliid, Hamamelid and Caryophyllid Families. The Families and Genera of Vascular Plants.*, K. Kubitzki, J. G. Rohwer, and V. Bittrich, Eds., Springer, Vol. 2, 438–453.

Sarvas, R., 1974: Investigations on the annual cycle of development of forest trees. Autumn dormancy and winter dormancy. *Communicationes Instituti Forestalis Fenniae*, **84**, 1–101.

Schaber, J. and F.-W. Badeck, 2003: Physiology-based phenology models for forest tree species in Germany. *International Journal of Biometeorology*, **47 (4)**, 193–201.

Schueler, S. and K. H. Schlünzen, 2006: Modeling of oak pollen dispersal on the landscape level with a mesoscale atmospheric model. *Environmental Modeling and Assessment*, **11**, 179–194.

Seinfeld, J. and S. Pandis, 2006: *Atmospheric chemistry and physics: from air pollution to climate change.* A Wiley-Interscience publication, John Wiley & Sons, URL `http://books.google.co.in/books?id=tZEpAQAAMAAJ`.

Siljamo, P., M. Sofiev, and H. Ranta, 2007: An Approach to Simulation of Long-Range Atmospheric Transport of Natural Allergens: An Example of Birch Pollen. *Air Pollution Modeling and Its Application XVII*, C. Borrego and A.-L. Norman, Eds., Springer US, 331–339, doi:10.1007/978-0-387-68854-1_36, URL `http://dx.doi.org/10.1007/978-0-387-68854-1_36`.

Skjøth, C. A., C. Geels, M. Hvidberg, O. Hertel, J. Brandt, L. M. Frohn, K. M. Hansen, G. B. Hedegård, J. H. Christensen, and L. Moseholm, 2008: An inventory of tree species in Europe - an essential data input for air pollution modelling. *Ecological Modelling*, **2217**, 292–304.

Skjøth, C. A., M. Smith, B. Šikoparija, A. Stach, D. Myszkowska, I. Kasprzyk, P. Radišić, B. Stjepanović, I. Hrga, D. Apatini, D. Magyar, A. Páldy, and N. Ianovici, 2010: A method for producing airborne pollen source inventories: An example of Ambrosia (ragweed) on the Pannonian Plain. *Agricultural and Forest Meteorology*, **150 (9)**, 1203–1210, doi:10.1016/j.agrformet.2010.05.002.

Sofiev, M., J. Belmonte, R. Gehrig, R. Izquierdo, M. Smith, A. Dahl, and P. Siljamo, 2013a: Airborne Pollen Transport. *Allergenic Pollen: A Review of the Production, Release, Distribution and Health Impacts*, M. Sofiev and K.-C. Bergmann, Eds., Springer Science+Business Media, Dordrecht, chap. 5, 133 ff, doi:10.1007/978-94-007-4881-1_5.

Sofiev, M., P. Siljamo, H. Ranta, and A. Rantio-Lehtimäki, 2006: Towards numerical forecasting of long-range air transport of birch pollen: theoretical considerations and a feasibility study. *International Journal of Biometeorology*, **50**, 392–402.

Sofiev, M., P. Siljamo, H. Ranta, T. Linkosalo, S. Jaeger, A. Rasmussen, A. Rantio-Lehtimaki, E. Severova, and J. Kukkonen, 2013b: A numerical model of birch pollen emission and dispersion in the atmosphere. Description of the emission module. *International Journal of Biometeorology*, **57**, 45–58, doi:10.1007/s00484-012-0532-z, URL `http://dx.doi.org/10.1007/s00484-012-0532-z`.

Steppeler, J., G. Doms, U. Schättler, H. Bitzer, A. Gassmann, U. Damrath, and G. Gregoric, 2002: Meso gamma scale forecasts using the nonhydrostatic model LM. *Meteorology and Atmospheric Physics*, **82**, 75–96.

Storkey, J., P. Stratonovitch, D. S. Chapman, F. Vidotto, and M. A. Semenov, 2014: A process-based approach to predicting the effect of climate change on the distribution of an invasive allergenic plant in Europe. *PloS one*, **9 (2)**, e88 156.

Sveinbjörnsson, B., H. Kauhanen, and O. Nordell, 1996: Treeline ecology of mountain birch in the Torneträsk area. *Ecological bulletins*, 65–70.

Swets, J. A., 1988: Measuring the accuracy of diagnostic systems. *Science*, **240 (4857)**, 1285–1293.

Taramarcaz, P., C. Lambelet, B. Clot, C. Keimer, and C. Hauser, 2005: Ragweed (Ambrosia) progression and its health risks: will Switzerland resist this invasion? *Swiss Medical Weekly*, **135**, 538–548.

Thibaudon, M., B. Šikoparija, G. Oliver, M. Smith, and C. A. Skjøth, 2014: Ragweed pollen source inventory for France – The second largest centre of Ambrosia in Europe. *Atmospheric Environment*, **83**, 62–71.

Thuiller, W., B. Lafourcade, R. Engler, and M. B. Araújo, 2009: BIOMOD – a platform for ensemble forecasting of species distributions. *Ecography*, **32 (3)**, 369–373.

Trabucco, A., R. J. Zomer, D. A. Bossio, O. van Straaten, and L. V. Verchot, 2008: Climate change mitigation through afforestation/reforestation: A global analysis of hydrologic impacts with four case studies. *Agriculture, Ecosystems & Environment*, **126 (1)**, 81–97.

Turolla, F., U. Känzig-Schoch, and E. Jörg, 2008: Bekämpfung pathogener oder invasiver Schadorganismen. Kantonale Strategie 2008. Tech. rep., Amt für Umweltkoordination und Energie.

van Moerbeke, D., (Ed.) , 1997: *European allergy white paper - Allergic diseases as a public health problem in Europe.* UCB Institute of Allergy, Braine-l'Alleud, 51 pp.

Verbruggen, H., L. Tyberghein, G. S. Belton, F. Mineur, A. Jueterbock, G. Hoarau, C. F. D. Gurgel, and O. De Clerck, 2013: Improving Transferability of Introduced Species' Distribution Models: New Tools to Forecast the Spread of a Highly Invasive Seaweed. *PloS one*, **8 (6)**, e68 337.

Viner, B. J., M. E. Westgate, and R. W. Arritt, 2010: A model to predict diurnal pollen shed in maize. *Crop Science*, **50**, 235 – 245, doi:10.2135/cropsci2008.11.0670.

Vogel, B., H. Vogel, D. Bäumer, M. Bangert, K. Lundgren, R. Rinke, and T. Stanelle, 2009: The comprehensive model system COSMO-ART - radiative impact of aerosol

on the state of the atmosphere on the regional scale. *Atmospheric Chemistry and Physics*, **9**, 8661–8680, doi:10.5194/acp-9-8661-2009.

Vogel, H., A. Pauling, and B. Vogel, 2008: Numerical Simulation of Birch Pollen Dispersion with an Operational Weather Forecast System. *International Journal of Biometeorology*, **52**, 805–814.

Wilks, D. S., 2006: *Forecast Verification*, 260–276. 2d ed., Academic Press, Amsterdam, 260-276.

Willmott, C. J., R. E. Davis, J. J. Feddema, K. M. Klink, D. R. Legates, C. M. Rowe, S. G. Ackleson, and J. O'Donnell, 1985: Statistics for the evaluation and comparison of models. *Journal of Geophysical Research*, **90**, 8995–9005, doi: 10.1029/JC090iC05p08995.

Zhang, R., T. Duhl, M. T. Salam, J. M. House, R. C. Flagan, E. L. Avol, F. D. Gilliland, A. Guenther, S. H. Chung, B. K. Lamb, and T. M. VanReken, 2014: Development of a regional-scale pollen emission and transport modeling framework for investigating the impact of climate change on allergic airway disease. *Biogeosciences*, **11 (6)**, 1461–1478, doi:10.5194/bg-11-1461-2014, URL http://www.biogeosciences.net/11/1461/2014/.

Zink, K., A. Pauling, M. W. Rotach, H. Vogel, P. Kaufmann, and B. Clot, 2013: EMPOL 1.0: a new parameterization of pollen emission in numerical weather prediction models. *Geoscientific Model Development*, **6 (6)**, 1961–1975, doi:10.5194/gmd-6-1961-2013, URL http://www.geosci-model-dev.net/6/1961/2013/.

Zink, K., H. Vogel, B. Vogel, D. Magyar, and C. Kottmeier, 2012: Modeling the dispersion of Ambrosia artemisiifolia L. pollen with the model system COSMO-ART. *International Journal of Biometeorology*, **56 (4)**, 669–680, doi:10.1007/s00484-011-0468-8.

Zink, K., M. W. Rotach, P. Kaufmann, E. Gentilini, F. Essl, B. Petitpierre, O. Broennimann, A. Guisan, and B. Clot, submitted: Using plant inventories to create source maps for pollen emission in numerical weather prediction systems: how detailed need they be? *Agricultural and Forest Meteorology*.

Ziska, L. H. and F. A. Caulfield, 2000: Rising CO2 and pollen production of common ragweed (Ambrosia artemisiifolia), a known allergy-inducing species: implications for public health. *Australian Journal of Plant Physiology*, **27**, 893–898.

Zweig, M. H. and G. Campbell, 1993: Receiver-operating characteristic (ROC) plots: a fundamental evaluation tool in clinical medicine. *Clinical Chemistry*, **39 (4)**, 561–577.

Thanks

Finally, the most personal part of the thesis: thanking everybody who has contributed to the successful completion of the PhD project.

Looking at the last four years, there is only one person that was present during the entire course of my PhD study: Prof. Dr. Mathias Rotach, first as the head of the group 'Bio- und Umweltmeteorologie' at MeteoSwiss, later as my supervisor at the University of Innsbruck. Thank you for taking over my supervision and always being available for Friday discussions whenever I needed them.

Due to organisational changes, I had several advisors that played an important role at different stages of my thesis. Especially, I would like to thank Dr. Bernard Clot for his warm welcome at Payerne and the fruitful discussions that formed the outline and focal points of my thesis. At a later point, this role was taken over by Dr. Pirmin Kaufmann whom I thank for his professional as well as personal advice in many different situations.

Naturally, this thesis contains ideas that arose from discussions with different members of the groups I was affiliated to: the group 'Bio- und Umweltmeteorologie' for the first three years and the group 'Numerical prediction' for the last year of my PhD. Several members of these groups provided invaluable help when computational problems came up: Dr. André Walser, Dr. Daniel Leuenberger, Dr. Oliver Fuhrer and Dr. Petra Baumann. A special thanks goes to my roommates Dr. Denis Hilaire, Dr. Martin Hirschi and Dr. Andreas Pauling. Apart from the groups at MeteoSwiss, I received a lot of advice and ideas from Dr. Heike Vogel at the Karlsruhe Institute of Technology. Thank you very much!

I also appreciated the constructive reviews of my co-authors, my advisors and the anonymous reviewers of the journals. In addition to my supervisor and advisors, my PhD thesis was reviewed by Dr. Bernhard Vogel and Michael J. Zink. Thank you very much for your valuable suggestions. Especially, I would like to thank Dr. Michel Thibaudon and Dr. Sylvain Dupont for taking over the role of external reviewers of my PhD thesis.

In addition to the people that contributed to the professional aspects of the thesis, I would also like to acknowledge the people that supported me privately. Without a precious and relaxing leisure time, writing a thesis would not be feasible. Particularly, I would like to thank my husband Marcel Thielmann. Only as a well-matched team was it possible to finish two PhD theses while becoming parents.

Curriculum Vitae

Katrin Zink
Born on 28 January 1983 in Weingarten, Germany

Education and professional training:

2010–2014   **Ph.D. study** at the University of Innsbruck, Austria
Supervisor: Prof. Dr. Mathias Rotach

Sep 2011   10th International NCCR Climate **Summer School**
Climate Change, Extremes and Ecosystem Services

2003–2009   **Diploma in Meteorology**
Modellierung der Ausbreitung von Ambrosiapollen mit COSMO-ART
Institute for Meteorology and Climate Research
University of Karlsruhe, Germany

Oct 2008   **Course**: Fortran for Scientific Computing
High Performance Computing Center Stuttgart (HLRS)
University of Stuttgart, Germany

1993–2003   **Abitur**
Studienkolleg St. Johann, Germany

1999–2000   **School year in the USA**
West Aurora High School, Illinois, USA

Work experience:

2009–2013   **Scientific assistant**
Federal Office of Meteorology and Climatology MeteoSwiss
Payerne and Zürich, Switzerland

2004–2007   **Student assistant**
Institute for Meteorology and Climate Research
Karlsruhe Institute of Technology, Germany

2005–2006   **Internship**
Centro de Estudios Avanzados en Zonas Aridas (CEAZA)
University of La Serena, Chile

Eidesstattliche Erklärung

Ich erkläre hiermit an Eides statt durch meine eigenhändige Unterschrift, dass ich die vorliegende Arbeit selbständig verfasst und keine anderen als die angegebenen Quellen und Hilfsmittel verwendet habe. Alle Stellen, die wörtlich oder inhaltlich den angegebenen Quellen entnommen wurden, sind als solche kenntlich gemacht.

Die vorliegende Arbeit wurde bisher in gleicher oder ähnlicher Form noch nicht als Magister-/Master-/Diplomarbeit oder Dissertation eingereicht.

July 4, 2014

Katrin Zink